The Influence of Gravity Upon Topology Changing Transitions and Warped Flux Compactifications

Neil Anthony Butcher

The University of Nottingham

Thesis submitted to the University of Nottingham
for the degree of Doctor of Philosophy, December 2009

"How wonderful that we have met with a paradox. Now we have some hope of making progress."

– Niels Bohr

Supervisor: Dr. Paul Saffin

Examiners: Prof. Elizabeth Winstanley
Prof. Ed Copeland

Abstract

We investigate the dynamics of the geometric transitions associated to compactified spacetimes. By including the effects of gravity we are able to follow the evolution of collapsing cycles as they attempt to undergo a topology changing transition. We perform investigations where we add a perturbation to the momentum of a static solution and observe the consequences this has on the spacetime, looking for evidence of black hole formation or collapsing cycles which could lead to singular geometry.

First we look into two possible four dimensional spacelike solutions to the Einstein equations called instantons. These both have a two-sphere at the origin, these are called bolt singularities. We introduce an initial perturbation to reduce the two-sphere to a point. Rather than achieving this singular geometry we find that either a horizon forms, shielding a curvature singularity, or the cycle re-expands after an initial contraction phase. For the case where a horizon forms we identify the final state with a known analytic black-hole solution.

In seven dimensions we simulate the gravitational dynamics of the conifold geometries (resolved and deformed) involved in the description of certain compact spacetimes. As the cycles of the conifold collapse towards a singular geometry we inevitably find that a horizon develops, shielding the external spacetime. The structure of the black hole is examined and we find a candidate for the final state of the collapse.

In ten dimensions we investigate the time evolution due to gravitational dynamics of a spacetime which is commonly used in brane-cosmology and string compactifications called the Klebanov-Strassler geometry. Here black holes are sometimes formed but more commonly the cycles are seen to re-expand after reaching a minimum value, showing the stability of the solution against perturbations which would change its size.

Contents

The Influence of Gravity Upon Topology Changing Transitions and Warped Flux Compactifications

1 Introduction **2**

1.1 String theory 4

1.2 Extra dimensions 4

1.2.1 Extra dimensions with regard to spherical symmetry 5

1.3 Branes 5

1.3.1 Compactification with incorporated branes 6

1.4 Outlook 6

2 Some background physics and maths **8**

2.1 Manifolds 8

2.1.1 Topology of a manifold 8

2.1.2 Differentiable and Riemannian manifolds 9

2.1.3 Holonomy 9

2.1.4 Identifying the topology of a manifold 10

2.1.5 Calabi-Yau manifolds 12

2.1.6 Moduli 13

2.2 Horizons and singularities 13

2.2.1 The event horizon 13

2.2.2 Apparent horizons 14

2.2.3 Other horizons 15

2.2.4 Singularities 15

2.2.5 Singularity theorems 16

2.2.6 Conical singularities 16

2.2.7 Cosmic censorship 17

2.3 Black hole spacetime solutions 17

2.3.1 Black hole properties 18
2.3.2 Black hole uniqueness 19
2.3.3 Black hole effects 19
2.3.4 Black hole evaporation 20
2.4 Cauchy problems 20
2.4.1 Moduli space approximation 21
2.4.2 Numerical Simulations 21
2.5 Supersymmetry 25
2.5.1 Properties and predictions 26
2.6 Supergravity and superstrings 27
2.6.1 11d supergravity 27
2.6.2 IIA superstrings 28
2.6.3 IIB superstrings 29
2.6.4 Other string theories 30
2.6.5 D-branes 32
2.6.6 Unifying superstring theories and supergravity 32
2.7 Compactifications 33
2.7.1 Flux free compactification 34
2.7.2 Flux compactifications 35
2.7.3 String landscape 36
2.8 Topology transitions 37
2.8.1 Obstacles to transitions 39

3 Five dimensional evolution 40
3.1 Five dimensional gravitational instantons 40
3.1.1 Features of gravitational instantons 41
3.2 Flop transitions 41
3.3 The Eguchi-Hanson instanton 42
3.4 Dynamical evolution of the Eguchi-Hanson instanton 43
3.4.1 Moduli space approximation 43
3.4.2 Numerical evolution of the Eguchi-Hanson instanton 44
3.4.3 Time dependent metric 44
3.4.4 The Einstein equations 46
3.4.5 Initial conditions 48

3.4.6 Results . . . 50
3.4.7 Smoother initial momentum . . . 57
3.4.8 Conclusions from numerics . . . 57
3.5 The Taub-bolt instanton . . . 58
3.6 Dynamical evolution of the Taub-bolt instanton . . . 59
3.6.1 Moduli space approximation . . . 59
3.6.2 Numerical evolution of the Taub-bolt instanton . . . 59
3.6.3 Initial perturbation . . . 60
3.6.4 Results . . . 60
3.6.5 Conclusions from numerics . . . 60
3.7 The Five dimensional black hole solution . . . 61
3.7.1 Uniqueness of the squashed 5d black hole . . . 62
3.7.2 Evaporation of the black hole . . . 62
3.8 Five dimensional summary . . . 63

4 Seven dimensional evolution 69
4.1 Singular conifold instanton . . . 69
4.2 Resolved conifold instanton . . . 70
4.3 Deformed conifold instanton . . . 71
4.4 Conifold transitions . . . 72
4.5 Dynamical evolution of the resolved conifold . . . 73
4.5.1 Moduli space approximation . . . 73
4.5.2 Numerical evolution of the resolved conifold . . . 73
4.5.3 Time dependent metric . . . 74
4.5.4 The Einstein equations . . . 75
4.5.5 Initial conditions . . . 75
4.5.6 Results . . . 76
4.5.7 Conclusions . . . 80
4.6 Dynamical evolution of the deformed conifold . . . 82
4.6.1 Time dependent metric . . . 82
4.6.2 The Einstein equations . . . 83
4.6.3 Initial conditions . . . 84
4.6.4 Results . . . 84
4.6.5 Conclusions . . . 85

4.7 The Seven dimensional black hole solution . . . 85
4.8 Seven dimensional summary . . . 90

5 Ten dimensional evolution 92
5.1 The Klebanov-Strassler static solution . . . 93
5.1.1 D-brane sourced fluxes . . . 93
5.1.2 Warp factor . . . 95
5.1.3 Superpotential and stabilised moduli . . . 96
5.2 Uses of the Klebanov-Strassler solution . . . 98
5.3 Dynamical evolution of the Klebanov-Strassler solution . . . 99
5.3.1 Moduli and perturbative approximations to the dynamics . . . 99
5.3.2 Numerical evolution of the Klebanov-Strassler solution . . . 101
5.3.3 Time dependent spacetime ansatz . . . 101
5.3.4 Initial conditions . . . 103
5.3.5 Results . . . 105
5.4 Ten dimensional summary . . . 109

6 Discussion 111
6.1 Hopes of transition . . . 112
6.2 Dynamical studies . . . 113
6.3 Evaporation of the black holes . . . 115
6.4 Closing statement . . . 116

Appendices

A Conventions and computation 118
A.1 Conventions . . . 118
A.2 Computational methods . . . 118

B Groups, forms and sets 119
B.1 Coset space geometry . . . 119
B.2 The Special unitary group; $SU(2)$ . . . 121
B.3 g^i one-forms . . . 124

C Five dimensional Einstein equations for Taub-Bolt 125
C.1 Equations of motion . . . 126
C.2 Constraint equations . . . 126

D Uniqueness of the squashed 5d black hole **127**

E Seven dimensional Einstein equations **130**

E.1 Resolved conifold Einstein equations 130

E.1.1 Equations of motion 131

E.1.2 Constraint equations 131

E.2 Deformed conifold Einstein equations 132

E.2.1 Equations of motion 132

E.2.2 Constraint equations 133

E.3 Static black hole equations 134

F Ten dimensional equations **135**

F.1 Equations of motion 137

F.2 Constraint equations 139

F.3 Flux equations 140

Bibliography **141**

The Influence of Gravity Upon Topology Changing Transitions and Warped Flux Compactifications

Chapter 1

Introduction

The term classical physics has been changed as our understanding of physics has progressed, at each stage it has referred to physics which is no longer modern.

Within the 1800's some physicists thought that theories of Newtonian motion, the gravitational force, thermodynamics and Maxwell's equations of electromagnetism meant that physics was close to completion and only had a few small difficulties. However these topics were later considered to be only classical physics when the small details turned out to be huge gaping holes in our understanding. Holes which demanded changes to our thoughts on what particles were made of, the fundamental electron interactions underlining chemistry, the fuel of stars and even the space and time we occupy.

General relativity interprets gravity as a geometric effect and has been adopted as a better description of gravity than Newton's laws due to general relativity's ability to correct earlier difficulties (such as an error in the orbit of Mercury) and make new predictions which have later been verified (curving of light from distant stars around the Sun). General relativity differs from Newton's gravity in some of the predictions it makes, it predicts that there will be gravitational radiation moving at the speed of light, there will be exotic objects called black holes, light will be bent around massive objects which can form optical illusions such as Einstein rings or light can get redshifted, objects will age at different rates in gravitational fields and general relativity even predicts (though it was not acknowledged as a prediction at the time) that the whole

universe can change in size. Some of these predictions have been verified but others have not yet been directly detected.

However (despite some features not yet being seen) even general relativity has now been delegated to the regime of classical physics, considered well understood and surpassed by theories which are quantised.

Quantum field theory has made the most accurate prediction of our time by predicting a property of the electron called the magnetic moment. It acts as a quantum mechanical method to describe fields such as the electromagnetic field and it mediates these fields and forces using vector bosons. This theory is also relativistic in that it is compatible with special relativity however it does not include gravity and does not include general relativity.

While each of these two improvements to the physics of the 19th century are exceptionally good at describing physics in their own regime, they cannot yet be combined together into a single theory of quantum gravity. In most cases such a combined theory is not needed because many physics problems do not need both of these improvements. While dealing with the interactions of particles, the effects of gravity can be mostly disregarded due to how weak this force is in comparison to the electromagnetic and nuclear forces. These stronger forces are very well described in quantum mechanics. On the scale of massive stars, galaxies and the universe, the quantum nature of the forces can be disregarded (even the existence of electromagnetism and nuclear forces is totally ignored in many cases).

However in some of the most interesting places in the universe such as black holes and the moments after the big bang, both of these effects must be considered simultaniously. These events will only finally be understood if we can consider the quantum mechanics while at the same time incorporating the very curved background of general relativity.

Quantum mechanics still has the privilege of being considered modern, however this title is now threatened by new and upcoming methods of physics which we hope will soon surpass both general relativity and quantum mechanics to become the new modern theory of physics. A good example of such a theory is string theory.

1.1 String theory

String theory is a leading research topic which attempts to bridge this gap by being both a quantum theory and also a theory which very naturally incorporates gravity. It relies on the idea that there exist small one dimensional objects upon each timeslice called strings. These have a tension which determines their favoured size but they can be stretched, split or jointed in time, they may be closed with no end points or open with two end points. Later other objects can be added to complement the theory of strings such as D-branes, surfaces upon which open strings may end. While string theory appeals due to the possibility of quantum gravity it also presents new challenges to overcome such as the low predictive power due to string theory being very dependent upon the background and the need for extra dimensions of space.

1.2 Extra dimensions

Extra dimensions are not exclusive to string theory and were suggested long before string theory came about. It was suggested by Theodor Kaluza[1] in the 1920's that extra dimensions could unite electromagnetism and four dimensional gravity into one theory of five dimensional gravity. Later Oskar Klein[2] interpreted this process physically as making one of the dimensions into a very small circle. This circle would have to be very small so that the dimension would so far have gone unrecognised, not being seen as a dimension but only as another force called the electromagnetic force.

We still use a similar process of compactification (making dimensions small) to hide the extra dimensions of string theory and produce a four dimensional gravity theory, just as in the Kaluza-Klein case this results in additional fields and forces like electromagnetism. Compactifications in ten or eleven dimensions have a great freedom of choice, with a range of possibilities in size and shape of the internal manifold. These possible ways to compact the extra dimensions are called the string vacua within string theory and the predictions of string theory are highly dependent upon the choice of vacuum, this is the cause of the low predictive power of string theory.

1.2.1 Extra dimensions with regard to spherical symmetry

As we wish to investigate possible transitions we require a solution which can change dynamically in time. Spherically symmetric vacuum solutions in four dimensions will not evolve dynamically as is shown by Birkhoff's theorem[3]:

"A spherically symmetric vacuum solution in the exterior region is necessarily static"

This is equivalent to the claim that there is no monopole radiation[4]. It means that if we wish to perform interesting dynamical simulations in the vacuum while maintaining spherical symmetry we must go to higher dimensional situations. This is true even using the Maxwell energy momentum tensor since there is an analogue of Birkhoff's theorem which is applicable to solutions of the Einstein-Maxwell field equations also.

This theorem is avoided by going to five dimensions or higher and this allows interesting dynamical situations which depend on only one codimension (a radius) and do not have any energy momentum tensor (vacuum). The extra dimensions permit more interesting gravitational instantons capable of evolving in time.

1.3 Branes

Compactification is not the unique method of hiding extra dimensions, other objects called D-branes have been added to string theory as objects upon which open strings may end. They are called "D" due to making the ends of strings obey Dirichlet boundary conditions and stay attached to the brane[5, 6, 7]. Being joined to D-branes imposes requirements on strings (for example strings with endpoints on two different branes will have a minimum length which is equivalent to a minimum relativistic mass) and the particle states which can emerge are determined by these requirements so the branes are crucial to the nature of emergent particles. We also note that branes can be dynamical and change in time in response to strings, this offers a great many possibilities and outcomes for particle physics. The suggestion of a braneworld cosmology hides the extra dimensions by making us and all we see confined to a lower dimensional brane[8]. This hides the extra dimensions without compactification by making gravity our only way to test for the extra dimensions in which case they could easily

have gone unseen. This is a method of hiding dimensions which we will not cover in the following chapters.

1.3.1 Compactification with incorporated branes

Though we do not consider braneworld cosmologies we will make use of D-branes as a source of fluxes into a spacetime. A D-brane will act as the elementary charge of Ramond-Ramond fluxes[7] and we will use these fluxes in a process of flux compactification which is described in more detail in section 2.7.2. This process adds an expectation value to the fluxes in the vacuum and overcomes some of the common difficulties which can be problematic for compactification, difficulties which we investigate in section 2.7.1. Adding D-branes to the compactified space can enhance the predictive power of string theory, the branes act to make some string vacua both static and stable and so these become preferable choices of vacua and the degeneracy is reduced. Despite being stable even these vacua can change in time in response to high energy effects or change only for a short period of time, making changes between these vacua possible. It is this evolution which we hope to investigate.

1.4 Outlook

In the coming chapter we will discuss in more detail string theory's need for the extra dimensional compact manifolds and the method of flux compactification to change a ten dimensional theory to a theory with only four extended dimensions which could be seen by us as an effective theory. We discuss the consequences of the distinct topologies this manifold takes and the effect of the continuous moduli which define the manifold. Then we discuss how the moduli and even the topology could possibly be changed in time and the ramifications this would have for string theory.

Then in the later chapters we shall go into detail about the actual simulations we performed, these are separated into chapters based upon the number of dimensions of the spacetime. In chapter 3 we discuss early investigations performed by taking a known static instanton in four spacelike dimensions and proceed to cause this to evolve in a

fifth timelike dimension, this is an example of a Cauchy problem. We perform this to both an Eguchi-Hanson instanton and a Taub-bolt instanton, these both possess points with a blown up cycle at the tip. We wished to find whether the cycle could be collapsed to zero size by some initial momentum, while at the same time avoiding the creation of a black hole spacetime. This would be a necessary requirement for a flop transition, a process we describe later.

Following this, in chapter 4 we take our initial surface to be six dimensional and perform a similar operation upon instantons which are six dimensional geometries which asymptote to a ”conifold” which is an instanton with a conical singularity at its tip. It can be resolved in two distinct ways, one where the tip is increased to a two-cycle (resolved conifold) or a method which makes the tip into a three-cycle (deformed conifold), we perform simulations on both these geometries to discover if a ”conifold transition” is a possibility. This is a more consequential transition which would change the topology of the spacetime drastically, it is described in more detail later.

In chapter 5 we go on to a ten dimensional simulation which starts with a warped deformed conifold. This is ten dimensional with fluxes and could make part of the manifold used in a flux compactification of string theory, it is also used in a great many models which require a stable throat in which to move probes such as branes.

We end with a discussion of our findings and some appendices giving a more thorough description of the equations of motion which we used to evolve the systems numerically.

Chapter 2

Some background physics and maths

2.1 Manifolds

A set of points X can be formed into manifolds of various mathematical structure, a topological manifold can be thought of as being continuous, the topology also means that the region close to a point looks like a patch of $\mathbb{R}^n$ giving n to be the dimension of the manifold. This requires the introduction of a topology to the set of points, the topology is a collection of open subsets U^i of the points. If all these open subsets are continuous and so can be described by coordinates x^n (called a chart), then the whole of X is continuous and the manifold is called topological. This continuity is not dependent upon the chart so there is some choice of which U^i to use. If we can always find another collection of open subsets which only keeps a finite number of the U^i's then the manifold is called compact. This compactness is a property of the topology.

2.1.1 Topology of a manifold

The manifold's topology is not determined by the exact shape or size but by the way the manifold is put together. One feature of the topology is the genus of the manifold (thus making the topology of a doughnut the same as the topology of a coffee cup, a common example).

2.1.2 Differentiable and Riemannian manifolds

Upon such a topological manifold we can improve on the continuity, we would want to make the manifold differentiable. This requirement means we have open subsets which agree within their overlapping regions (making the transitions functions between the different patches differentiable). If this is imposed it allows functions to be differentiated upon the manifold without having conflicting results in regions of overlap between the patches. Giving such a manifold a metric makes it a Riemannian manifold.

The metric (if it exists) is unlikely to be unique and there is likely to be a range of possibilities (as a doughnut differs from a teacup only in its metric). Some of these may be discrete but many will only differ by continuous parameters we call these parameters moduli.

2.1.3 Holonomy

Once endowed with a metric, manifolds also have a property known as their holonomy which depends upon the topology and also the Levi-Civita connections (which are solely dependent upon the metric). Using the Levi-Civita connections we can perform parallel transport of a vector around some path upon the manifold. Parallel transporting a vector around a closed path will not in general leave it unchanged, upon returning to its starting position it may point in a different direction. By choosing different starting points and different closed paths we can possibly change the orientation of the vector in a great many ways, for a sphere we can change any vector to any other. However this is not always the case, no path on a perfect doughnut (or a flat sheet) will change the vector. The group of all these transformations is called the holonomy, spheres have $SO(n)$ holonomy, tori have identity holonomy.

2.1.3.1 Almost complex structure and complex manifolds

It may be possible to endow an even dimensional manifold with an almost complex structure[9] defined by a (1,1) tensor J. This structure is a map which also obeys $J^2 = -1$. It has the eigenvalues $\pm i$ with eigenvectors which we take to be the complex

coordinates. Note that any even dimensional manifold admits such a tensor field locally however upon a complex manifold, J can be be defined globally. The existence of such a globally defined J is a requirement for a manifold to be complex and its existence depends upon the topology.

A manifold with the the additional feature that the transition functions between all the charts be holomorphic (a much stronger condition than real differentiability as it implies that the function is infinitely differentiable and can be described by its Taylor series) is called a complex manifold.

The existence of a complex structure does not mean that it is unique, there may be multiple ways to define the complex coordinates. As we choose one set of coordinates (one J) we select one from the range of possible complex manifolds many of these will differ only by continuous parameters we call the complex structure moduli.

2.1.3.2 Symplectic and Kähler manifolds

A manifold with a closed almost complex structure is called symplectic and a manifold which is symplectic and complex is Kähler. This is actually a requirement on the manifold along with its connection and it means that all terms of the metric can be found from the derivatives of one function, the Kähler potential (which need only be defined locally). The Kähler manifold has $U(d)$ holonomy where d is the dimension, if the holonomy is further reduced to $Sp\left(\frac{d}{4}\right)$ (where the dimension is a multiple of four) then the manifold is called hyper-Kähler. While the metric of a Kähler manifold is more tightly constrained than a Riemannian manifold, it is still not generally unique and will still vary by continuous parameters called the Kähler moduli.

2.1.4 Identifying the topology of a manifold

Though the topology must be determined in full using set theory, there exist invariants specific to the topology of the spacetime, these characteristic numbers help identify the specific topology.

2.1.4.1 Euler characteristic χ

The Euler characteristic is a topological constant which was classically defined for the surfaces of polyhedra in terms of the number of faces, edges and vertices possessed. It is defined for higher dimensional topological spaces in terms of an alternating sum of the numbers and dimension of cells upon the space,

$$\chi = k_0 - k_1 + k_2 - k_3 + ... \tag{2.1}$$

where k_i gives the number of cells of dimension i.

e.g. upon a two dimensional surface k_0 is the number of vertices (0d cells), k_1 gives the number of edges (1d cells) and k_2 is the number of faces (2d cells). This constant always takes the value 2 for the topology of a two-sphere and it always takes the value 0 for a torus.

However the important point for our uses is the knowledge that it is invariant for a single topology. Any change to this characteristic number will show beyond doubt that the topology of the space has been changed by some process, such processes are the most drastic form of topology changing transition.

2.1.4.2 Betti numbers, Hodge numbers and intersection numbers

The Betti numbers of a manifold are topological invariants which extend the concept of the genus (number of holes) into higher dimensions. The nth Betti number b_n is the number of n-dimensional independent generators of the homology group[10]. So for a connected manifold b_0=1, all points are linked by a common generator. b_1 is related to the genus of the manifold and the higher Betti numbers give higher dimensional equivalents of the genus. Any change to these numbers indicates a change of topology.

Betti numbers also describe the possibility of closed differential forms on the manifold, any exact differential form will be closed but there is also the possibility of closed forms which are not exact. If the group of all closed p-forms which are equal up to an exact form is labelled H^p the the pth Betti number b_p gives the dimension of H^p.

The differential forms can be split depending upon their type, the vector space of one-forms can be split into a space of type (1,0) forms and another of (0,1) forms. The

dimensions of these vector spaces are called the Hodge numbers[9], $h^{1,0}$ and $h^{0,1}$, these numbers can be arranged into a Hodge diamond. Note that

$$\Sigma_{p+q=n}\, h^{p,q} = b_n \tag{2.2}$$

These new Hodge numbers are also topological invariants and two manifolds with different Hodge numbers must be topologically distinct. However the reverse is not true, Hodge structures are not unique to topologies.

In cases where different topologies share the same Hodge structure and Betti numbers, the difference may be seen by the intersection numbers of the topologies. These are again topological invariants which describe the number of points where cycles (closed surfaces of specified dimension) intersect (weighted by orientation)[5].

2.1.5 Calabi-Yau manifolds

Manifolds which occupy n dimensions are called Calabi-Yau manifolds if they obey a small selection of properties. They are named after a mathematician who made a conjecture about the existence of a Ricci-flat metric upon such manifolds and then a second who proved it. The requirements upon the manifold to be Calabi-Yau demand that it is compact, complex, Kähler and it must also have $SU(d)$ for its holonomy group, this is equivalent to the requirement that its torsion vanish[11].

The key theorem concerning these manifolds is that they definitely have a unique metric which is Ricci flat (they also need to obey another restriction upon the Chern class however this is simple to determine, see [12, 13]). The conjecture and theorem that these manifolds shall admit a Ricci flat metric is not a trivial one since this is not in general true for compact manifolds, often even Kähler manifolds have topological obstructions to Ricci flatness. These topological difficulties are avoided by the restriction to $SU(d)$ holonomy. Showing that the Ricci flat metric exists does not tell us what the metric is but is enough for us to continue to use them in string theory.

A conformal Calabi-Yau manifold is a manifold whose metric is related to that of a Calabi-Yau by a conformal factor.

2.1.6 Moduli

The moduli are the continuous parameters which identify one manifold from the numerous possibilities of Calabi-Yau manifolds (or conformal Calabi-Yau manifolds). They can be split into the complex structure moduli and the Kähler moduli. Small changes to these parameters give rise to small continuous deformations to the manifold. These moduli will become important when we use the manifold as the vacuum of our spacetime.

2.2 Horizons and singularities

Spacetimes may include both horizons and singularities. Both these are closely linked to the existence of a black hole though this is not a given and there are multiple theorems which attempt to show that horizons imply singularities and singularities require horizons. There are a range of different horizons and a range of different singularities, some of these depend upon the coordinate system and can even be removed by an adequate coordinate choice, others however are physical effects which cannot be avoided.

2.2.1 The event horizon

The event horizon is a boundary within a spacetime, it surrounds a region from which timelike and null paths cannot leave and so cannot affect any outside observer. The event horizon seals off all internal events from any external observer. This means that points within the event horizon are never within the past light cone of the outside observer and so cannot be observed or influence the outside[14, 4]. The presence and position of an event horizon is not dependent upon the coordinate system used. On a thermodynamic side-note, the event horizon has a spatial area which has been shown to always increase if two black holes combine. With the discovery that black holes radiate with some temperature, the area has been taken as the entropy of a black hole[15], this Bekenstein-Hawking entropy prevents the second law of thermodynamics from being violated by the creation of black holes[16, 17, 18]. The event horizon, though it is well

defined within a complete spacetime, can be hard to identify if we do not yet know the future evolution of a dynamical spacetime. Other horizons can be detected upon a single Cauchy surface or timeslice so can be of more use in numerical simulation, which run for a finite time and so will not show the event horizon.

As we perform our simulation, one possible outcome can be the creation of a black hole. In fact this is the expected result for sufficiently high initial energy input. This is defined by the existence of an event horizon within the space time, however this is not easy to test for a single given time. The event horizon contains all points for which all null geodesics are unable to diverge to $\mathcal{I}^+$ (the future null infinity), this is only known once the entire future evolution of the system has been calculated. Since we do not intend to run each simulation infinitely far into the future we must use a different method to detect the creation of the black hole.

2.2.2 Apparent horizons

In contrast to the event horizon, an apparent horizon[19, 14] (also known as a marginally outer trapped surface) is defined locally in time and so can be detected upon a single time-slice and as soon as it forms. An apparent horizon encompasses a region of space where outgoing null geodesics have zero expansion. This means that, upon the single timeslice and at the apparent horizon

$$0 = \left[\frac{d\,Area}{dt}\right]_{null}. \tag{2.3}$$

In more general cases, upon any spacelike surface (not necessarily a timeslice) with extrinsic curvature K_{ij}, the apparent horizon has the unit normal n^i which obeys

$$0 = \nabla_i n^i + K_{ij} n^i n^j - K \tag{2.4}$$

(K is the trace of K_{ij}). The lack of expansion indicates that the null geodesics do not diverge and so these points must be within an event horizon. All points behind the apparent horizon are also behind some event horizon, this can be used to show that an event horizon has formed. The converse is not true generally, the event horizon may contain points not enclosed in an apparent horizon, or an event horizon may exist where no apparent horizon has been formed. As the situation tends to a steady state

the two should coincide and the apparent horizon becomes a good approximation to the event horizon.

2.2.3 Other horizons

Though the event horizon acts as the boundary of any black hole we may produce, and the apparent horizon will allow us to prove that the black hole has been formed, other horizons exist which will play less important roles. Charged and rotating black holes will include an additional inner horizon and rotating black holes are surrounded by an ergosphere within which rotation is unavoidable. The Cauchy horizon of a spacelike surface S encompasses all the events which are entirely determined by the initial condition upon the base, S. There also exist cosmological horizons which mark the limit of our observations due to the finite age of the universe, though these horizons exist they will not feature in our systems.

2.2.4 Singularities

The intuitive picture of a singularity, as a region of spacetime which exhibits catastrophic behaviour, can lead to points looking singular which are in fact regular. Regions where the metric is zero (preventing it from being invertible) or where the metric is not defined or infinite will look like singularities upon first inspection, however they may not be. There exist coordinate singularities which can be removed by a suitable choice of coordinate system. Singularities can be proven to be true singularities if the curvature of the spacetime diverges, however coordinate singularities may also cause the curvature tensor (R^a_{bcd}) to diverge. To be sure of a divergence of the curvature we must show that scalar quantities formed from the curvature (eg R,$R_{ab}R^{ab}$,$R_{abcd}R^{abcd}$ etc) diverge, these scalars are independent of the coordinate choice and so will diverge in any coordinate system. Though this method will identify a curvature singularity, it may not find other singularities such as the conical singularities of section 2.2.6.

Due to this range of different types of singularity, some of which involve a diverging curvature and others which do not, we need to define the presence of a singularity in terms of geodesics. A geodesic is said to be incomplete if they have finite range of

affine parameter, despite being inextensible in at least one direction (they have been fully extended in some direction but still have finite affine length), the incomplete geodesic may be null, timelike or spacelike. An incomplete timelike geodesic indicates that an observer may not exist after a finite time, this objectionable feature indicates a singularity. We also have a singularity if a null geodesic is incomplete (this method would also give singularities if we artificially removed points from the manifold, so we also need the additional condition that the spacetime is inextensible). An incomplete null geodesic or an incomplete timelike geodesic indicate the presence of a singularity. The existence of such incomplete geodesics can be shown in some cases by the singularity theorems.

2.2.5 Singularity theorems

These theorems show[14] that singularities are a true feature of the results of physical processes such as gravitational collapse, though they shed little light on the nature or properties of the singularities produced. They rely on assumptions about the nature of the matter and energy in question and the nature of the spacetime. These theorems can be used to show that singularities do in fact exist within the event horizons.

2.2.6 Conical singularities

A key feature of what follows is called a conical singularity. These are singular spacetimes despite having no bad behaviour of the curvature tensor. Below is a simple example in 2+1 dimensions but we will later discuss the possibility of conical singularities in higher dimensions and also the possibility of replacing the singular tip and so recovering a smooth, non singular manifold. A key point for our following work is that the way we replace the tip, and so the resulting non-singular manifold may not be unique, alternative resolutions with differing topologies may be acceptable.

e.g. radial cone

The three dimensional Minkowski metric can be written in radial coordinates as

$$ds^2 = -dt^2 + dr^2 + r^2\, d\theta^2 :\ 0 < r < \infty :\ 0 < \theta < 2\pi. \tag{2.5}$$

However we can change this space by redefining the range of θ, making it less than a new value $\theta_0 < 2\pi$, this has the effect of removing a wedge from the space at the origin, we also need to exclude the origin itself from the spacetime, it is now a conical singularity

$$ds^2 = -dt^2 + dr^2 + r^2\, d\theta^2 :\ 0 < r < \infty :\ 0 < \theta < \theta_0 < 2\pi. \tag{2.6}$$

This process has left the local metric unchanged (meaning the curvature tensor still vanishes everywhere) however the spacetime is now singular. The spacetime takes the form of a cone, with a singular point at the top but being flat and smooth everywhere else.

2.2.7 Cosmic censorship

This conjecture claims that any singularity cannot be observed due to a surrounding event horizon[4], a singularity without any horizon is called a naked singularity and such an artifact will be excluded if this conjecture holds. Such a naked singularity would be observable from the outside and even the possibility of its existence would cause determinism to fail (the future evolution of spacetime could not be determined from the current state). The circumstances under which this conjecture holds is still an open question.

2.3 Black hole spacetime solutions

Black hole spacetimes have been proposed as early as the 18th century[20], using only Newton's laws of gravitation. The black hole had a gravitational field so strong that light could not escape making them totally dark. Modern day black holes are even more ominous since the inescapable trap caused by their gravity extends to all objects and

not just to light. We can say that a spacetime contains a black hole if there are events which are not within the causal history of the future null infinity, they are behind an event horizon. So if a spacetime contains an event horizon of section 2.2.1 then it is a black hole solution (by extension if a spacetime contains an apparent horizon of section 2.2.2 then it must contain an event horizon and so it too is a black hole solution). The presence of this event horizon means that events behind it are completely hidden from the outside and so cannot be observed or influence outside events.

2.3.1 Black hole properties

The event horizon of the black hole has a defined area which allows us to think of the black hole having a size even if we never define or use a metric within its interior. The area of the event horizon is shown to never decrease, even if multiple black holes merge then the sum of all the areas must increase[21]. Alongside the discovery that black holes are not perfectly black and radiate, the area of the event horizon has been associated with the entropy of the black hole, partially due to the lack of a way to decrease it within general relativity (without the introduction of quantum processes) which is analogous to the second law of thermodynamics[21].

The black hole also has a defined energy (closely linked to the mass, M) which by energy conservation must match the energy used to form the black hole. One method of defining the energy of a whole spacetime which is asymptotically flat was given by Arnowitt, Deser and Misner and is appropriately called the ADM energy[22, 23]. Another definition of energy for asymptotically AdS spacetime was presented by Abbott and Deser[24] though other measures of the energy exist such as the Bondi energy[4]. An important measure of energy for us is the gravitational Hamiltonian, which can be applied to spacetimes which are not asymptotically flat, it also allows there to be horizons within the spacetime (though it implies that the spacetime inside continues to evolve just as the outside does). This Hamiltonian agrees with the ADM energy or that of Abbott and Deser, in the appropriate circumstances[25]. This Hamiltonian compares the action of the spacetime to the action of some stationary background and takes this difference to be the spacetime's Hamiltonian.

The surface gravity of the black hole tells us the effect upon the energy which a small

change in area will have, since we treat the area like an entropy we can compare this value to the temperature of thermodynamics. This comparison seems to hold since the surface gravity is proportional to the Hawking temperature, the surface gravity is constant over a stationary black hole horizon (just as the temperature is constant within a state of thermal equilibrium) and the surface gravity cannot be reduced to zero by physical processes (just like the temperature of thermodynamics).

In Einstein Maxwell theory the black hole will also have a charge which directly gives the electric field outside the black hole. The charge along with the mass and any rotation uniquely define any stationary black hole in 4d Einstein Maxwell theory.

2.3.2 Black hole uniqueness

Just as a 4d stationary black hole with charge, mass and rotation is unique. This has been called the no-hair theorem and it means we can limit the possible stationary black hole solutions which could result from any classical simulation. This uniqueness sometimes extends to higher dimensions also. A common result in the following simulations is the formation of a black hole solution which then tends to a stationary black hole solution, in one of these cases in section 3.7 we identify the result to be a unique black hole.

2.3.3 Black hole effects

The principal effect of the black hole is the enclosure of events within it. Events in string theory have been envisaged which could be both incredible to see and used to add weight to the claims of string theory, of note are topology changing transitions or brane collisions. If we believe that some fascinating event of general relativity, supergravity or even string theory has happened we must also check that it can have some effect on the outside observer, us. If the events are totally hidden behind an event horizon and cannot be seen then they cannot be an influence upon the universe which we would wish to describe, giving no predictions or observable effects.

2.3.4 Black hole evaporation

Classical black holes have an area which (like the entropy of thermodynamics) can never shrink and so black holes will always be there once they have been created, however with the inclusion of quantum mechanical effects there has been the suggestion that the black holes will radiate while at the same time reducing in mass and in area. If the black hole continues to radiate faster than it acquires new mass it will eventually reach a very small size and go on to vanish completely leaving behind either a common background such as a Minkowski spacetime or possibly some relic, this is called its evaporation.

2.4 Cauchy problems

We intend to find the future evolution of a spacetime to see the unavoidable effects of changes we make. These simulations are commonly referred to as Cauchy problems, they involve taking some $d-1$ dimensional spacelike timeslice, the Cauchy surface or initial surface, and proceeding to use the Einstein equations to construct a sequence of subsequent spacelike hypersurfaces and inferring from these the d dimensional spacetime. A fundamental difference from other numerical simulations is that the system we evolve is not defined at a position in space and at a time, it is the space and the time! Simulations in general relativity have great freedom in the choice of coordinate system, extending even to a choice of what time will be. This all comes from the tensor nature of the Einstein equations and from the equivalence principle itself. The initial surface we will start with can be described in any coordinate system and distances between the points of this system can (and will) change throughout the course of the dynamical simulation.

As we choose the time coordinate we have to choose both a lapse α and a shift β^μ[26, 27, 23]. These are determined by our choice of normal to the timeslice n^μ,

$$n^\mu = -\alpha \nabla^\mu t \tag{2.7}$$

$$\beta^\mu = t^\mu - \alpha n^\mu. \tag{2.8}$$

The lapse α describes the proper time separating timeslices as viewed by observers

moving only along the time direction (it will very likely differ across the spacetime). A large lapse means that fewer timesteps are needed to evolve to late times. A small lapse increases time resolution and makes for a more accurate program. The shift β^μ allows the spatial coordinates to alter as time evolves and allow changes to the nature of a timeslice. Choices of lapse and shift do not change the physical results, they represent the coordinate freedom of the late time evolution, however changing them must be accompanied by a change to any initial momenta in order to keep the same physical system, changing them leads to a new time coordinate and so an alteration to the momentum. Choosing the best slicing can improve the efficiency, stability and the accuracy and there are a range of suggested possibilities[27].

2.4.1 Moduli space approximation

It is possible to predict the outcome of some features of the spacetime evolution before resorting to a full numerical investigation using methods such as those suggested for BPS monopoles in [28]. These give existing parameters time dependence and use the Lagrangian to find equations of motion for just these few parameters, this is a low energy approximation as it does not permit the full evolution of spacetime, keeping many features and profiles constant which would otherwise change. While these approximations are good only for low energies and may become invalid after a short time period they can be used to predict the evolution of a feature of the spacetime which would otherwise be considered static. Such features may include the motion of monopole configurations, the evolution of a topological defect or the changing size of a cycle in a spacetime. These methods can be used to predict the evolution of key features of the string compactification such as the moduli of the vacuum manifold, predicting whether they will be stable against small additions of momentum.

2.4.2 Numerical Simulations

In order to study the evolution of the spacetime beyond the low energy analytic approximations we need to permit all the functions which define the metric to evolve and not just some of the parameters which define the static case. This usually requires a nu-

merical simulation due to the number of inseparable second order differential equations needed to satisfy the Einstein equations. These simulations can be made applicable to higher energy initial momentum and go on to late times beyond the approximations. The numerical simulations often allow new features to arise which are not permitted in moduli space approximations, an example would be a static case which never has an event horizon regardless of the values of the parameters there could however be a horizon in the numerical simulation as the lack of one is an artificial effect coming from the restricted evolution. Methods for numerical simulation vary so we must choose wisely to best evolve our spacetime.

2.4.2.1 ADM simulations

In order to simulate the evolution of spacetime numerically we needed to select a good system of coordinates and make good gauge choices. We followed well established (but not unique) techniques used for Cauchy formulations of numerical relativity commonly call an ADM formulation. Previously they have been used primarily for four dimensional spacetimes however we applied these techniques to our higher dimensional simulations, taking advantage of the symmetries. We selected some of the less complicated methods and algorithms of numerical simulation and elaborated on these as necessary to form a resultant program both stable and accurate. In addition to the numerical algorithms used to evolve the system we had to select both initial conditions and boundary conditions on both inner and outer boundaries.

2.4.2.2 Inner boundaries

These pose potentially catastrophic problems for numerical relativity, singularities which will form in black hole spacetimes bring infinite terms which cannot be dealt with by the simulation. Possible ways to deal with this include using a slicing which freezes the origin, not evolving it, however this will not work for extended periods of time. Alternatively it is possible to apply cosmic censorship of section 2.2.7 to argue that the singularity is hidden behind an event horizon, it will not affect the outside and so we can remove it from the region simulated. This however requires a knowledge of the event horizon which may not be available at the time, or the use of an apparent

horizon (if it exists) and the difficulties of a moving boundary or boundaries which only appear at later times. Luckily many of our own simulations did not start with singularities, and formed them well after the apparent horizon had already formed. This was sufficient to produce our results because by the time the singularity ended the simulation we already knew that there was a horizon and we could also already make a good estimate of its final area.

2.4.2.3 Outer boundaries

While the time slices of the spacetime extend all the way to the spacelike infinity i^0, it is almost essential to select only a small region to simulate, severing all space outside from the simulation. This region should be large enough that the outer effects do not change the results. This artificial outer boundary brings other problems however as outgoing waves can be reflected from it or grow to high frequencies causing instabilities. We tried to avoid problems by moving this surface far from the area of interest and selecting initial momenta which decayed asymptotically reducing the effects and possible instabilities at this distance from the origin.

2.4.2.4 Runge Kutta method

Given that we wish to evolve a system using a first order differential equation

$$\frac{d}{dt}y = f\left(t, y\right), \tag{2.9}$$

we would wish to use methods of higher order than the simple Euler method, both for their increased accuracy and the better stability. It is preferable to use a fourth order Runge Kutta method[29], which involves making a small trial step to a position half way through the actual step, calculating the derivative at this point and then using this approximation to the derivative as we attempt to progress a step in time. In order to progress a distance of Δt from step n to $n+1$ using the fourth order Runge Kutta method we first find the derivative at the current timestep.

$$k_1 = \Delta t \; f(t_n, y_n) \tag{2.10}$$

Using this we approximate the value of the derivative at a point half way between the current point and the next one, we then improve upon it.

$$k_2 = \Delta t \; f(t_n + \frac{\Delta t}{2}, y_n + \frac{k_1}{2}), \tag{2.11}$$

$$k_3 = \Delta t \; f(t_n + \frac{\Delta t}{2}, y_n + \frac{k_2}{2}). \tag{2.12}$$

We then make an approximation about the derivative at the point we are heading for

$$k_4 = \Delta t \; f(t_n + \Delta t, y_n + k_3). \tag{2.13}$$

Knowing that none of these approximations shall be perfect, we use all four as we progress to the next timestep

$$y_{n+1} = y_n + \frac{k_1 + 2k_2 + 2k_3 + k_4}{6}. \tag{2.14}$$

In this way we treat each timestep in the same manner and ignore all the prior behaviour as we propagate, it is a fourth order method, generally superior to a first or second order method, and adequate for our time evolution purposes.

2.4.2.5 Adams-Bashforth-Moulton method

An alternative to the Runge Kutta method, this algorithm involves storing information about the past evolution for use as we progress to a new timestep. The act of storing earlier information makes this a multistep method[29, 30], the function and its derivative from multiple timesteps are required to progress to the future. The Runge Kutta method uses only the information upon this timestep y_n to find the next y_{n+1}, by storing previous information about the derivatives at earlier timesteps f_{n-1}, f_{n-2} and f_{n-3}, we can reach fourth order without estimations regarding a trial step to a midpoint. This requires less computation at any one timestep but more information to be stored and used at later times. The method begins with a predictor step and is later refined by a corrector step. The predictor calculation is found using the fourth order Adams-Bashforth algorithm,

$$y_{n+1}^{predictor} = y_n + \frac{\Delta t}{24}\left(55 f_n - 59 f_{n-1} + 37 f_{n-2} - 9 f_{n-3}\right). \tag{2.15}$$

The corrector step uses this prediction to refine our final timestep using the Adams-Moulton method

$$f_{n+1} = f(t_{n+1}, y_{n+1}^{predictor}), \tag{2.16}$$

$$y_{n+1}^{corrector} = y_n + \frac{\Delta t}{24}\left(9f_{n+1} + 19f_n - 5f_{n-1} + f_{n-2}\right). \tag{2.17}$$

The predictor equation is an explicit one (y_{n+1} appears only on the left hand side) whereas the corrector equation is implicit, by combining both of these we formed a predictor-corrector algorithm.

We tended to find that this method was faster than, but could not run for as long as, the Runge Kutta method.

2.5 Supersymmetry

This suggestion came about by attempts to combine additional internal symmetry with the existing theories. People wanted a group which would combine with the Poincare group (including translations, rotations and boosts) leading to non trivial physics. Non were found and a theorem was later introduced by Colemann and Mandula [31] which used a small number of assumptions regarding the S-matrix, a nondegenerate vacuum and the spectrum of particles to show that no symmetry was possible within the context of Lie groups. A different type of symmetry was later suggested, this theory bypassed the earlier proof by expanding the Lie group concept[32] to include generators Q_α^i which obey anticommutation relations, the anti-commutator of two generators being defined as:

$$\{Q_\alpha^i, Q_\beta^j\} = Q_\alpha^i\, Q_\beta^j + Q_\beta^j\, Q_\alpha^i. \tag{2.18}$$

The exact algebra is not necessary here but can be found in many books on the topic such as [33, 34]. The supersymmetric charges will transform as spinors under Lorentz group transformations (leading to the subscript α), there may be more than one such spinor (described by the index i). The number of spinors can be 1,2,4 or 8, described by N=1,N=2,N=4 or N=8 supersymmetry (N higher than eight brings problems in the form of at least one particle with spin higher than two). Limiting N to eight also limits

the number of dimensions to eleven[5]. This choice in the number of spinors along with other choices lead to a whole range of supersymmetric theories and models.

2.5.1 Properties and predictions

The existence of supersymmetry has immediate implications for the possible particles, acting with the supersymmetry generators mixes particles of different spin, it acts to mix bosons and fermions. It forces each fermionic particle to have a bosonic supersymmetric partner with a different spin but the same mass (also each boson must have a fermion particle). These particles could include a heavy particle which is stable, this particle would be a candidate for dark matter.

The additional particles predicted by supersymmetry help the hierarchy problem of the Higgs mass. Field theory predicts the size of the Higgs mass to fall at about the Planck scale, this is due to the very large contributions by quantum mechanical interactions. These large radiative corrections are reduced by the introduction of supersymmetry as the supersymmetric particles cancel the interactions and reduce the mass contribution. This predicts a Higgs mass around the scale of supersymmetry breaking, this may be much smaller than the Planck scale and so preferable in view of experiment.

One benefit comes to those hoping to unify both the nuclear forces to the electromagnetic force into a grand unified force. The gauge couplings of these forces would be expected to meet at a common energy scale, the scale at which GUT is broken, however by looking at the running of these coupling constants this does not seem to be the case. If we add the minimal supersymmetry to the standard model (MSSM, minimal supersymmetric standard model) then the coupling come a lot closer to meeting at a common energy scale, giving increased strength to the existence of a GUT theory.

The failure to observe any such partner particles (or even particles with masses close to those predicted) shows that any manifest supersymmetry must be a broken symmetry. However breaking the symmetry threatens its predictive power and risks jeopardising all the potential benefits supersymmetry brings.

2.6 Supergravity and superstrings

If we promote supersymmetry to a local symmetry, while also including general relativity we form a theory of supergravity. These theories can exist with different numbers of supersymmetries (N) and in various dimensional spacetimes. If we wish to avoid particles with a spin greater than two we must limit the number of dimensions to eleven and N is limited to eight. These supergravity theories can be formed by taking the effective action at the low energy limit of some other theory such as a superstring theory. Using different superstring theories at the start will result in supergravity theories with different fields. We will discuss a few of these in passing but elaborate further on type IIB string theory since this supergravity theory will be used as an effective Lagrangian later in our simulations. Initial formulations of string theory were not supersymmetric and included only a bosonic sector. These were later supplemented with fermionic fields in order to create a superstring theory. The strings produce a range of fields depending upon the state and boundary conditions which the individual string adopts. One of these fields being the spin-two massless particle we see as a graviton (the quantum boson of the gravitational force). Some of the fields need to be censored by means of a GSO projection [35], primarily to remove a tachyon. Potential theories are in general hindered by the possibility of gravitational anomalies and divergences, if we attempt to add Yang-Mills fields we can also generate gauge anomalies/divergences in the gauge currents. There are five superstring theories which seem to avoid these anomalies which differ on the details of the strings. From each of these strings we can take a low energy limit to find a supergravity or we can begin with the supergravity at the start. The field theory which exhibits Poincare invariance while also having the greatest collection of supersymmetry is eleven dimensional supergravity.

2.6.1 11d supergravity

Eleven dimensional supergravity has features which make it popular to work with, we know of a classical action which may be used to describe it [36] and it had possible explanations for the four dimensions we can see [37]. It has been studied in the past and even considered as a theory of everything for a while, however supergravity alone

could not be the full theory of everything due to problems with nonrenormalisability and a high cosmological constant, though it is still thought of as a good low energy approximation. Supergravity was later complemented by studying a ten dimensional theory which had superstrings in it.

2.6.2 IIA superstrings

If we restrict ourselves to only closed strings then we get type II string theories. These have the maximal amount of supersymmetry, the full 32 supercharges. One result of the supersymmetry are two fermionic partners to the graviton, called gravitinos these are massless. One of these theories, designated IIA, has a non-chiral spectrum, i.e. it is left-right symmetric. If we take the low energy limit then we are left with the content of massless particles in the form of IIA supergravity.

2.6.2.1 IIA supergravity

If we take the low energy effective field theory of the type IIA superstring we arrive at a theory including gravity and some fields. This massless content is determined primarily by the large amount of supersymmetry.

It was noted that unexpectedly the dimensional reduction of the eleven dimensional supergravity to ten dimensional supergravity gives the same massless content[38]. Both methods produce the same action containing a ten dimensional spacetime metric, a scalar which we call the dilaton, an antisymmetric tensor, a one-form and a three-form flux. It is later considered that this is not a coincidence and hints at a deeper connection between the two.

2.6.2.2 Massive IIA supergravity

We can generalise the IIA supergravity theory at the expense of losing its simple connection to eleven dimensional supergravity by including an additional field, a ten-form field (to complete the 2,4,6 and 8 pattern of even fields)[5]. The equation of motion means that this field must be a constant, with no propagating degrees of freedom, but

it can still contribute an energy density and so have physical implications. This field does indeed result from the IIA superstring.

2.6.3 IIB superstrings

We can introduce chirality as we form our closed string theory by a different choice when we carry out the GSO projection. This results in that the two gravitinos have the same chirality and an asymmetry between left handed and right handedness. This theory is free of gravitational anomalies since all anomalies cancel in the low-energy supergravity approximation.

2.6.3.1 IIB supergravity

If we take the low energy limit of IIB superstring theory we arrive at a theory of supergravity. This theory of ten dimensional supergravity is not obtainable directly by compactifying some eleven dimensional theory, it shows the massless content of the IIB superstrings. This spectrum includes the graviton, a dilaton ϕ, another scalar C_0, 2 antisymmetric two-forms B and C_2 and a four-form C_4. We write the Lagrangian for IIB supergravity in the Einstein frame as follows[39, 5],

$$\begin{aligned}\mathcal{L}_{10}^{IIB} = \quad & R * \mathbb{I} + \frac{1}{2} d\phi \wedge *d\phi - \frac{1}{2} e^{2\phi} F_1 \wedge *F_1 - \frac{1}{4} F_5 \wedge *F_5 \\ & - \frac{1}{2} e^{-\phi} H \wedge *H - \frac{1}{2} e^{\phi} F_3 \wedge *F_3 - \frac{1}{2} C_4 \wedge H \wedge F_3, \end{aligned} \tag{2.19}$$

where the fields comprise[40] our dilaton ϕ, an axion F_1, an NS-NS three-form field H, an R-R three-form field F_3 and a self dual five-form field strength F_5. These are linked to the potentials via,

$$F_1 = dC_0 \tag{2.20}$$

$$F_3 = dC_2 - C_0\, dB \tag{2.21}$$

$$F_5 = dC_4 + \frac{1}{2} B \wedge dC_2 - \frac{1}{2} C_2 \wedge dB \tag{2.22}$$

$$H = dB. \tag{2.23}$$

There is a great deal of gauge freedom there, even though the four potential, C_4, appears in the Chern-Simons term of the Lagrangian this term is still gauge invariant. We

need to separately impose the self duality condition upon F_5 by hand, as it is unconstrained by the Lagrangian

$$F_5 = *F_5, \tag{2.24}$$

we need to impose this at the level of the equations of motion, not at the level of the Lagrangian or else the kinetic term of F_5 vanishes trivially. The Lagrangian does however give all the other equations of motion for these fields:

$$\begin{aligned}
d(*F_5) &= -F_3 \wedge H && (2.25)\\
d(e^{\phi} * F_3) &= F_5 \wedge H && (2.26)\\
d(e^{2\phi} * F_1) &= e^{\phi} * F_3 \wedge H && (2.27)\\
d(e^{-\phi} * H) &= e^{\phi} F_1 \wedge *F_3 - F_5 \wedge F_3 && (2.28)\\
d * d\phi &= -e^{2\phi} * F_1 \wedge F_1 - \frac{1}{2} e^{\phi} * F_3 \wedge F_3 + \frac{1}{2} e^{-\phi} * H \wedge H && (2.29)
\end{aligned}$$

The fluxes also contribute to the energy momentum tensor, which means that our spacetime will not be Ricci flat but will obey the Einstein equation with the Einstein tensor (B.15) [41],

$$\begin{aligned}
G^{ab} &= T^{ab}, && (2.30)\\
T^{ab} &= \frac{1}{\sqrt{-g}} \frac{\partial \mathcal{L}}{\partial g_{ab}}. && (2.31)
\end{aligned}$$

Leading to the equation of motion (written in terms of fluxes),

$$\begin{aligned}
R_{MN} &= \frac{1}{2}\partial_M \phi \, \partial_N \phi + \frac{1}{2} e^{2\phi} F_{(1)\ M} F_{(1)\ N} + \frac{1}{96} F_{(5)\ M}{}^{abcd} F_{(5)\ Nabcd} \\
&\quad + \frac{1}{4} e^{+\phi} \left(F_{(3)\ M}{}^{ab} F_{(3)\ Nab} - \frac{1}{12} F_{(3)}{}^2 g_{MN} \right) \\
&\quad + \frac{1}{4} e^{-\phi} \left(H_{\ M}{}^{ab} H_{\ Nab} - \frac{1}{12} H^2 g_{MN} \right). && (2.32)
\end{aligned}$$

2.6.4 Other string theories

In addition to type II string theory there are an additional three theories involving strings which are just as important, they include open strings and the fascinating heterotic strings.

2.6.4.1 I superstrings

If we also add open strings to the theory then we get a type I theory, it involves introducing gauge groups in the form of quantum numbers associated with the string ends. This theory has $N = 1$ supersymmetry and the gauge group is $SO(32)$, it turns out to be finite and free of anomalies[42]. It has the advantage of specifying the gauge group to uniquely be $SO(32)$, this group is sufficiently large to yield sufficient low energy gauge groups upon compactification, along with massless fermionic generators. The fact that this superstring theory contains gauge fields and is also chiral makes it appealing to study. The anomaly cancellation is a result of the group $SO(32)$ and the same theoretical properties are shared by another group, $E8$x$E8$. The gauge group $E8$x$E8$ can not be used in the setting of open strings however since it can not be formed by the method of adding quantum numbers to string ends. Both of these gauge groups can however be exploited in heterotic strings.

2.6.4.2 Heterotic superstrings

Heterotic strings[43, 44, 45] take advantage of the independent nature of the left handed and right handed components. The two can be treated asymmetrically provided each sector is internally consistent. The difference can extend even to the number of degrees of freedom they experience and the nature of the movers. The left movers and the right movers act as though they were in different dimensions, one (usually the right-movers) being those of the ten dimensional fermionic string but the other from the twenty six dimensional bosonic theory, it has some strengths from both. This theory is free of tachyons but in order to avoid possible gravitational or gauge anomalies we must carefully choose how to compactify the additional sixteen dimensions of the bosonic coordinates, this compactification is performed upon a sixteen dimensional torus and allows us to form either the $SO(32)$ or the $E8$x$E8$ gauge groups. The low energy limit of these strings is always an $N = 2$ ten dimensional supergravity but there are two different Yang-Mills gauge groups which can result from the low energy limit, $SO(32)$ and $E8$x$E8$. These theories (mostly the $E8$x$E8$ one) offer the solutions which most closely resemble the standard model, creating a lot of interest in the way the remaining ten dimensions may be compactified.

2.6.5 D-branes

A further object which can be added to complement string theory is a D-brane. D-branes initially acted as a surface upon which open strings could end[6], forcing the string end to stay on the brane is equivalent to imposing Dirichet boundary conditions upon the endpoint leading to the title D-brane. The possibilities for strings are increased by these branes, they can still differ in vibrational modes and they can also differ in their attachment to branes, leading to a very rich variety of particles. D-branes themselves are also dynamical and evolve according to their own action (Dirac-Born-Infeld action). D-branes are classified by their dimension, leading to titles such as ”D3-brane”, a brane occupying three dimensions.

The existence, position and state of the D-branes will be crucial in determining the possibilities of particles. The particles arise from the state of the strings and the string states will be dependent upon the branes. If two branes are separated by some distance then there is the possibility of a string stretched between the two. This string has a minimum length (the distance between the branes), the tension of the string means this length corresponds to a minimum energy and the relativistic nature of the energy means this leads to a minimum mass. The distant placement of the branes has led to a massive particle. D-branes will also act to break some supersymmetry, the extent of supersymmetry breaking will depend on the branes, their placement and also their mutual intersections. This can be useful in obtaining theories with reduced supersymmetry and can also restrict our brane placement if we want to preserve some of the supersymmetry. It is common to wish to break most of the supersymmetry leaving only N=1 supersymmetry, this allows us to retain all the advantages of supersymmetry.

Just as the presence of a charged particle will contribute as a source of the electric field so Dp-branes can act as the elementary charge of the p-form Ramond-Ramond fields and will contribute as a source to these fields[7].

2.6.6 Unifying superstring theories and supergravity

The observation that the IIA low-energy action can be obtained by compactifying one dimension of eleven dimensional supergravity leads us to believe there could be a more

fundamental reason for this, maybe these theories are more deeply connected.

Just as there is a duality between IIA string theory and supergravity, there are also dualities which connect the string theories to each other. So called S-duality (also called a strong-weak duality) links a type I string theory with strong coupling to the SO(32) heterotic string theory where the coupling is weak (or vise versa). S-duality also duals type IIB superstring theory to itself with a different coupling. T-dualities dual type II supergravities to each other and heterotic supergravities to each other, they work by changing the internal manifold we compactify upon when we reduce to lower dimensions in the following chapters.

In these ways all the string theories are now thought of to be unified as possible ways to reduce some ”M theory” which is eleven dimensional and contains membranes, the higher generalisation of strings. This higher dimensional theory must also have a low energy limit matching eleven dimensional supergravity. Even if string theories are already the dimensionally compacted form of a higher dimensional theory, further compactification will be needed to reach the four dimensional physical world, we need to compactify another six of the dimensions.

2.7 Compactifications

For any string theories to be applicable to our own universe they need to be seen by us as our own 3+1 dimensional spacetime[46]. This requires that the additional six dimensions go unobserved, this is possibly due to their small size as a compact six dimensional manifold. The idea of extra dimensions which are unseen due to their small compact size, was presented as early as 1919. Then it was found that compactification was capable of unifying the electromagnetic theory with gravity as a five dimensional theory. If we compactify a five dimensional metric by making one dimension (x^4) periodic,

$$x^4 \tilde{=} x^4 + 2\pi R \tag{2.33}$$

we can split the metric to a 4 dimensional metric (general relativity is still seen upon the remaining four dimensions), a scalar (g_{55}) and a vector (g_{a5}). This has changed the

theory involving only gravity to be seen as a theory with a vector and a scalar field, this has massless modes which act like electromagnetism and gravity coupled together in four dimensions.

The possibility of compactifying dimensions so as to reduce the observational dimension of the spacetime while at the same time introducing new fields to the theory is a useful tool in string theory as it allows the extra dimensions of string theory to have gone unnoticed. The manifolds we could compactify upon can vary in their sizes and also their topologies. This manifold's topology would then be responsible for the number of generations of particles we see and also other quantum numbers, though the gauge field on the manifold (such as $E8$x$E8$) would also contribute some quantum numbers of its own. This gives great incentive for us to find the nature and topology of this internal manifold and so hopefully explain some observations of physics and make some predictions with string theory.

When we perform the compactification there is the potential to break all the supersymmetry and so lose all the useful benefits we observe in section 2.5. We would want at least N=1 supersymmetry to still be observed after we perform the compactification.

Our compactification should arrive at a spacetime with four extended dimensions and a six dimensional compact manifold called the internal manifold. We would hope to arrive at a vacuum with the maximal amount of space-time symmetry in the four dimensions which are not compact, this means the extended dimensions form either a Minkowski metric (with Poincare invariance), de Sitter(with $SO(2,3)$ invariance) or anti-de Sitter (with $SO(1,4)$ invariance). The maximal symmetry also means that the vacuum expectation for all the fermionic fields should vanish and the bosonic fluxes should be comprised of only internal forms or four-forms of the non-compact spacetime (which is the hypervolume and treats all the extended dimensions equally).

2.7.1 Flux free compactification

If no fluxes are present then demanding some remaining supersymmetry and also keeping maximal 4D spacetime symmetry means that there must exist a covariantly constant spinor[47, 11] (this comes from the requirement that the gravitino must have

vanishing expectation value).

The existence of the covariantly constant spinor is a strong statement with topological and differential implications for the choice of manifold. This imposes a restraint upon the possible internal manifolds we can select, it in fact restricts our choice to a manifold with $SU(3)$ holonomy. It also means that there is a real two-form J which can act as an almost complex structure and a complex (3,0) form Ω making them complex manifolds. This means that the manifold is a Calabi-Yau manifold of section 2.1.5 which we already know can be given a Ricci flat metric (even though we generally do not know the metric explicitly) and so are perfect candidates for our internal compact manifold. The covariantly constant property means that the four dimensional spacetime must be an unwarped Minkowski metric (one with a trivial scale factor). These compactifications will also preserve N=2 supersymmetry.

Calabi-Yau manifolds are not unique and there exist a large number of possible Calabi-Yau manifolds with distinct topology and so selecting one topology over others seems to be a free choice. The choice of topology will determine the observations we see about particles and so if we cannot find a preferred topology then string theory loses much of its predictive power and so cannot be used or verified by any experiment. The Calabi-Yau manifold is not even defined uniquely by its topology and there will exist infinitesimal deformations which preserve the Calabi-Yau condition. These are called the metric moduli and these give rise to light scalar fields which are unacceptable to phenomenology due to their unobserved long range effects such as the violation of the equivalence principle. Such violations have not been observed and so such fields are tightly constrained[48, 49], as such a method is introduced to prevent these fields being seen, we add expectation value to the fluxes in the compactification.

2.7.2 Flux compactifications

Adding fluxes to the six dimensional internal manifold allows for more freedom in our compactification, the fluxes lead to a non-zero energy-momentum tensor meaning that the spacetime is no longer Ricci flat and the internal manifold is not restricted to a Calabi-Yau, though there are still many restrictions due to the equations of supergravity. As we still want to maintain the maximal amount of four dimensional symmetry

we arrive at a metric of the form.

$$ds^2 = e^{2A(y)}\,\tilde{g}_{\mu,\nu}dx^\mu dx^\nu + g_{mn}dy^m dy^n \tag{2.34}$$

where μ goes from 0 to 3 and m goes from 1 to 6. $\tilde{g}_{\mu,\nu}$ must be a four dimensional metric with maximal symmetry, either Minkowski, de Sitter or anti de Sitter. The term $e^{2A(y)}$ is called the warp factor and it permits the extended four dimensional manifold to vary across the internal manifold however it cannot break the maximal symmetry of the four space and so does not break Lorentz invariance of our four dimensional observations. In order to avoid breaking all the supersymmetry we need to have supercurrents which are well defined globally which means that even with fluxes (even fluxes which may break the supersymmetry spontaneously) we still need an internal manifold $g_{mn}dy^m dy^n$ without the full $SO(6)$ holonomy group. With the addition of fluxes our internal manifold need not be a Calabi-Yau manifold but should still be a conformal Calabi-Yau manifold.

With the addition of flux to the compactified dimensions we may also solve the difficulty of moduli because the fluxes make some values of the moduli preferred by introducing a potential to the deformations of the manifold. The potential has minima which act as the vacuum and any other internal manifold would not be a static situation. In the dimensionally reduced picture the addition of fluxes works to counter the problem of light moduli fields by giving them a mass, with mass the moduli no longer act to infinite range and so can exist without violating tests of the equivalence principle.

2.7.3 String landscape

The range of possible string vacua is huge and very diverse, there is a large range of topologies which each have their own collection of continuous parameters and on top of this we can add an unimaginable variety of fluxes sourced by D-branes. This immense collection of possibilities has been dubbed the string landscape[50]. As we mentioned earlier the addition of fluxes to the range of vacua brings the advantage of a superpotential which means that local minima of this potential are the only vacua which can be stable and of these the global minima will be preferable. Without this

superpotential there would be no method of vacua selection and so no way to decide upon a good candidate (it would have to be identified by observations and so string theory would make no predictions about particle properties), with the superpotential we can isolate the preferred static vacua to predict the combinations of moduli and flux which will be preferred.

We would wish to know whether the topology also could be predicted by the superpotential. Unlike the other features defined by continuous parameters, the topology would seem to be a discontinuous choice leading to isolated islands in the string landscape. The prefered moduli can then be reached dynamically because there is a continuous path of finite length in the landscape along which the vacuum could dynamically flow in the early universe. On first impression it does not seem that there is any such path to changing the topologies. The possibility of being ”trapped” in one topology with no path to change would severely limit the predictions string theory could make.

2.8 Topology transitions

Despite the discontinuous nature of the topologies a possible method for changing the topology in time has been suggested, this method offers the possibility of finite paths between manifolds with different topology and so unifying the seemingly disjoint regions of the string landscape.

The hope comes from manifolds which possess conical singularities and singular points[51, 52, 13]. While these manifolds are usually not considered as part of the string landscape they can be reached by taking some of the moduli to their absolute limits, such as taking the moduli giving the diameter of a circle to zero. Since the moduli can be changed continuously, it is possible that the vacuum could continuously change until one of these singular manifolds is reached at the limit. Though the singular manifold can be the limit of a topology, it does not have to possess a defined topology itself, and so one singular manifold could be the limiting case of two different topologies. If this is the case then it has been suggested that the singular manifold could form the link between different topologies and allow a path in moduli space between vacua with differing topology. By continuously deforming the moduli we arrive at the singular

manifold, then we treat the singular manifold as the limit of the new topology and begin to continuously deform the new moduli to move away from the singular point and back to a defined string vacua. One way to picture these transitions between manifolds is to study the cycles within them, for example it may be that certain cycles collapse to zero size on one side of the transition and expand as different cycles on the other.

These processes differ between individual cases but the extent of the transition can be seen by looking at which topological invariants are changed by the process. A more mild form of transition is called the flop transition which will change only the intersection numbers of the topology[53], this is described in more detail in chapter 3. The most profound transitions will change the Hodge numbers, the Betti numbers and the Euler number of the topology, these are drastic changes to the vacuum and one example is the conifold transition which is discussed in the chapter 4 .

A lower dimensional analogy to this is the transition from a two dimensional surface of a sphere to the two dimensional surface of a torus (doughnut). These two closed surfaces have different topology however they share a common limit which is a manifold with a singular point which looks like a sphere so squashed that it intersects itself at one point or it can be viewed as a doughnut so fat that the hole has shrunk to a point. By passing through this ”manifold” it may be possible to pass from one topology to the other, by continuously deforming the doughnut making it fatter and fatter we can form the singular manifold, then instead of deforming the doughnut we treat this manifold as a sphere and continuously reduce the squashing of the sphere we arrive at a new topology (this process could also be reversed).

If the transition is possible it would offer a way to change the topology of the string vacuum and so to unify two disjoint regions of the string landscape. By finding a great many of these transition types, each linking two topologies, it may be possible to interconnect all the string landscape together and so circumvent the risk of getting trapped in a topology. This restores some predictive power to string theory by making it possible to move to a flux vacua more favourable, given the superpotential.

There are many reasons why this process may fail, we wish to see if they can possibly be overcome.

2.8.1 Obstacles to transitions

The clearest danger point is the moment of transition, the formation of the singular point and the moment at which the topology changes. This clear risk to the transition needs to be thoroughly assessed if any transition is to be viable. Remarkably this seemingly catastrophic event can be made regular within string theory[54] and the low energy dynamics can be studied both for flop transitions[55, 56, 57] and the more severe transitions capable of changing Hodge numbers[53, 58, 59]. This is interpreted as D-branes wrapping the cycles and making new light states appear.

Another possible danger while performing the collapse comes from the gravitational properties of the collapsing cycle, there is the risk that horizons could form as the size of the cycle reduces, this is a risk even before the singular point is reached. The appearance of a horizon would mean that the point of transition would be hidden behind the event horizon of a black hole and so would be of no consequence to the outside observer. This would mean that the low energy theory would be inapplicable and that there are risks to the transition which would go unseen in any low energy description.

It is these gravitational effects which we wish to investigate and we wish to find the risk to topology changing transitions being manifest as we include the gravitational effects. We start with a five dimensional flop transition and then move to the more severe transitions in higher dimensional situations.

Chapter 3

Five dimensional evolution

Five dimensions offer a great many more possible situations than can even be conceived in our usual four dimensions. Notably there is the possibility in five dimensions of dynamical spherical vacuum solutions. Such an evolution is not permitted in four dimensions, as is shown by Birkhoff's theorem. Previous numerical work has been performed in five dimensions[60] and we can use these techniques as we progress to the higher dimensional simulations of string theory, however first we discuss our own work in five dimensions. These five dimensional studies investigate some transitions between topologies however these are only of gravitational interest, in the later chapters we will progress to transitons possible in six dimensional compact manifolds which could be used in string theory.

3.1 Five dimensional gravitational instantons

A gravitational instanton is a collective name for some of the solutions to the classical field equations. They exist in 4 dimensions of space (no time!) and have a finite action. Within our simulations we use such instantons as a single timeslice through the (4+1) spacetime we are interested in, we use this timeslice as the initial condition which we go on to evolve to later time. Being solutions to the field equations themselves, the instantons would not evolve were some initial momentum not applied.

3.1.1 Features of gravitational instantons

The gravitational instantons alone, before we introduce a time coordinate or any momentum, exhibit interesting mathematical properties which have been named ”nuts” and ”bolts”[61]. These points are apparently singularities when the metric is written using polar coordinates and the $SU(2)$ one-forms, however they can be shown to be only coordinate singularities if the metric is changed to Cartesian coordinates. Like the coordinate singularity at the origin of the polar coordinates, the manifold is regular despite the presence of these objects. Given a metric written in terms of the $SU(2)$ forms,

$$ds^2 = d\tau^2 + a(\tau)^2\,\sigma_1^2 + b(\tau)^2\,\sigma_2^2 + c(\tau)^2\,\sigma_3^2, \tag{3.1}$$

this metric is called a Bianchi type IX metric. The metric has a ”nut” singularity at the origin ($\tau = 0$) if that, near to $\tau = 0$,

$$a^2 = b^2 = c^2 = \tau^2. \tag{3.2}$$

This singularity is the singularity of the polar coordinate system. Alternatively a metric possesses a bolt singularity if, close to $\tau = 0$

$$a^2 = b^2 = finite \qquad c^2 = \left(\frac{n}{2}\right)^2 \tau^2. \tag{3.3}$$

where n is some integer. This apparent singularity can be thought of as the coordinate singularity of an $\mathbb{R}^2$ provided the range of the angular coordinate ψ is aptly chosen. The topology of the manifold is locally $\mathbb{R}^2$xS^2 where the $\mathbb{R}^2$ shrinks to a point as $\tau \to 0$. However the S^2 two-cycle remains even at the tip of the origin.

3.2 Flop transitions

If we begin with a spacetime containing a bolt singularity and proceed to evolve it in time then it is conceivable that the size of the two-sphere could be changed dynamically and so would act like a scalar moduli. The size changing in time would be viewed in the four dimensional theory as a scalar field varying in time. It is also conceivable that the scalar could be dynamically changed to lower and lower values, even going

all the way to zero. If the value could be taken to zero we would recover the singular manifold $\mathbb{C}^2/\mathbb{Z}_2$. Having recovered the singularity at the origin it may be possible to go on to instigate a "flop transition" [55, 56, 57]. This involves the dynamical reduction of the two-cycle at the origin to zero and then blowing up another new two-cycle at the origin. This would result in the change of the topology of the spacetime, however this change is less drastic than other topology changes because it leaves the Hodge numbers unchanged and has no effect on the spectrum of massless moduli. Previous investigations involving only the moduli and their low energy dynamics[55, 56, 57] have omitted the possible gravitational effects upon the collapsing cycles. The gravitation may cause a horizon to form in the higher dimensional theory, this in turn would render the moduli investigation inapplicable and mean that the dynamics of the topology changing transition are more complicated than the low energy theory implies. In order to establish whether there is a possibility of flop transitions being carried out dynamically or whether the creation of black holes with horizons is inevitable, we must carry out analytical approximations and numerical simulations upon individual instantons.

3.3 The Eguchi-Hanson instanton

One particular instanton of great interest to us is the Eguchi-Hanson instanton. This instanton is spherically symmetric in 4 dimensions of space. Its metric is a regular self-dual, hyper-Kähler metric in four-dimensions and has the asymptotic structure of $\mathbb{C}^2/\mathbb{Z}_2$ [62, 63], i.e. it is a resolution of the $\mathbb{C}^2/\mathbb{Z}_2$ conical singularity. It is constructed as a cohomogeneity-one metric with squashed three-spheres as the level surfaces and has the explicit form

$$ds^2_{EH}(l) = \alpha(\rho)^{-1}\, d\rho^2 + \frac{1}{4}\rho^2 \left[(\sigma_1^2 + \sigma_2^2) + \alpha(\rho)\sigma_3^2\right], \tag{3.4}$$

$$\alpha(\rho) = 1 - \left(\frac{l}{\rho}\right)^4. \tag{3.5}$$

We have used the conventional left-invariant one-forms of $SU(2)$ which satisfy (B.18) and the parameter l is a constant parameter i.e. a modulus of the solution. From the above form of the metric we see that there is an apparent singularity at $\rho = l$, we get

a clearer understanding of its nature if we look close to this region using the following coordinates,

$$\rho = l + \frac{R^2}{l}. \tag{3.6}$$

This results in the metric taking the form

$$ds^2|_{R\to 0} \to \left[dR^2 + R^2\sigma_3^2\right] + \frac{l^2}{4}(\sigma_1^2 + \sigma_2^2), \tag{3.7}$$

which clearly shows that the apparent singularity at $R = 0$ ($\rho = l$) is just a coordinate artefact, and that the manifold looks locally like a product of flat space and a two-sphere of radius $l/2$; this type of removable singularity is a bolt singularity (3.3). It is the finite size of this two-sphere which has resolved the singularity, by taking l to zero in (3.4) we can see the metric becomes $\mathbb{C}^2/\mathbb{Z}_2$. (The $\mathbb{Z}_2$ comes from an identification required to make the origin of the resolved space regular [62].)

3.4 Dynamical evolution of the Eguchi-Hanson instanton

3.4.1 Moduli space approximation

Using a moduli space approximation as described in section 2.4.1 we can find a low energy prediction for what the dynamics of the evolution may be. This analytical approximation involves giving the moduli a small time dependence and calculating the resultant Einstein-Hilbert action. It relies on the assumption that the form of the spacetime remains as a Eguchi-Hanson instanton and only the moduli changes. By introducing a new timelike coordinate and allowing the moduli to change in time we get a new metric,

$$ds^2 = -dt^2 + \left(1 - \left(\frac{l(t)}{\rho}\right)^4\right)^{-1} d\rho^2 + \frac{1}{4}\rho^2\left[(\sigma_1^2 + \sigma_2^2) + \left(1 - \left(\frac{l(t)}{\rho}\right)^4\right)\sigma_3^2\right] \tag{3.8}$$

This metric gives the Einstein-Hilbert action to be

$$S = \int dt\, d^4x\sqrt{-g}R \tag{3.9}$$

$$= \int dt\left[\pi^2 l(t)^2\dot{l}(t)^2\right]. \tag{3.10}$$

This action shows the Lagrangian to be

$$L = \pi^2 l(t)^2 \dot{l}(t)^2. \tag{3.11}$$

This Lagrangian can be used in the Euler Lagrange equations

$$\begin{aligned} 0 &= \frac{d}{dt}\left[2\pi^2 l(t)^2 \dot{l}(t)\right] - \left[2\pi^2 l(t)\dot{l}(t)^2\right] \\ 0 &= 2l(t)\dot{l}(t)^2 + l(t)^2\ddot{l}(t) - l(t)\dot{l}(t)^2 \\ 0 &= l(t)\dot{l}(t)^2 + l(t)^2\ddot{l}(t) \\ 0 &= \frac{1}{2}\frac{d^2}{dt^2}\left[l(t)^2\right]. \end{aligned} \tag{3.12}$$

Equation (3.12) shows $l(t)^2$ is linear in time. This is a promising result, if this approximation holds true then it suggests that once an initial momentum causes the size of the two-cycle to reduce, it will continue to fall linearly, vanishing within a finite time and so giving the conical singularity needed for the flop transition. To see if this approximation holds true we must perform a numerical simulation upon a metric with more freedom to evolve in time and space and to leave the form of an Eguchi-Hanson instanton.

3.4.2 Numerical evolution of the Eguchi-Hanson instanton

In order to test the accuracy of the moduli space approximation and to establish the possibility of initiating a flop transition we must perform a numerical simulation upon a metric with the capacity to evolve freely in time[64, 65].

3.4.3 Time dependent metric

To aid the stability of the algorithm, particularly in establishing sensible boundary conditions, we require that

1. All three variables and all three momenta to remain even and finite at the origin.
2. All three variables and all three momenta to tend to finite (maybe zero) values asymptotically.

3. We minimise the amount of division by variables in all equations of motion.

To that end we evolved the following form for the metric

$$ds^2 = -dt^2 + \left[1 + 4\left(\frac{r}{l}\right)^2\right] e^{2A} dr^2 \;+\; l^2 \left[1 + \left(\frac{r}{l}\right)^4\right] e^{2B}(\sigma_1^2 + \sigma_2^2) \;+\; r^2 \left[1 + \left(\frac{r}{l}\right)^2\right] e^{2C}\sigma_3^2, \tag{3.13}$$

where

$$A = A(r,t), \tag{3.14}$$

$$B = B(r,t), \tag{3.15}$$

$$C = C(r,t). \tag{3.16}$$

In order to impose all the necessary boundary conditions at once, keeping the equations regular at the origin, we used techniques outlined in [66, 67]. This involved the introduction of three new variables D_A, D_B and D_C, to replace the spatial derivatives,

$$D_A = A' + \frac{4r}{l^2 + 4r^2}, \tag{3.17}$$

$$D_B = B' + \frac{2r^3}{l^4 + r^4}, \tag{3.18}$$

$$D_C = C' + \frac{r}{l^2 + r^2}. \tag{3.19}$$

We also introduced the momenta K_A, K_B and K_C, defined as

$$K_A = -\dot{A}, \tag{3.20}$$

$$K_B = -\dot{B}, \tag{3.21}$$

$$K_C = -\dot{C}, \tag{3.22}$$

where $\dot{}$ indicates derivative with respect to time and $'$ indicates derivative with respect to r. The D_i were chosen so as to be odd at the origin as these were simple boundary conditions to impose. Actually, the full set of boundary conditions at the origin may be found by requiring local flatness [66], in which case we find

$$A(t,r) \sim A^0(t) + \mathcal{O}(r^2), \tag{3.23}$$

$$D_A(t,r) \sim \mathcal{O}(r), \tag{3.24}$$

$$K_A(t,r) \sim K_A^0(t) + \mathcal{O}(r^2), \tag{3.25}$$

with similar relations for the functions $B(t,r)$, $C(t,r)$, $K_B(t,r)$, $K_C(t,r)$ at the origin. We also find that

$$A^0(t) = C^0(t), \quad K_A^0 = K_C^0. \tag{3.26}$$

By giving the metric functions some initial momentum the spatial part of the metric will cease to remain Eguchi-Hanson, however it will retain some Eguchi-Hanson features, at least for early times. Notably, the bolt singularity at the origin will remain, still describing a two-sphere of radius $L(t)/2$. We used the value of B at the origin to define this $L(t)$ at later times.

$$L(t) = 2\exp(B^0(t)) \tag{3.27}$$

Note that for $L(t)$ to vanish, then $B(t, r = 0)$ must diverge.

3.4.4 The Einstein equations

We found the equations of motion and the constraint equations from the Einstein-Hilbert action,

$$S = \int dt\, d^4x\sqrt{-g}R. \tag{3.28}$$

In a vacuum this action leads to the conclusion that the metric obeys the Einstein field equations

$$R_{\mu\nu} - \frac{1}{2}g_{\mu\nu}R = 0, \tag{3.29}$$

which is solved by a Ricci flat metric

$$R_{\mu\nu} = 0. \tag{3.30}$$

This set of equations can be split into three equations which describe the evolution of K_A, K_B and K_C, and a further two equations which impose additional constraints upon the system.

3.4.4.1 Constraint equations

The metric produced the following constraints, equations which the variables must always conform to. These were imposed as initial conditions and later monitored to test the program's accuracy.

If we define some new parameters

$$\begin{aligned} a^2 = &\quad \left(1 + 4\left(\tfrac{r}{l}\right)^2\right) \quad e^{(2A)} \\ b^2 = &\quad 4l^2\left(1 + \left(\tfrac{r}{l}\right)^4\right) \quad e^{(2B)} \\ c^2 = &\quad 4\,r^2\left(1 + \left(\tfrac{r}{l}\right)^2\right) \quad e^{(2C)}. \end{aligned} \tag{3.31}$$

Then the Hamiltonian constraint comes from $R_{00} = 0$ and is given by

$$\begin{aligned} 0 = &- K_A\,(2\,K_B + K_C) - K_B\,(K_B + 2\,K_C) + \frac{c^2}{b^4} - \frac{4}{b^2} \\ &+ \frac{1}{a^2}\left(-D_A\,(D_C + \frac{1}{r}) + 2\,D_B\,(D_C + \frac{1}{r}) + \frac{2\,D_C}{r}\right) \\ &+ \frac{1}{a^2}\left(-2\,D_A\,D_B + 3\,D_B^2 + 2\,D_B' + D_C' + D_C^2\right). \end{aligned} \tag{3.32}$$

Additionally the momentum constraint comes from $R_{0i} = 0$ and is

$$K_A\,(D_C + 2\,D_B + \frac{1}{r}) = 2\,K_B' + K_C' + 2\,K_B\,D_B + K_C\,(D_C + \frac{1}{r}). \tag{3.33}$$

Apparently singular terms within these constraints did not produce any instabilities as they do not feed back into the equations used to evolve the system, they were only used for testing purposes. We kept a check that the constraints remained small; typically they were of order 0.005.

3.4.4.2 Equations of motion

We found the equations of motion from the field equations using the ADM formalism [23, 68]. Also we added multiples of the momentum and Hamiltonian constraints to remove as many potentially singular terms from our equations of motion. This resulted

in the following equations of motion.

$$\begin{aligned}
\dot{A} &= -K_A \\
\dot{B} &= -K_B \\
\dot{C} &= -K_C
\end{aligned}$$

$$\begin{aligned}
\dot{K_A} &= K_A^2 - K_B^2 - 2\,K_B\,K_C + \frac{c^2}{b^4} - \frac{4}{b^2} + \frac{1}{a^2}(D_B^2 + 2\,D_B\,(D_C + \frac{1}{r})) \\
\dot{K_B} &= 2\,K_B^2 + K_B\,K_C + K_B\,K_A - \frac{2\,c^2}{b^4} + \frac{4}{b^2} \\
&\quad + \frac{1}{a^2}(D_B\,D_A - 2\,D_B^2 - D_B' - D_B\,(D_C + \frac{1}{r})) \\
\dot{K_C} &= -K_B^2 + K_C^2 - 2\,K_B\,K_A + \frac{3\,c^2}{b^4} - \frac{4}{b^2} + \frac{1}{a^2}(3\,D_B^2 - 2\,D_B\,D_A + 2\,D_B')
\end{aligned}$$

$$\begin{aligned}
\dot{D_A} &= -K_A' \\
\dot{D_B} &= -K_B' \\
\dot{D_C} &= -K_C', \qquad (3.34)
\end{aligned}$$

where a, b and c are defined in (3.31). The only potentially singular term remaining (which could have produced instabilities) is D_B/r, analytically this is regular as D_B is odd. Numerically it was sufficiently stable to allow the program to run its course.

3.4.5 Initial conditions

In the parametrisation of (3.13), using the coordinate $r = R$ of (3.6) and the Eguchi-Hanson instanton of (3.4) we find that our initial conditions for the metric functions take the form

$$\begin{aligned}
A &= \frac{1}{2}\,ln\left[4\left(\frac{r}{l}\right)^2\left(1 - \left(\frac{l^2}{l^2+r^2}\right)^4\right)^{-1}\left(1 + 4\left(\frac{r}{l}\right)^2\right)^{-1}\right] \\
B &= \frac{1}{2}\,ln\left[\frac{1}{4}\left(1 + \left(\frac{r}{l}\right)^2\right)^2\left(1 + \left(\frac{r}{l}\right)^4\right)^{-1}\right] \\
C &= \frac{1}{2}\,ln\left[\frac{1}{4r^2}\left(1 - \left(\frac{l^2}{l^2+r^2}\right)^4\right)\left(l + \frac{r^2}{l}\right)^2\left(1 + \left(\frac{r}{l}\right)^2\right)^{-1}\right].
\end{aligned} \qquad (3.35)$$

If we impose vanishing momenta then this would constitute an exact solution of the equations of motion. As a check of our numerics we do indeed find that the system remains static. As we want to evolve the Eguchi-Hanson metric toward the conical singularity we must impose some non-vanishing momentum for the metric functions.

3.4.5.1 Initial momentum

Adding the initial momentum is not a trivial task given that general relativity imposes constraints coming from the gauge fixing (section 3.4.4.1). The two constraints, Hamiltonian and momentum, mean that once $A(t=0,r)$, $B(t=0,r)$ and $C(t=0,r)$ are fixed according to (3.35) there is only one free function left to describe the momentum. To fix this function we take our motivation from the moduli space approximation of section 3.4.1 and find that initially we have

$$K_B = -\dot{B} = -\frac{\dot{L}}{l}\left(\frac{l^2 - r^2}{l^2 + r^2}\right), \tag{3.36}$$

so we are able to choose an $\dot{L}$ and derive from this K_B. We imposed that $\dot{L}$ was required to be:

1. even at the origin.
2. finite and negative at the origin.
3. vanishes far from the origin.
4. continuous and differentiable to first order.

The first condition ensures that K_B is even, the second means that we push the Eguchi-Hanson space towards the conical singularity. The third condition is imposed so that only the form near the origin is important, and that the non-compact nature of Eguchi-Hanson does not affect the evolution. The final condition gives a smooth profile for us to evolve.

Only one of the three momenta, K_B, was specified explicitly by $\dot{L}$, with the other two being derived from the constraints (3.32) and (3.33) using a 4th order Runge-Kutta algorithm.

We require a momentum which tends to zero sufficiently quickly to make the energy we introduce finite. We found that a momentum which tended to vanish as a Gaussian gave a black hole solution with an ever-increasing area. This is not a physical result as a black hole of divergent area could only be caused by a perturbation of infinite energy. The momentum needs to decay faster than a Gaussian and as such we chose an $\dot{L}$ which was exactly zero outside some radius.

We decided on an $\dot{L}$, taking the form:

$$\dot{L} = \begin{cases} -\dot{L_0}\,(1-(\frac{r}{r0})^2)^2 & r < r0 \\ 0 & r > r0 \end{cases} \tag{3.37}$$

where $\dot{L_0}$ is a positive constant (the magnitude of $\dot{L}$ at the origin) and r0 is another constant which determines the outer radius of the non-zero $\dot{L}$.

3.4.6 Results

Depending upon our input parameters, $\dot{L_0}$ and r0, there were three possible outcomes to adding the momentum:

1. For sufficiently low $\dot{L_0}$ and r0, there was insufficient initial momentum to observe the creation of either a black hole or a singular topology.

2. For an intermediate range in the parameters the system produced an apparent horizon. After initially increasing, the area of the apparent horizon converged to a constant value.

3. For large initial parameters the system already contained an apparent horizon simply due to the initial conditions.

3.4.6.1 Bouncing cycles - case 1

In the case that very little initial momentum was added to the origin, with sufficiently low $\dot{L_0}$ and r0, the evolution of the spacetime did not result in an apparent horizon and so there was the possibility of avoiding creating a black hole. In order to test the outcome of these cases we monitored the size of the two-cycle which was centred on

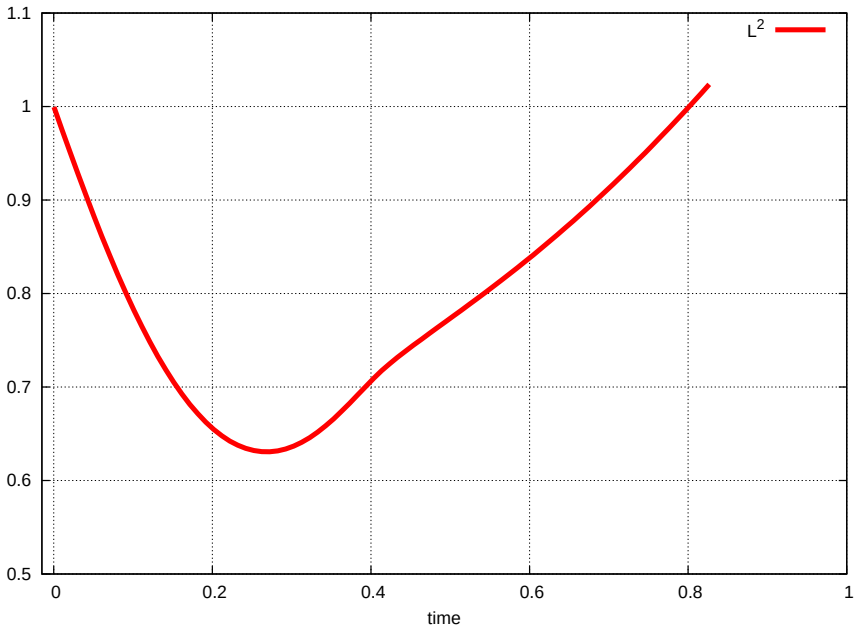

Figure 3.1: The change to the size of the two-cycle over time in a situation with no apparent horizon creation. $r0 = 0.4$, $\dot{L_0} = 1.2$

the origin. The collapse of this two-cycle to a point would indicate the production of a singular topology, having produced this manifold with a singular point it may then be possible to go on to initiate a flop transition as described in section 3.2. We plotted the size of this two-cycle against time shown in Fig. 3.1, this shows that the size of the two-cycle does begin to fall, initially looking like it could fall linearly as the approximation of section 3.4.1 predicts. However this approximation is very quickly violated and the collapse begins to slow down, in time the two-cycle ceases collapsing and begins to increase again. The area of the two-cycle is seen to rise above its starting value and continue rising. The two-cycle never falls to zero and no flop transition could ever be initiated.

3.4.6.2 Collapsing cycles - case 2

In this case a black hole forms, which was not initially present. We focus on a single example where we took $r0 = 1.0$, $\dot{L_0} = 2.3$. In Fig. 3.2 we plot the time dependence of L as measured at the origin, and also give the area of the horizon - both in units of l. What the figure shows is that L is monotonically decreasing, with L^2 decreasing approximately linearly in the initial phase. This is consistent with the expectations from the moduli space approximation of section 3.4.1. However, at some point an

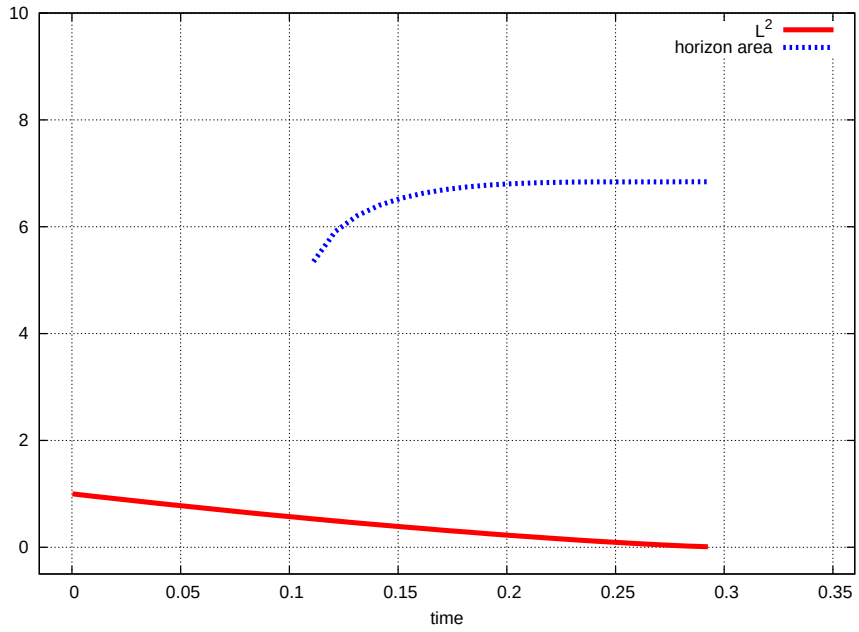

Figure 3.2: The falling area of the two-cycle and the creation and convergence of the apparent horizon. $r0 = 1.0$, $\dot{L}_0 = 2.3$

apparent horizon forms ($t \sim 0.11$ in the simulation) which then implies an event horizon exists - something the moduli space approximation does not account for. At this point we can no longer trust any low-energy dynamics derived from the moduli space approximation.

We also see from Fig. 3.2 that the area of the apparent horizon increases initially, but then settles down to a fixed value. Presumably this corresponds to the formation of what would become a static black hole; we shall discuss this further in section 3.7. The figure also shows that L, as defined at the origin, reaches zero in finite coordinate time t ($t \sim 0.3$ in the simulation). This corresponds to a divergence in the metric function $B(t, r)$ and is in fact a curvature singularity. Fortunately this is hidden behind the horizon.

In order to get a clearer understanding of the causal structure of our solution we present in Fig. 3.3 a plot showing various radial outgoing null geodesics. Superimposed on this is the curve showing the location of the apparent horizon. We see that initially the null rays continue outwards and, given the asymptotically locally flat structure of Eguchi-Hanson, reach null infinity. However, some time later the outgoing null rays near the origin turn around and head towards $r = 0$. The presence of such null rays indicates that a horizon has formed, and this is confirmed by the existence of the

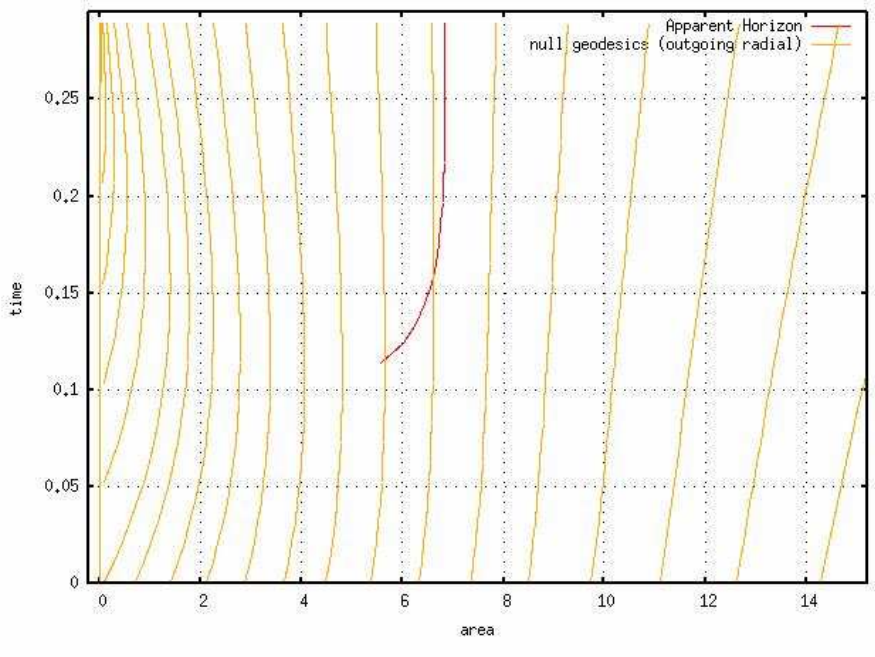

Figure 3.3: The apparent horizon and the outgoing congruence of null radial geodesics. Those behind the horizon can be seen to be trapped.

apparent horizon.

In Fig. 3.3 the apparent horizon is formed at $t \sim 1.1$ however the event horizon must have already existed before the creation of the apparent horizon. In fact all the null geodesics which are contained behind the horizon must have always been contained behind an event horizon. In the case in Fig. 3.3, the event horizon must have existed from the start of the simulation and already had an area ~ 6.5. In contrast Fig. 3.4 there is no event horizon at the start of the simulation, all the null geodesics upon the initial surface manage to escape and so are not behind any event horizon.

3.4.6.3 Results for a range of initial conditions

The black hole's area and the extent to which the angular isometry is broken (squashing) depends on the initial conditions; in our parametrisation (3.37) this means changing $\dot{L}_0$ and $r0$. A range of graphs resulting from varying $\dot{L}_0$ while keeping $r0$ constant are shown in Fig. 3.5 and the final areas are summed up in in Fig. 3.6. As we increase the value of $\dot{L}_0$ it causes the size of the two-cycle at the origin to fall more swiftly, resulting in the earlier termination of the simulation. It also results in the apparent horizon being formed earlier and converging to a higher area.

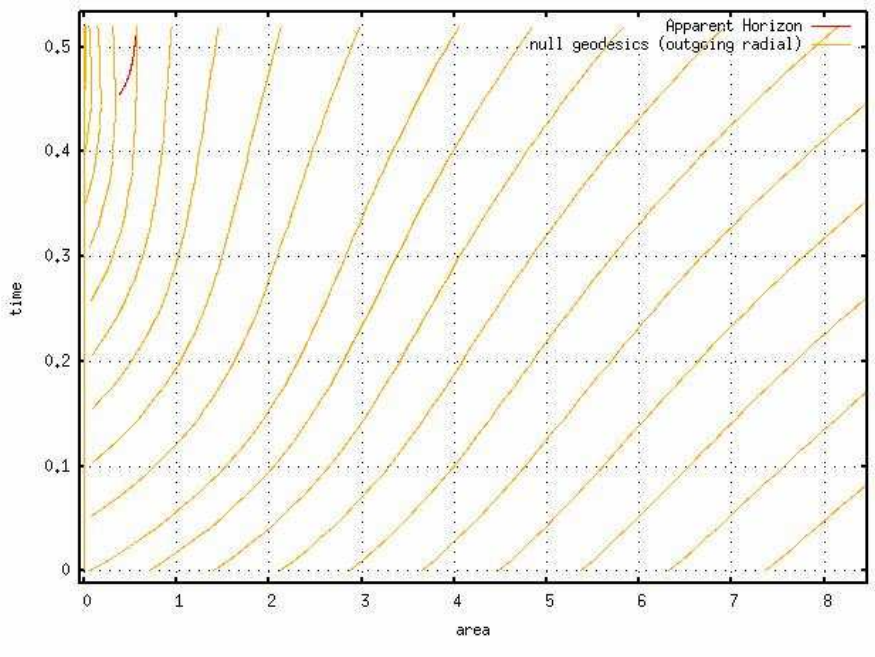

Figure 3.4: The apparent horizon and the outgoing congruence of null radial geodesics in a case where the event horizon is formed at a later time and does not exist within the initial surface

For values of $\dot{L}$ which are very small the system never produces any sort of horizon, no singularity is formed and the value of L drops for a small amount then begins to rise again, there is not enough energy to form a black hole or a singularity. Alternatively, if we take $\dot{L_0}$ to be very large then the initial data already contains an apparent horizon, rather than forming one dynamically. The results we present in Fig. 3.6 cover the intermediate range where there is enough localised energy to form a black hole, but not so much that it is there at the start of the simulation. In Fig. 3.6, where $r0 = 1.0$, the apparent horizon forms dynamically for $0.7 < \dot{L_0} < 2.8$ and its area can be seen to converge and be measured. Over the duration of the simulation the squashing parameter was seen to converge for the range $2.0 < \dot{L_0} < 2.8$, and in all these cases it converges to a value greater than 1.0. This will be seen to be consistent with the numerical squashing parameter being identified with the analytic form of k_+, given in (3.46), which must also remain greater than one at the horizon.

Alternatively we can let $r0$ vary while we keep the size of $\dot{L_0}$ fixed at 2.3, the results are given in the form of graphs shown in Fig. 3.7. Altering the value of $r0$ causes little or no change to the evolution of the two-cycle at the origin, however it does cause the apparent horizon to form at a larger radius (with a higher area) though the profile evolves and asymptotes in the same way.

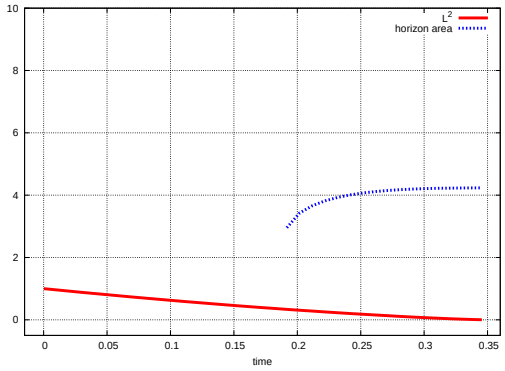

(a) $\dot{L}_0 = 2.0$

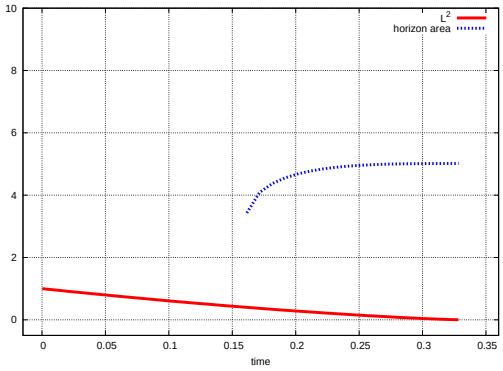

(b) $\dot{L}_0 = 2.1$

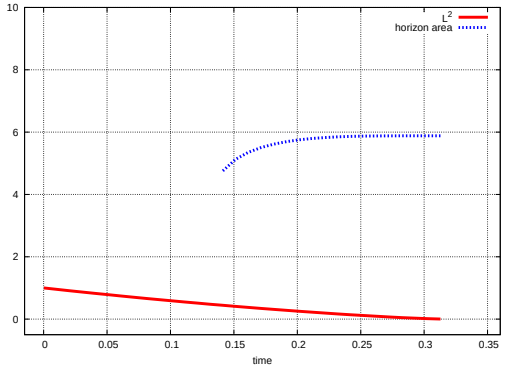

(c) $\dot{L}_0 = 2.2$

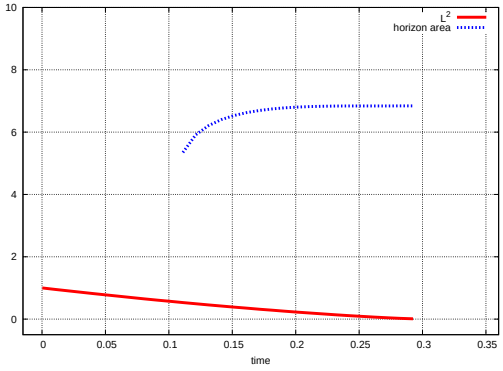

(d) $\dot{L}_0 = 2.3$

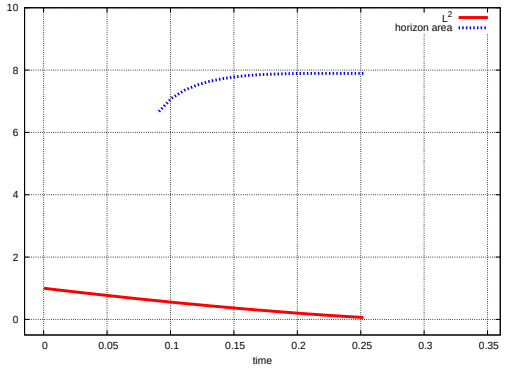

(e) $\dot{L}_0 = 2.4$

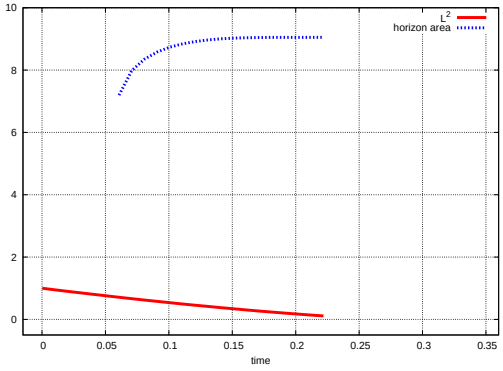

(f) $\dot{L}_0 = 2.5$

Figure 3.5: The effect of changing the value of $\dot{L}_0$ while keeping $r0 = 1.0$

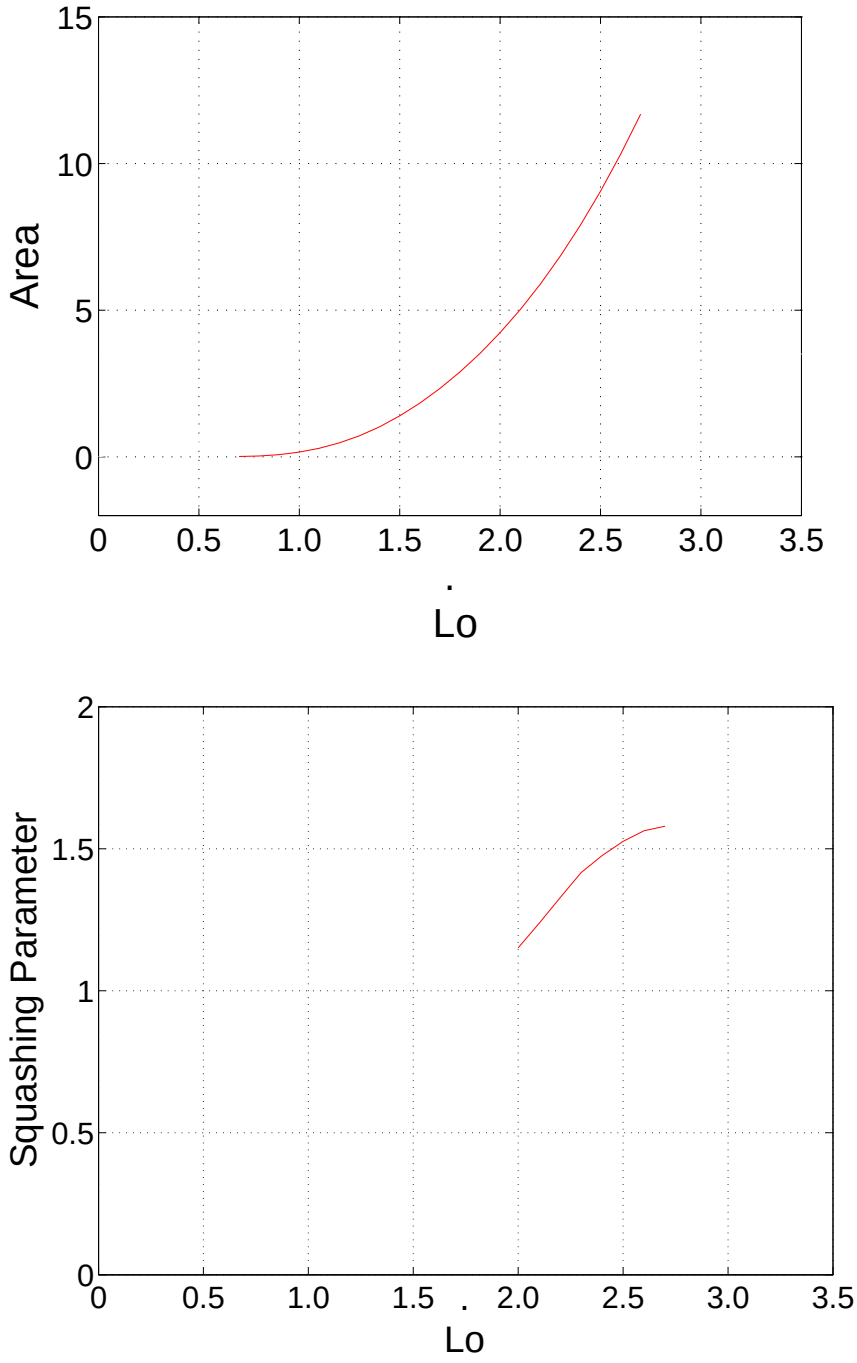

Figure 3.6: The effect on the final area and extent of squashing (only for values for which it has converged) at the horizon due to differing the initial $\dot{L}_0$ ($r0 = 1.0$).

If we vary both the values of $\dot{L_0}$ and $r0$ we can find the resulting area in a great many cases. this is shown in Fig. 3.8. The range in which a horizon forms at a late time is shown and given a shading scale to indicate the area of that horizon. Within the region marked A, there is insufficient energy to form a horizon at all. Region B marks the existence of a horizon within the initial conditions.

3.4.7 Smoother initial momentum

We also attempted to add momentum with a profile smoother than that of (3.37), which was only smooth to second order, and there was a question as to whether this could have influenced the result. We performed another series of simulations, this time with a profile smooth to a higher order, given by

$$\dot{L} = \begin{cases} -\dot{L_0}\,(1-(\frac{r}{r0})^2)^n & r < r0 \\ 0 & r > r0 \end{cases} \tag{3.38}$$

The higher the value of n the higher the derivative to which the momentum is smooth, we tried a range of values going from the starting value of two to a highest value of six. This resulted in the same possible outcomes, the cycle could bounce or alternatively a black hole apparent horizon was created before the cycle collapsed to zero. The question of whether there was a bounce or a horizon and the area of the apparent horizon created again depend upon the exact starting parameters which define the momentum. Using a smoother form of the momentum and achieving such similar results showed that our black hole creation was not caused by the order of the initial momentum's differentiability.

In Fig. 3.9 we show the effect of changing the order (the value of n in (3.38)) without changing the parameters, in all these cases the size of the two-cycle bounces but the exact details change (such as the time taken to bounce and how pronounced the bounce is).

3.4.8 Conclusions from numerics

Using a variety of initial momentum with different strength, range and profiles which are smooth to different orders we have produced the range of results described, some

of which have apparent horizons and so black holes. Our simulations find no evidence that the addition of momentum to an Eguchi-Hanson instanton can result in a conical singularity. This is seen by monitoring the size of the two-cycle at the origin and seeing that it never collapses to zero size without being enclosed in a black hole event horizon. We will later go on to describe the properties of the resulting black hole.

3.5 The Taub-bolt instanton

An alternative gravitational instanton which also exhibits a bolt singularity is Taub-bolt[69]. It too is a spherically symmetric four dimensional instanton though it is not self-dual, nor is it Kähler. We can describe it by the cohomogeneity-one metric[62] in a spherical form using the one-forms of $SU(2)$ which satisfy (B.18),

$$\begin{aligned} ds^2_{Taub\,bolt} &= \frac{r^2-N^2}{(r-2N)(r-N/2)}dr^2 \\ &\quad +4N^2\frac{(r-2N)(r-N/2)}{r^2-N^2}\sigma_3^2 \\ &\quad +(r^2-N^2)(\sigma_1^2+\sigma_2^2). \end{aligned} \tag{3.39}$$

The bolt exists at $r=2N$, this is a bolt coordinate singularity as is seen by the substitution

$$r = 2N + \frac{R^2}{8N}. \tag{3.40}$$

This results in the metric taking the form

$$ds^2|_{R\to 0} \to \left[dR^2 + \frac{R^2}{4}\sigma_3^2\right] + 3N^2(\sigma_1^2+\sigma_2^2), \tag{3.41}$$

which clearly shows that the apparent singularity at $R=0$ ($r=2N$) is a bolt singularity (3.3), it has a two-cycle blow up of radius $\sqrt{3}N$. This single modulus N describing the size of the bolt singularity, is the single modulus we intend to smoothly collapse to zero in order to initiate a flop transition by making the two-cycle at the origin vanish. In collapsing the two-cycle we may inadvertently cause the creation of a black hole solution and not a collapsed cycle, this may be an unavoidable outcome. We also applied similar numerical techniques to simulate addition of momentum to this instanton in our attempt to collapse the two-cycle at its tip.

3.6 Dynamical evolution of the Taub-bolt instanton

3.6.1 Moduli space approximation

Performing a moduli space approximation upon the Taub-bolt solution involves using the Einstein-Hilbert action upon a metric with a time dependent modulus:

$$\begin{aligned} ds^2 &= -dt^2 + \frac{r^2 - N(t)^2}{(r-2N(t))(r-N(t)/2)}dr^2 \\ &\quad +4N(t)^2\frac{(r-2N(t))(r-N(t)/2)}{r^2-N(t)^2}\sigma_3^2 \\ &\quad +(r^2-N(t)^2)(\sigma_1^2+\sigma_2^2). \end{aligned} \tag{3.42}$$

This leads to the Lagrangian

$$L = -18\pi N(t)^2 \dot{N(t)}^2, \tag{3.43}$$

which in turn gives the prediction that N^2 will be linear in time, since N^2 is proportional to the area of the blown up two-cycle, this predicts a linear fall in area. If this prediction holds it will allow the size of the two-cycle to vanish in a finite time, we must evolve the system numerically to see the accuracy of this prediction and look for the creation of black hole horizons.

3.6.2 Numerical evolution of the Taub-bolt instanton

Following methods nearly identical to those of section 3.4.2 we went on to perform a numerical simulation of the evolution of the Taub-bolt instanton to see how our results compared. This required that we use a metric with the capacity to evolve freely in time, where not just the modulus but all the metric functions are free to evolve independently in time and in the one codimension of space (the radius). The metric is given by:

$$\begin{aligned} ds^2 &= -dt^2 + \left(1+\frac{R^2}{N^2}\right)e^{2A(t,R)}dR^2 \\ &\quad +\frac{R^2}{\left(4+\frac{R^2}{N^2}\right)}e^{2C(t,R)}\sigma_3^2 \\ &\quad +N^2\left(1+\frac{R^4}{N^4}\right)e^{2B(t,R)}(\sigma_1^2+\sigma_2^2). \end{aligned} \tag{3.44}$$

We again used the vacuum Einstein equations to give both equations of motion, with which to evolve the system, and also some constraint equations which had to be imposed upon our initial momentum and which could later be used to test the evolution, these are all listed in appendix C.

3.6.3 Initial perturbation

To produce any evolution we had to apply a perturbation to the initial conditions, defined by its magnitude and its length scale, we chose a profile following the form

$$\dot{B} \sim \dot{N}_0 e^{-\left(\frac{R}{R_0}\right)^2} \tag{3.45}$$

3.6.4 Results

This initial momentum produces dynamical change to the spacetime, the effect of this change was invariably to create an apparent horizon. Unlike the previous simulation which used the Eguchi-Hanson metric as the initial condition, we never caused a bounce event and always created a black hole spacetime instead. The fall in the area of the two-cycle at the tip of the bolt was not linear, its exact profile was dependent on the parameters of the initial momentum, the strength of the momentum and the range it extended away from the origin. As is shown in Fig. 3.10 and Fig. 3.11, changing these two parameters has little effect upon the final area of the apparent horizon, although it has more influence upon the time it takes to create an apparent horizon and the time it takes for the area of the two-cycle to drop to zero.

3.6.5 Conclusions from numerics

Adding momentum to the Taub-bolt instanton never resulted in the creation of a conical singularity at the origin of the spacetime. Instead it always resulted in the creation of an apparent horizon and so created a black hole spacetime. The creation and final properties of the black hole (such as the area) seem to be only weakly dependent on changes to the initial momentum. The black hole outcome occurs even when we add

only a little momentum, though at these small momenta the convergence is not sufficient to determine the final area. The nature of the resultant black hole is described below.

3.7 The Five dimensional black hole solution

By the time the program ends (due to the curvature singularity at $r = 0$) the apparent horizon has settled to a single area which can be measured. The natural question is "what is the final state?". Given that we cannot run the simulations beyond the curvature singularity we can only offer a conjecture to answer this question. However, given that the horizon has converged to a constant value we believe that it is reasonable to suggest a five-dimensional black-hole is in the process of forming. The black-hole which fits our requirements was written down in its Kaluza-Klein dimensionally reduced form in [70, 71]. Written in its five-dimensional form this black hole looks like [72]

$$ds^2 = -f dt^2 + \frac{k^2}{f} dr^2 + \frac{r^2}{4}\left[k(\sigma_1^2 + \sigma_2^2) + \sigma_3^2\right], \tag{3.46}$$

$$f(r) = \frac{(r^2 - r_+^2)}{r^2} \tag{3.47}$$

$$k(r) = \frac{(r_\infty^2 - r_+^2) r_\infty^2}{(r_\infty^2 - r^2)^2} \tag{3.48}$$

and describes a static black-hole with a squashed three-sphere for a horizon at $r = r_+$. The radial coordinate range is $0 < r < r_\infty$ and the parameter range is $0 < r_+ < r_\infty$. If we accept that this is the end state of the Eguchi-Hanson or the Taub-bolt collapse then we are free to evaluate the squashing function $k(r)$ at the horizon, provided it too has settled to a single value before the program's end.

The asymptotic structure of the black-hole is interesting in that it is not asymptotically flat, rather it is asymptotically locally flat and takes the form [72]

$$ds^2 = -dT^2 + dR^2 + R^2 d\Omega_{S^2} + \frac{r_\infty^2}{4}\chi^2. \tag{3.49}$$

So, locally this looks like $\mathbb{R}^{(1,3)} \times S^1$, where the circle has radius $r_\infty/2$. we can find the parameters r_+ and r_∞ by evaluating the area of the horizon, and the squashing

parameter on the horizon ($k(r_+) = k_+$),

$$r_+ \sim \left(area/k_+^2\right)^{\frac{1}{3}} \tag{3.50}$$

$$r_\infty = r_+\sqrt{\frac{k_+}{k_+ - 1}} \tag{3.51}$$

This result gives us a rather novel method for dynamical compactification. Suppose that instead of starting with a compact manifold, where a portion of Eguchi-Hanson space has been glued in, we start with the full Eguchi-Hanson space with its four ”large” spatial dimensions. Then our results show that this evolves to a space where one of the spatial dimensions compactifies to a circle, giving three ”large” dimensions and one ”small”.

3.7.1 Uniqueness of the squashed 5d black hole

Since the black hole is known to be squashed and five dimensional with spherical symmetry the possibilities for the final black hole are very limited and we believe that there is only one static black hole solution which the simulation can be tending towards. As described in appendix D it seems that the black hole in (3.46) is the only possible black hole which could be coming out of our simulation. Knowing the form of the black hole analytically means that we have some hope of seeing what will happen if that hole evaporates.

3.7.2 Evaporation of the black hole

As described in section 2.3.4, the resultant black hole should begin to quantum mechanically radiate until it eventually evaporates leaving only a relic. The consequence of an evaporating black hole of the form (3.46) has been studied previously and it has been seen that the relic left behind can be a Taub-nut instanton[63, 73, 60]. Since our initial instanton can classically collapse to a black hole of the form (3.46) and this black hole can later quantum mechanically evaporate leaving a Taub-nut instanton by combining these two effects there has been a transition of the topology. This is not the flop transition discussed earlier (which is still ruled out by the black hole forma-

tion) but requires that a black hole be formed mid-process but later evaporate, which classical GR does not allow but could be permitted quantum mechanically.

3.8 Five dimensional summary

Five dimensions offers possibilities above and beyond those conceivable in four dimensions. We have investigated the possibilities of transitions within five dimensions, notably the flop transitions in which the two-cycle at the tip of a bolt singularity is collapsed to zero and then re-expanded and in doing so there is a transition of the topology. These flop transitions depend on the possibility that the cycle can be successfully reduced to zero size. The moduli space approximation (which involves predicting the behaviour based only on low energy changes to the moduli) predicts that such a collapse may be possible however this prediction disregards the possibility of creating black holes. Numerical simulation has shown that the creation of black holes is a significant risk to any flop transition, and even if no horizon is created the moduli space approximation does not hold for later times. In fact even for a range of initial momentum with differing profile, strength and range, and even for two different possible bolt singularities, there was no creation of conical singularities without creating black hole horizons around them, this impedes the initiation of flop transitions. We now go on to ask if these findings are still true for more severe transitions in higher dimensions.

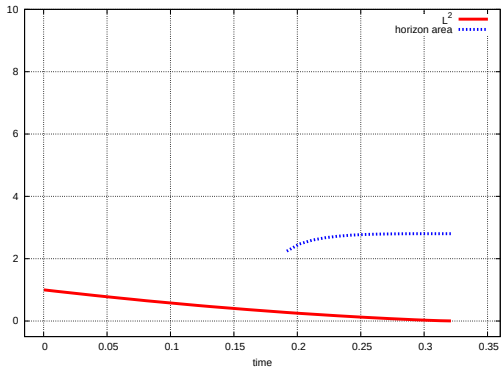

(a) $r0 = 0.7$

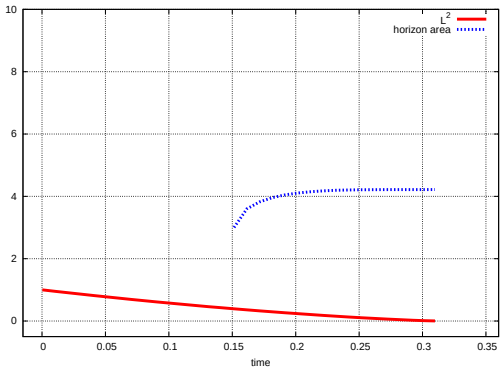

(b) $r0 = 0.8$

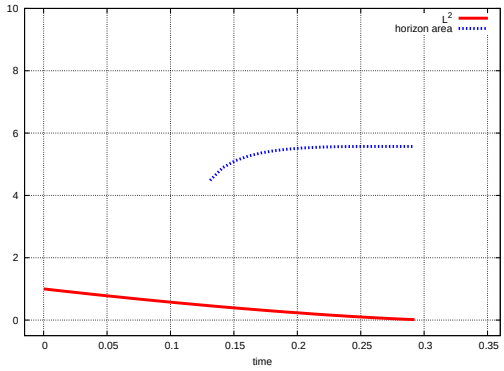

(c) $r0 = 0.9$

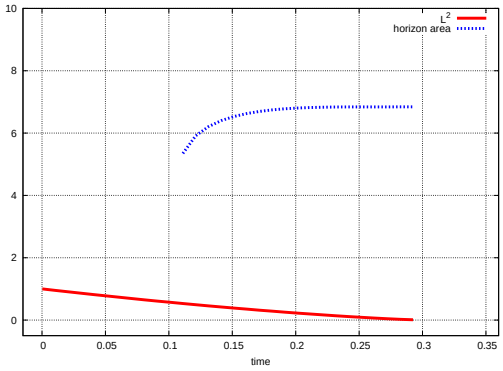

(d) $r0 = 1.0$

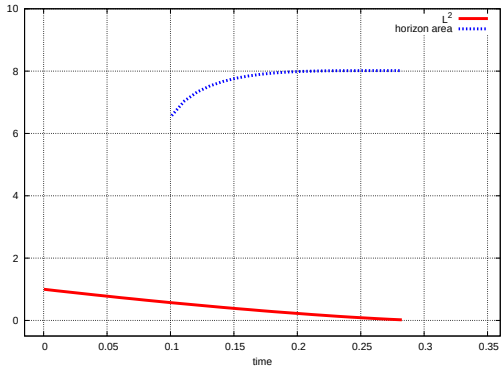

(e) $r0 = 1.1$

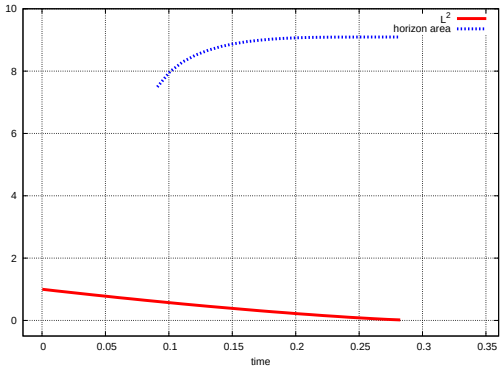

(f) $r0 = 1.2$

Figure 3.7: The effect of changing the value of $r0$ while keeping $\dot{L}_0 = 2.3$

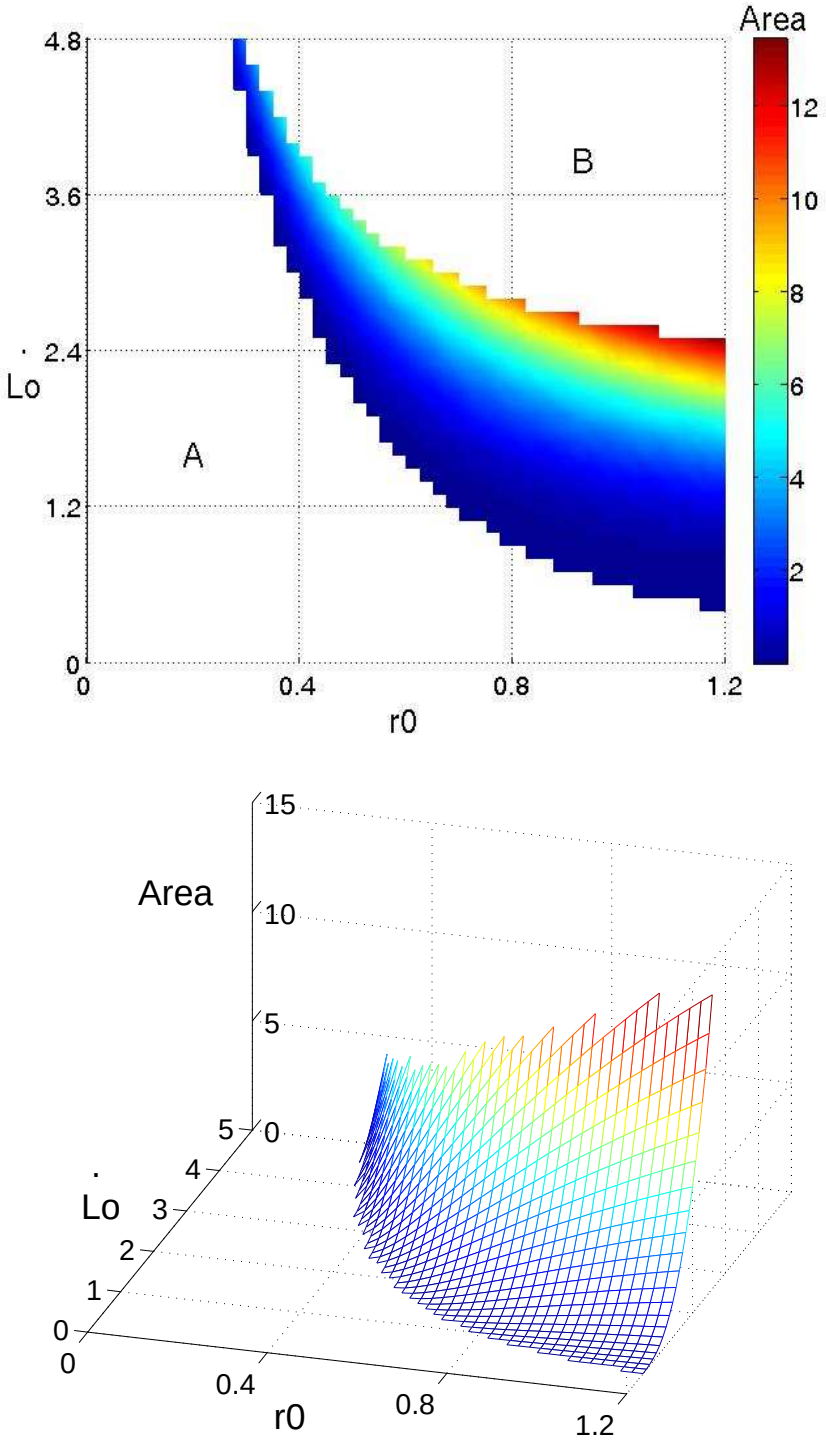

Figure 3.8: The effects on the creation of a black hole and its final area due to differing the initial $\dot{L}_0$ and r0.

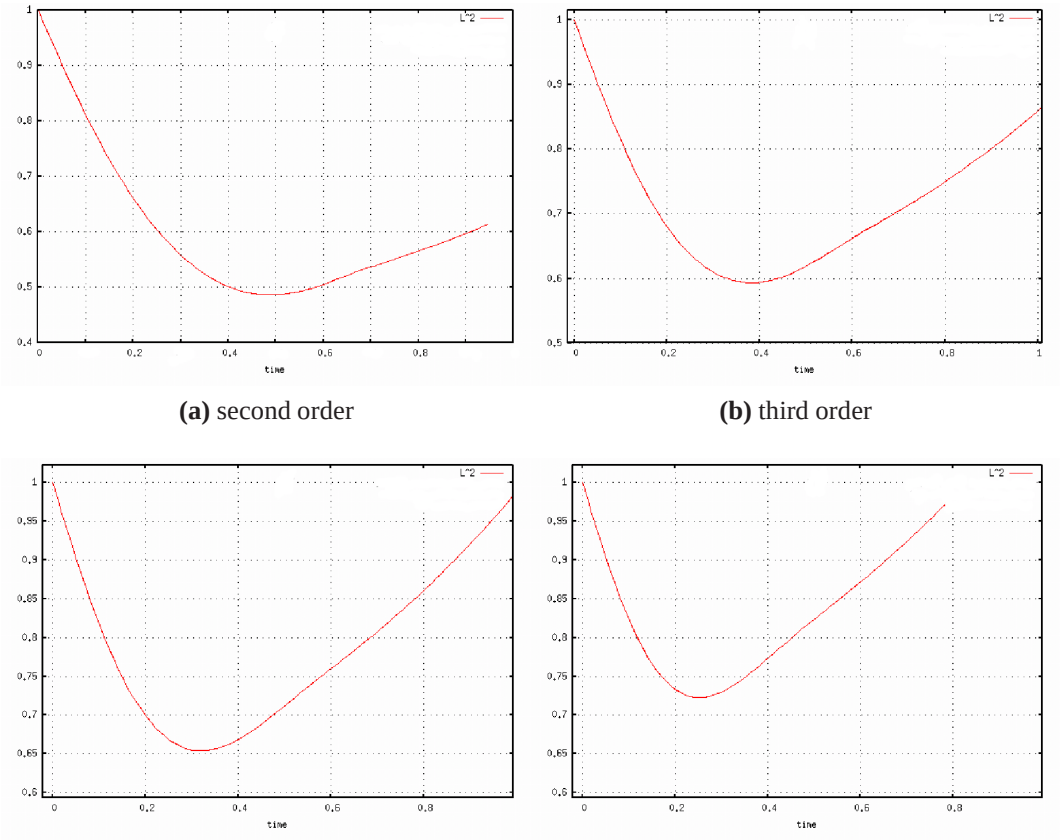

(a) second order **(b)** third order

(c) fourth order **(d)** sixth order

Figure 3.9: The effect of changing the differentiability (n in (3.38)) while keeping $\dot{L}_0 = 1.0$ $r0 = 0.8$

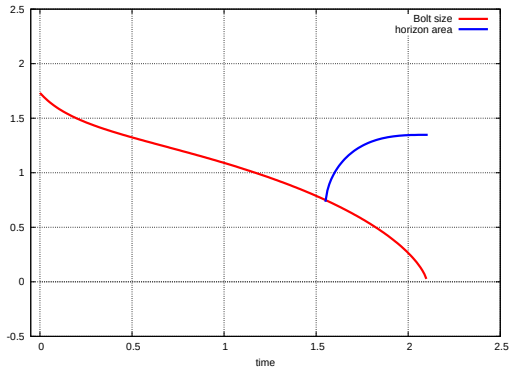

(a) $\dot{N}_0 = 1.1$

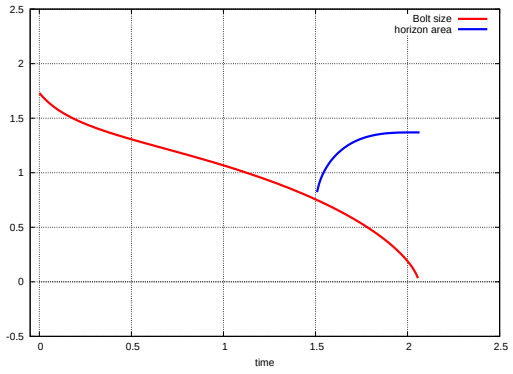

(b) $\dot{N}_0 = 1.2$

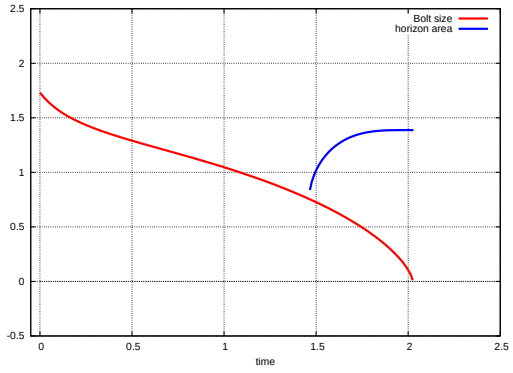

(c) $\dot{N}_0 = 1.3$

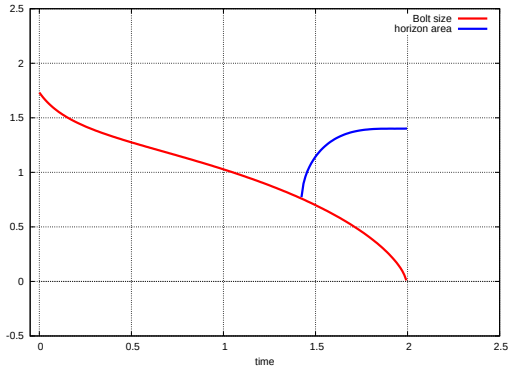

(d) $\dot{N}_0 = 1.4$

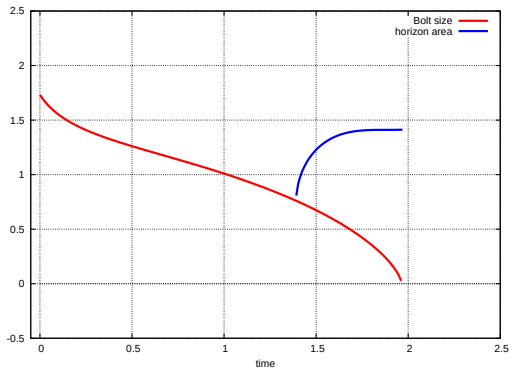

(e) $\dot{N}_0 = 1.5$

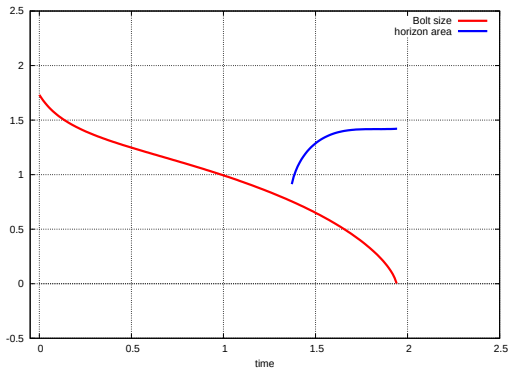

(f) $\dot{N}_0 = 1.6$

Figure 3.10: Taub-bolt: The effect of changing the strength of the momentum while keeping its range as 1.0

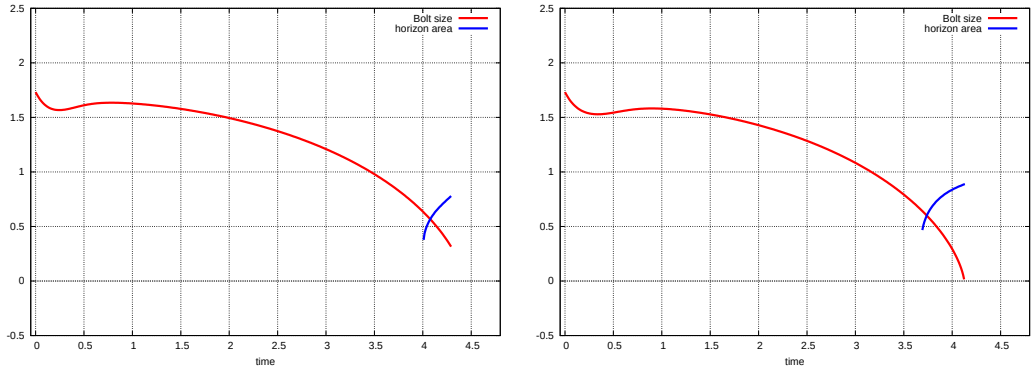

(a) $R_0 = 0.20$ **(b)** $R_0 = 0.25$

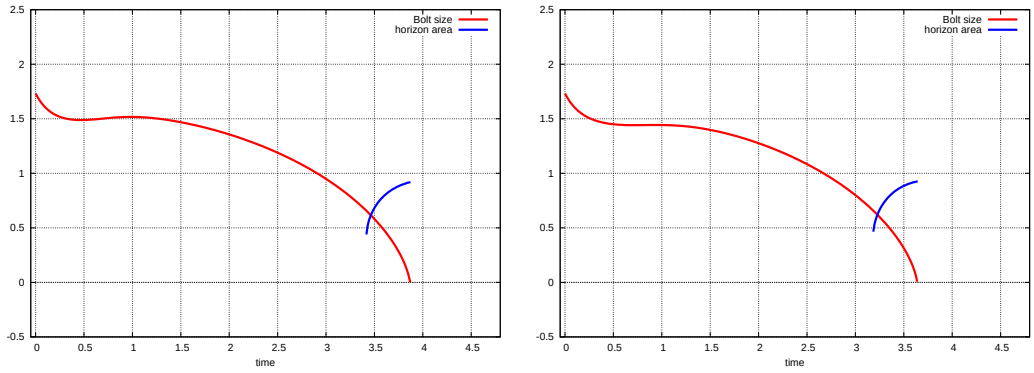

(c) $R_0 = 0.30$ **(d)** $R_0 = 0.35$

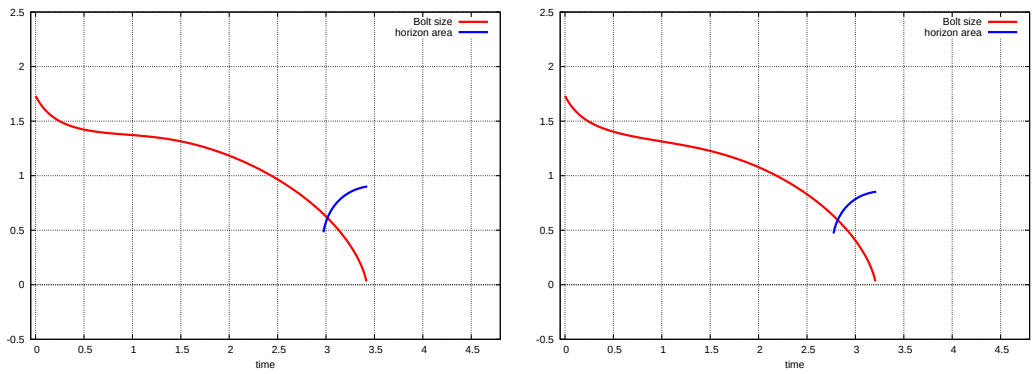

(e) $R_0 = 0.40$ **(f)** $R_0 = 0.45$

Figure 3.11: Taub-bolt: The effect of changing the range of the momentum while keeping its strength at the origin as 1.0

Chapter 4

Seven dimensional evolution

Though our ambition was to perform simulations in the ten dimensions of superstring theory, we first progress from five dimensions to seven dimensions. The Calabi-Yau manifolds which are used as an internal manifold for compactification in string theory are all six dimensional (seven dimensional when we evolve in time) and so these simulations will have applicability to compactification and to topology changing transitions. In seven dimensions there have already been studies[74, 54, 75, 76, 77, 52] into more drastic transitions than the previous flop transition, called conifold transitions they rely on the more elaborate instantons possible in higher dimensions.

4.1 Singular conifold instanton

One example of a singular manifold is the singular conifold[74], a Calabi-Yau threefold, it takes the form of a cone with a five-dimensional base. In the region close to the singular point can be described by a quadratic in $\mathbb{C}^4$

$$\sum_{A=1}^{i=4}(\omega^A)^2 = 0 \tag{4.1}$$

where ω^A are four complex coordinates. The conifold can have a Ricci flat metric given by[74, 78]

$$ds^2 = dr^2 + r^2 ds^2_{base}. \tag{4.2}$$

Such a base is labelled $T^{(1,1)}$ and has the topology of S^3xS^2[74], it can be written

in terms of two $SU(2)$ groups. Using the two distinct sets of the conventional left-invariant one-forms of $SU(2)$ which obey the equations of (B.20), we can write the base of the conifold in a form known as the Sasaki-Einstein metric:

$$ds^2_{T^{(1,1)}} = \frac{1}{6}(\sigma_1^2 + \sigma_2^2 + \Sigma_1^2 + \Sigma_2^2) + \frac{1}{9}(\sigma_3 + \Sigma_3)^2. \tag{4.3}$$

The reason to investigate the singular conifold is that the singular point at its tip can be made smooth in two distinct ways, due to the S^3xS^2 topology (as opposed to a trivial S^5 topology), we can expand the two-cycle at the origin, giving the resolved conifold, or expand the three-cycle to produce a deformed conifold.

4.2 Resolved conifold instanton

The resolved conifold is the alteration to the singular conifold achieved by expanding the singular point into an S^2[79, 74]. It is further defined by a parameter determining the radius of the S^2, we call this parameter α. In the limit that this radius drops to zero, we recover the singular conifold. Using the one-forms of (B.20) to represent $SU(2)$ the resolved conifold can be expressed as follows.

$$\begin{aligned} ds^2_{res} = \quad &+ \quad \frac{r^2 + 6\alpha^2}{r^2 + 9\alpha^2} dr^2 + \frac{1}{6} r^2 (\sigma_1^2 + \sigma_2^2) \\ &+ \quad \frac{1}{6}(6\alpha^2 + r^2)(\Sigma_1^2 + \Sigma_2^2) + \frac{r^2}{9}\left(\frac{r^2 + 9\alpha^2}{r^2 + 6\alpha^2}\right)(\sigma_3 + \Sigma_3)^2. \end{aligned} \tag{4.4}$$

At the origin this metric does not degenerate to a point, instead we find an S^2 which can be seen by setting r=0,

$$ds^2|_{r=0} = \alpha^2(\Sigma_1^2 + \Sigma_2^2). \tag{4.5}$$

This is a two-sphere of area, $4\pi\alpha^2$ (crossed with a 1+1 Minkowski geometry) which has replaced the origin of the singular conifold, and in doing so has smoothed the manifold. Clearly the resolved conifold approaches the singular conifold in either the high r or low α limits.

4.3 Deformed conifold instanton

There also exists the deformed conifold solution, which uses another method to rectify the singularity of the singular conifold [74, 80, 78, 81]. It involves expanding the singularity to the form of an S^3. This is also described by a parameter, one which defines the radius of the S^3, called ϵ. This is defined by

$$\sum_{A=1}^{i=4}(\omega^A)^2 = \epsilon^2. \tag{4.6}$$

Using two sets of left-invariant one-forms which satisfy (B.20), and defining K by

$$K = \frac{(\sinh(2r) - 2r)^{\frac{1}{3}}}{2^{\frac{1}{3}}\sinh(r)}, \tag{4.7}$$

we can write a Ricci flat metric upon the deformed conifold as,

$$\begin{aligned} ds^2_{Def} = \quad & \frac{\epsilon^{\frac{4}{3}}K}{2}\left[\frac{1}{3K^3}dr^2 + \frac{1}{3K^3}\left(\sigma_3+\Sigma_3\right)^2\right. \\ & +\frac{1}{2}\sinh^2\left(\frac{r}{2}\right)\left(\left(\sigma_1-\Sigma_1\right)^2+\left(\sigma_2+\Sigma_2\right)^2\right) \\ & \left.+\frac{1}{2}\cosh^2\left(\frac{r}{2}\right)\left(\left(\sigma_1+\Sigma_1\right)^2+\left(\sigma_2-\Sigma_2\right)^2\right)\right]. \end{aligned} \tag{4.8}$$

At the origin, this metric is also smooth as it does not degenerate to a point but to an S^3 [74, 82], this three-sphere has replaced the origin and so removed the conical singularity.

In the limit of high r values we can see that this tends to the same form as the singular conifold by noting that for large r

$$K \to \left(\frac{2}{e^r}\right)^{\frac{1}{3}}, \tag{4.9}$$

and so for large r,

$$\begin{aligned} ds^2|_{r\to\infty} \to \quad & \frac{\epsilon^{\frac{4}{3}}}{6}\left(\frac{e^r}{2}\right)^{\frac{2}{3}}dr^2 \\ + \quad & \frac{3}{4}\epsilon^{\frac{4}{3}}\left(2e^{2r}\right)^{\frac{1}{3}}\left(\frac{1}{6}\left(\sigma_1^2+\Sigma_1^2+\sigma_2^2+\Sigma_2^2\right)+\frac{1}{9}\left(\sigma_3+\Sigma_3\right)^2\right). \end{aligned} \tag{4.10}$$

This can be written, in terms of a new radial coordinate ρ, as

$$\rho^2 = \frac{3}{4}\epsilon^{\frac{4}{3}}\left(2e^{2r}\right)^{\frac{1}{3}}, \tag{4.11}$$

$$ds^2|_{r=\infty} = d\rho^2 + \rho^2\left(\frac{1}{6}\left(\sigma_1^2+\Sigma_1^2+\sigma_2^2+\Sigma_2^2\right)+\frac{1}{9}\left(\sigma_3+\Sigma_3\right)^2\right). \tag{4.12}$$

This clearly shows that the asymptotic forms of both the singular conifold and the deformed conifold are the same, they only differ sufficiently close to the origin.

We can alternatively write the deformed conifold in terms of the more convenient one-forms, the g^i forms described in section B.3.

$$ds^2_{Def} = \frac{\epsilon^{\frac{4}{3}}K}{2}\left[\frac{1}{3K^3}dr^2 + \frac{1}{3K^3}\left(g^5\right)^2 + \sinh^2\left(\frac{r}{2}\right)\left(\left(g^1\right)^2 + \left(g^2\right)^2\right) + \cosh^2\left(\frac{r}{2}\right)\left(\left(g^3\right)^2 + \left(g^4\right)^2\right)\right]. \quad (4.13)$$

4.4 Conifold transitions

The fact that there are two distinct ways of smoothing the singular point at the tip of the singular conifold means that another type of topology changing transition can be conceived. Called a conifold transition, it involves collapsing the three-cycle at the tip of a deformed conifold and then re-expanding the tip in the form of the two-cycle exhibited by a resolved conifold[74, 53]. This process results in changing the three-cycle into a two-cycle, which is a more drastic process than was described in section 3.2 because it results in changing Hodge numbers and it changes the spectrum of massless moduli fields which could be observed. This process will occur in a seven dimensional setting which means it has direct applications to the topology changes between Calabi-Yau manifolds with distinct topologies. The topology change can occur in the opposite direction also, where a two-sphere is reduced in time until it collapses all the way to zero then the tip is re-expanded as a three-sphere. This involves the creation of a singular manifold within the process. Though it would seem that that these singularities would destroy the low energy theory also, it is a feature of string theory that these potentially singular situations can actually be interpreted in a consistent and definitive manner[74, 54, 75, 76, 77, 52] or at least the associated mathematics can be described. The physics which the singular transitions imply is less well understood and its full implications will be of great importance to string theory. If these transitions are possible they could allow us to unify the string landscape and form general predictions of string models. These transitions rely on the ability to collapse the cycle all the way to zero and continuously re-inflate it as a cycle of a different dimension. Possible problems may hamper this process, and they have been investigated in previous work concen-

trating on the low energy dynamics in the reduced dimensional theory. The possibility of creating black holes in the higher dimensional theory is often overlooked and it is this risk which we attempt to investigate numerically. This will involve simulating the addition of momentum to the smooth instantons to see if the singular spacetime can be created without an apparent horizon to accompany it.

4.5 Dynamical evolution of the resolved conifold

4.5.1 Moduli space approximation

In order to estimate the low energy dynamics of the resolved conifold we can allow the modulus α to vary in time to a small extent [28]. This involves introducing a new, time dependent modulus, which we called $\alpha(t)$ where $\alpha(0) = \alpha$. This is comparable to allowing the size of the two-cycle to change in time, while confining the r dependence to remain that of the resolved conifold. Having made this assumption we can find the dynamics by using the Einstein-Hilbert action and the curvature resolved conifold metric, including this new dependence, we get an effective action:

$$S_{eff} = \int dt \left(\frac{d}{dt}\sqrt{\alpha}\right)^2. \tag{4.14}$$

This gives the approximation that $\sqrt{\alpha(t)}$ is linear in time, implying that if we set $\alpha(t)$ on a course towards hitting zero, then the moduli approximation says that it will reach zero in finite time. As $\alpha = 0$ corresponds to the singular geometry then we see no obstruction to the geometry becoming singular within this approximation. By extending this approximation to include the full gravitational dynamics we hope to achieve a better understanding of this process.

4.5.2 Numerical evolution of the resolved conifold

Having described the resolved conifold instanton and made a prediction for the dynamics its moduli may undergo, we must go on to test that prediction and find the full effects gravity will have upon the dynamics of the system. In contrast to the low energy approximation, we now give the metric total time dependence and allow it to

vary freely in time[83, 65], following only the Einstein equations and constraints of symmetry.

4.5.3 Time dependent metric

To perform the simulations we need a suitable form for the metric which is general enough to give a consistent time evolution of the equations of motion, but with enough symmetry to ensure that numerical simulation is possible. For both the deformed and resolved conifold simulations we evolve a metric with four functions, each of which has an associated momentum. In order to improve numerical stability, and to simplify the application of boundary conditions, we follow the method of section 3.4.3 and choose functions which extract out various factors such that the functions we evolve are initially finite and asymptote to constant values, moreover they are symmetric under $r \to -r$.

$$\begin{aligned} ds^2 = -dt^2 + A^2(t,r)dr^2 &+ r^2 B^2(t,r)(\sigma_1^2 + \sigma_2^2) \\ &+ (6{\alpha_0}^2 + r^2)C^2(t,r)(\Sigma_1^2 + \Sigma_2^2) \\ &+ r^2 D^2(t,r)(\sigma_3 + \Sigma_3)^2. \end{aligned} \tag{4.15}$$

At $r = 0$ we need to impose some boundary conditions, these follow by requiring local flatness at the origin [66] and by maintaining A, B, C and D as even functions at the origin.

$$A^0(t) = B^0(t) = C^0(t), \tag{4.16}$$

$$\begin{aligned} A(t,r) &\sim A^0(t) + \mathcal{O}(r^2), \\ B(t,r) &\sim B^0(t) + \mathcal{O}(r^2), \\ C(t,r) &\sim C^0(t) + \mathcal{O}(r^2), \\ D(t,r) &\sim D^0(t) + \mathcal{O}(r^2). \end{aligned} \tag{4.17}$$

4.5.4 The Einstein equations

Given that we are using the Einstein-Hilbert action, without any modification to gravity and with no fluxes or other additions to the action, and also having decided upon a metric, we can go on to find the resulting Einstein equations which will give both our equations of motion and constraints for the coming evolution, see appendix E.1.

4.5.5 Initial conditions

By comparing (4.15) and (4.4), we can read off the initial conditions for the resolved conifold,

$$\begin{aligned} A(0,r) &= \sqrt{\frac{r^2+6{\alpha_0}^2}{r^2+9{\alpha_0}^2}} \\ B(0,r) &= \frac{1}{\sqrt{6}}, \\ C(0,r) &= \frac{1}{\sqrt{6}}, \\ D(0,r) &= \frac{1}{3}\sqrt{\frac{r^2+9{\alpha_0}^2}{r^2+6{\alpha_0}^2}}. \end{aligned} \tag{4.18}$$

This is a static metric, so if no initial momentum is added then no evolution occurs (this was used to test stability of our code). To see any dynamical effects we must add additional momentum.

4.5.5.1 Initial momentum

We added momentum and in doing so initiated the dynamical process, making sure that the momentum and Hamiltonian constraints were satisfied. Our specific algorithm was to add momentum to C (which describes the size of the two-sphere) according to the form given below (4.19). This depends upon two parameters giving the strength of the momentum (P) and the range the momentum extended away from the origin (r_0). The momentum for B was taken as (4.20), in order to aid the stability of the tip, this

actually has the tendency to maintain an unsquashed three-sphere close to the origin.

$$\dot{C}(0,r) = -P\left(\frac{r}{r_0}\right)^4 e^{-\left(\frac{r}{r_0}\right)^2} \tag{4.19}$$

$$\frac{\dot{B}(0,r)}{B(0,r)} = \frac{\dot{D}(0,r)}{D(0,r)}. \tag{4.20}$$

The form of the momentum is required to fall off sufficiently fast asymptotically so that we are not adding an infinite amount of energy, the exponential decay in (4.19) achieves that and means we could have a final state of a finite mass black hole. The other two initial conditions for the C and D momenta were determined by the momentum constraint and the Hamiltonian constraint.

4.5.6 Results

We monitored the evolving system for the formation of an apparent horizon as described in section 2.2.2. For radial null geodesics we may write,

$$0 = \left[\frac{d\,Area}{dt}\right]_{null}, \tag{4.21}$$

$$= \left[\frac{\partial\,Area}{\partial t}\right]_r + \left[\frac{\partial\,Area}{\partial r}\right]_t \left[\frac{\mathrm{d}r}{\mathrm{d}t}\right]_{null}, \tag{4.22}$$

at the apparent horizon. We also measure the area of the apparent horizon at each time slice and so discover its evolution. For our simulations we find that its area increased monotonically but, as shown in Fig. 4.1, asymptotes to a constant value. This constant value we took to be a good approximation to the area of the resulting event horizon. The exact value it asymptotes to will depend upon the exact initial momentum we put in.

In addition to the area of the horizon another property of the resultant black hole is the squashing of the angular part of the metric. This exists because the functions B, C and D within (4.15) are not determined solely by the area at the horizon, their various ratios are referred to as the squashings of the metric at the horizon. The parameters defining the extent of the squashing also change in time but, like the horizon area, converge as time goes on, as shown in Fig. 4.2 for a particular example. The fact that both the apparent horizon area, and the squashing at the horizon are asymptoting to constant values is evidence that the final state is settling on a static black hole.

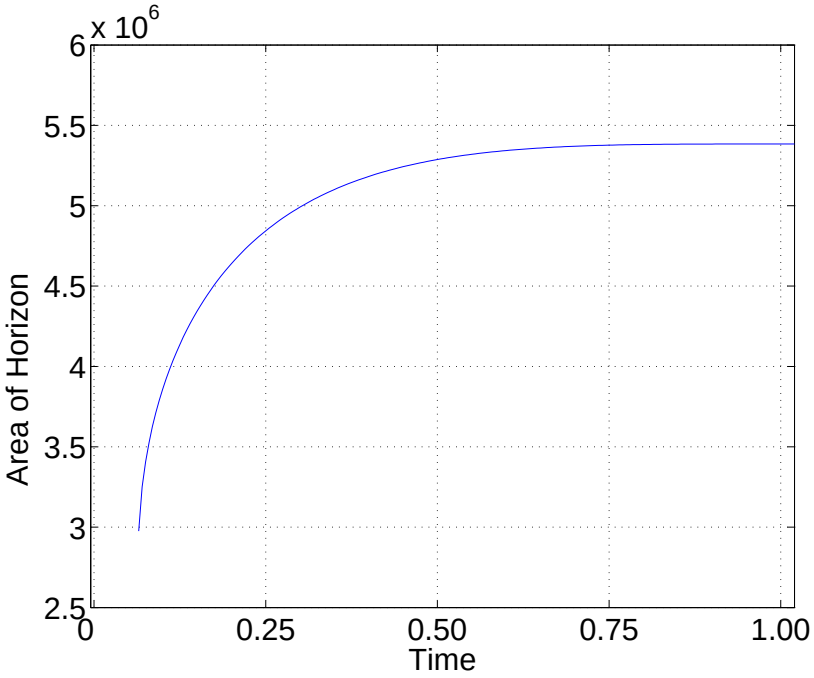

Figure 4.1: The area of the apparent horizon of the collapsing resolved conifold, changing in time, for the parameters $P = 0.5$ and $r_0 = 3$.

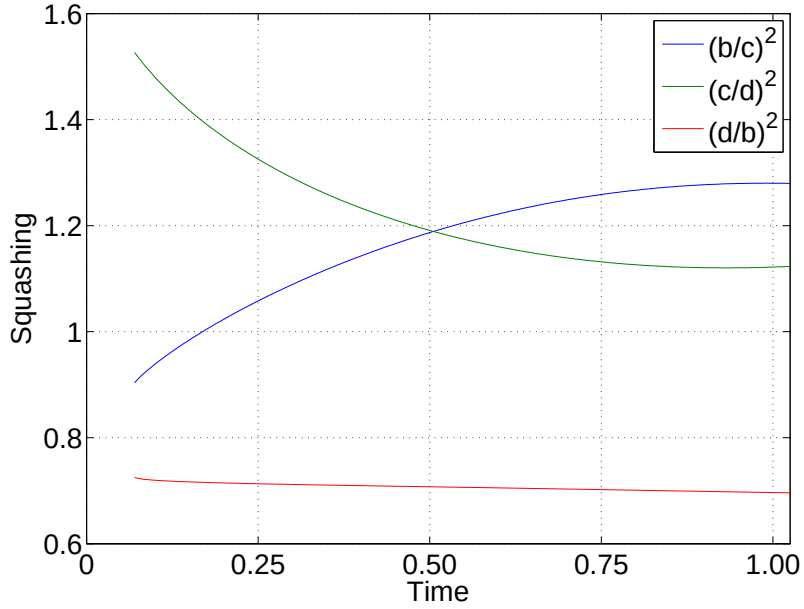

Figure 4.2: The squashing values of (what was initially) the resolved conifold, seen to be converging in time. Note the slow change to the squashing (d/b) due to the initial condition (4.20)

4.5.6.1 Results for a range of initial conditions

We varied the parameters P and r_0 and assessed the resulting size of any resultant black hole, the results are presented in Fig. 4.3. For small values of P and r_0 we were not able to reliably extract a value for the final area of the apparent horizon and so this portion of the plot has been left blank. This was due to the large timescale needed to produce such black holes, and was beyond the dynamic range of our simulations. What we see from the data is that for all the cases which could be reliably tested we did observe the formation of a black hole. This is in contradistinction to the results of the Eguchi-Hanson system examined in section 3.4.2 as there was no result for which the modulus bounced, in fact there were no simulations which did not result in the creation of a horizon (though sometimes the area could not be measured).

While Fig. 4.3 shows only the final area of the resultant black hole, it is also interesting to view the time evolution which leads to this value asymptotically. If we change the strength while keeping the range at some fixed value we can form families of results as shown in Fig. 4.4. Note that increasing the strength causes the apparent horizon to form at an earlier time and to have a higher area at all times in addition to having a higher final area (which we have already seen in Fig. 4.3). Note that for very high strengths ($P > \ 0.55$), the program has to be terminated at an earlier time since the size of the two-cycle at the origin has dropped to zero earlier, fortunately the area has already converged by this point.

Similar graphs can be plotted for which the strength is fixed but the range is varied, as in Fig. 4.5. These have to be plotted as a log scale due to the profound change the variation of r_0 has on the final area. Note that for lower strength and range the rate of convergence is lower and so for the lowest strengths the final area of the simulation is not a good estimate for the event horizon area (hence these points are not included in Fig. 4.3).

4.5.6.2 Moduli space comparison

In section 4.5.1 we presented a prediction for the behaviour of $\alpha(t)$ based on the moduli space approximation, given that the static resolved conifold is a solution for any fixed

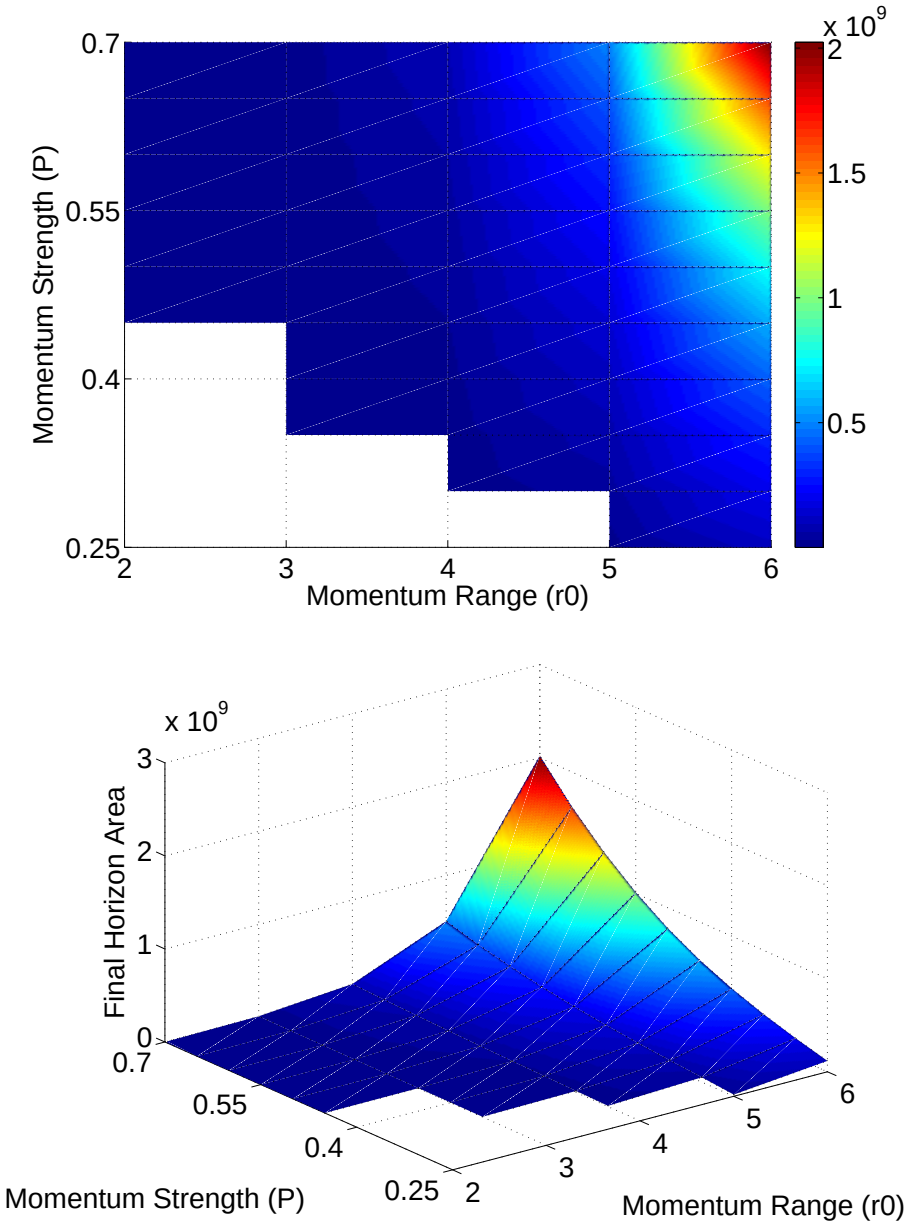

Figure 4.3: The effects on the creation of a black hole and its final area due to differing the initial P and r_0.

α; this led us to conclude that $\sqrt{\alpha(t)}$ should evolve linearly in time. We would like to check this result against the full numerical solutions that we have obtained, but this involves some ambiguity in defining what we mean by α once the metric has evolved away from the precise form of the resolved conifold. That is to say, once the profile functions have evolved away from the functional form given by (4.18), how do we extract a value for α? In practise we chose to define $\alpha(t)$ using the value of $C(t,r)$ at the origin, $C(t,0)$ to extract a value for $\sqrt{\alpha(t)}$ by comparing expressions (4.15) and

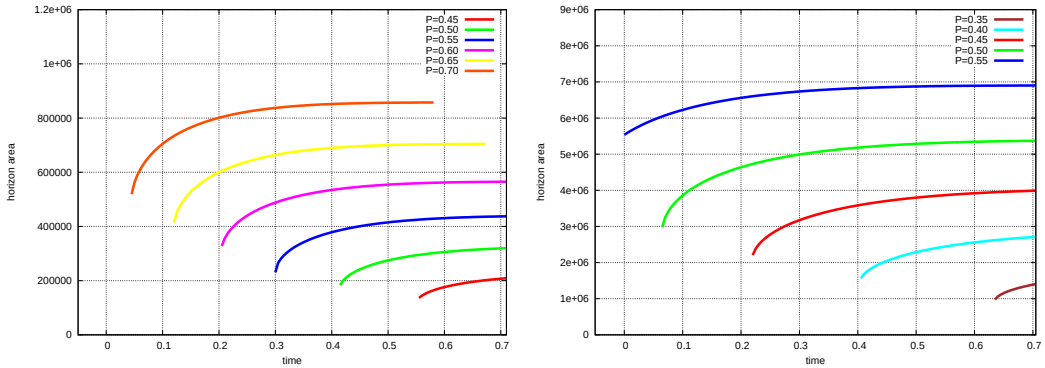

(a) $r_0 = 2$ **(b)** $r_0 = 3$

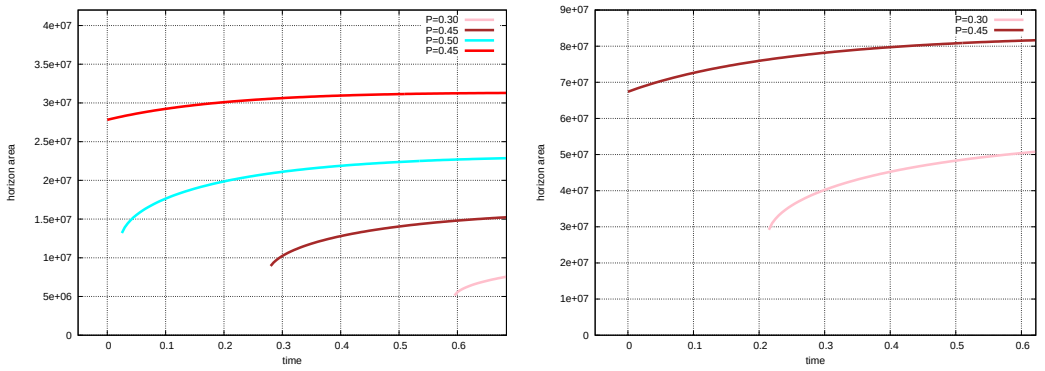

(c) $r_0 = 4$ **(d)** $r_0 = 5$

Figure 4.4: The effect of changing the strength of the momentum while keeping its range as a fixed value

(4.4),

$$\sqrt{\alpha}(t) = \sqrt{6}\alpha_0 C(t, 0). \tag{4.23}$$

As shown in Fig. 4.6 the time evolution of $\sqrt{\alpha}$ is indeed linear in the initial stages, however this prediction only holds for early times.

4.5.7 Conclusions

From these numerical simulations of the evolution of the resolved conifold, it seems that a conical singularity cannot be formed. Instead of forming a spacetime with a conical singularity (from which we could perform a conifold transition) we get an apparent horizon, indication of a true event horizon and hence a black hole spacetime. The formation of this black hole spacetime seems unavoidable even though we tried a range of initial momentum, extending even to very small momentum. While changing the initial momentum cannot avoid creating a black hole, it will cause changes to the

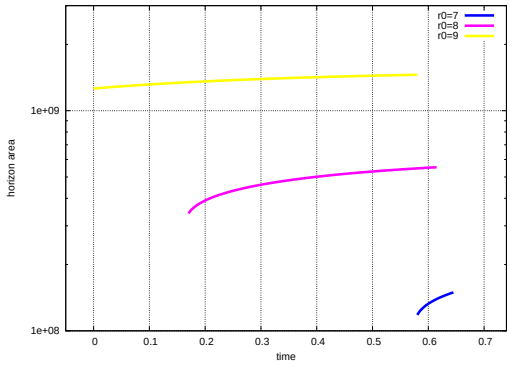

(a) $P = 0.20$

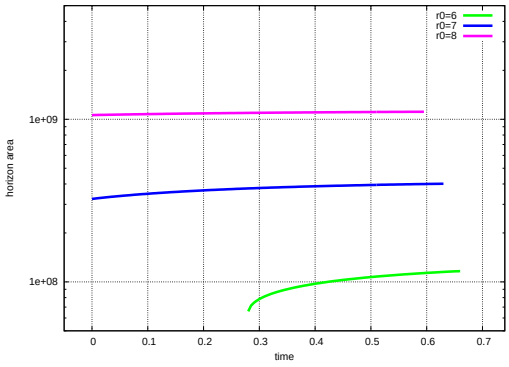

(b) $P = 0.25$

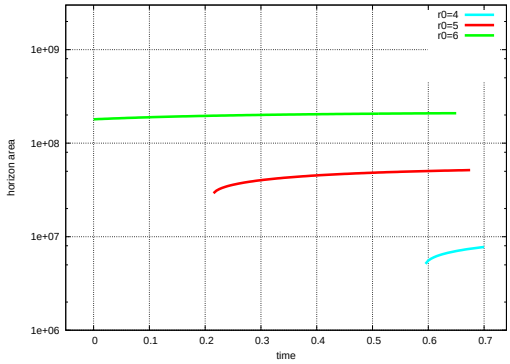

(c) $P = 0.30$

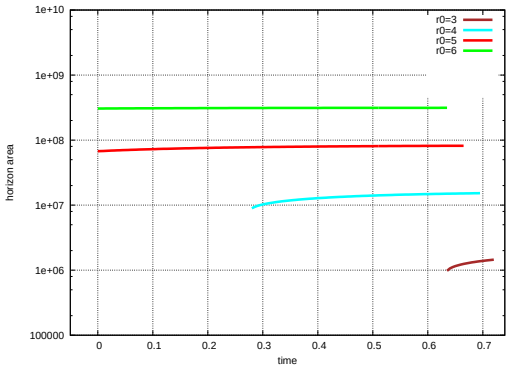

(d) $P = 0.35$

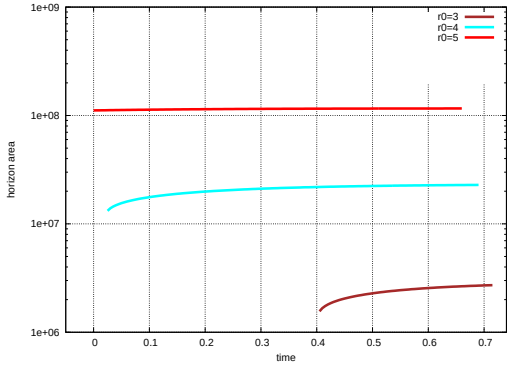

(e) $P = 0.40$

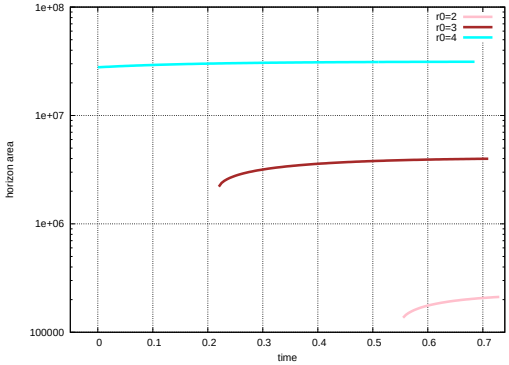

(f) $P = 0.45$

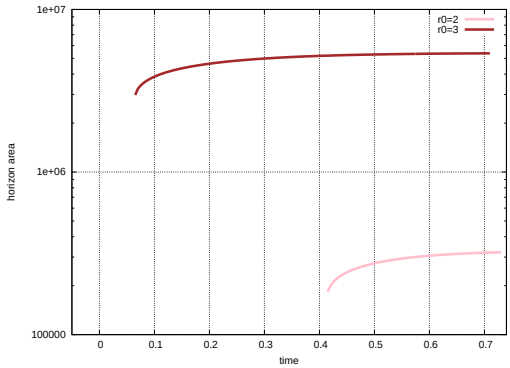

(g) $P = 0.50$

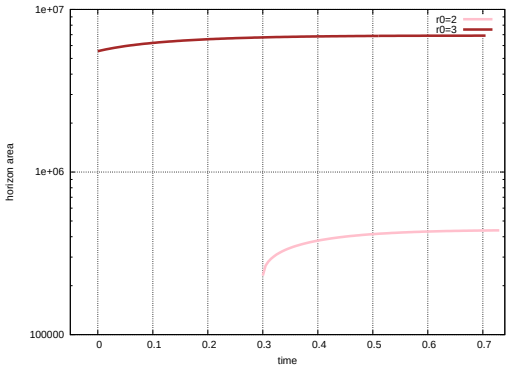

(h) $P = 0.55$

Figure 4.5: The effect of changing the range of the momentum while keeping its strength at a fixed value (log scale)

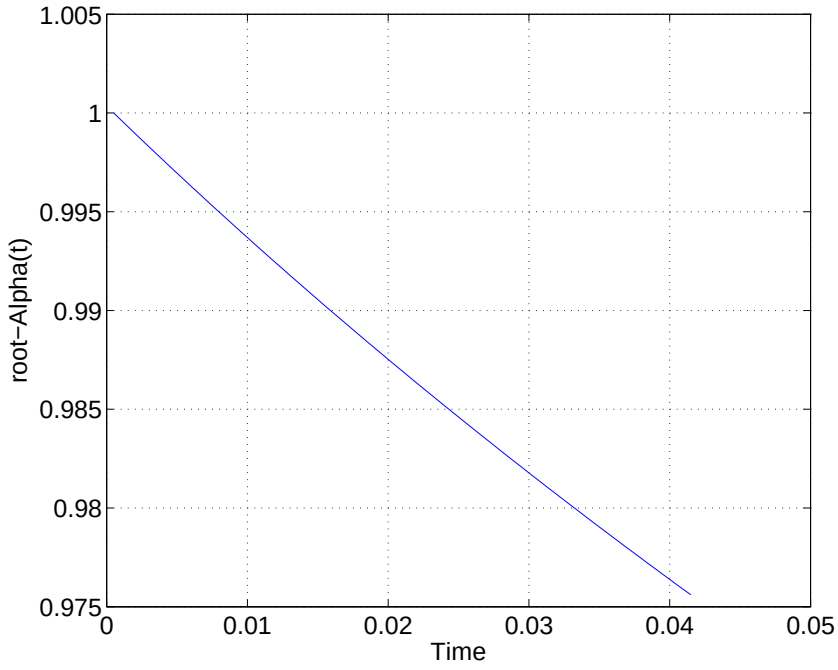

Figure 4.6: The evolution of the the moduli of the resolved conifold at very early times. The approximation predicts this shall be linear.

process of creation and the evolution of the apparent horizon. For some profiles of initial momentum it is possible to extract reliable information about the nature of the resultant black hole (most notable is the final area of the black hole).

4.6 Dynamical evolution of the deformed conifold

We performed a second numerical simulation, this time involving the collapse of a three-sphere at the origin, the deformed conifold instanton has such a three-sphere and so we go on to simulate the changes to this instanton as we add momentum[83, 65].

4.6.1 Time dependent metric

We wanted a simulation capable of going on for a long time, at least long enough to see the creation of the apparent horizon or the collapse of the sphere. To this end we choose a metric for which we have explicitly extracted the problematic terms, leaving us with smooth, finite functions to evolve, as well as allowing us to make the profiles

symmetric under $r \to -r$. We therefore take the simulation metric to be

$$\begin{aligned} ds^2 = -dt^2 &+ \left(A(t,r)\cosh\left(\frac{r}{3}\right)\right)^2 dr^2 \\ &+ \left(B(t,r)\sinh\left(\frac{r}{3}\right)\right)^2 \left(\left(g^1\right)^2 + \left(g^2\right)^2\right) \\ &+ \left(C(t,r)\cosh\left(\frac{r}{3}\right)\right)^2 \left(\left(g^3\right)^2 + \left(g^4\right)^2\right) \\ &+ \left(D(t,r)\cosh\left(\frac{r}{3}\right)\right)^2 \left(\sigma_3 + \Sigma_3\right)^2 \end{aligned} \tag{4.24}$$

so that, A, B, C and D are all even at the origin and also they asymptote to constant values. This allows for more accurate application of boundary conditions arising due to maintaining even variables at the origin (implying (4.25)) and from requiring local flatness at the origin as described in [66] (leading to (4.26)).

$$\begin{aligned} A(t,r) &\sim A^0(t) + \mathcal{O}(r^2), \\ B(t,r) &\sim B^0(t) + \mathcal{O}(r^2), \\ C(t,r) &\sim C^0(t) + \mathcal{O}(r^2), \\ D(t,r) &\sim D^0(t) + \mathcal{O}(r^2), \end{aligned} \tag{4.25}$$

$$A^0(t) = B^0(t), \quad C^0(t) = D^0(t) \tag{4.26}$$

These conditions are imposed at the boundary.

4.6.2 The Einstein equations

The Einstein-Hilbert action gives us the equations we use to evolve and constrain the simulation, these are given in appendix E.2.

4.6.3 Initial conditions

By comparing (4.24) and (4.8), we can read off the initial conditions to be

$$\begin{aligned} A(0,r)^2 &= \frac{\epsilon^{\frac{4}{3}}}{6K^2\cosh^2\left(\frac{r}{3}\right)} \\ B(0,r)^2 &= \frac{1}{4}\epsilon^{\frac{4}{3}}K\frac{\sinh^2\left(\frac{r}{2}\right)}{\sinh^2\left(\frac{r}{3}\right)}, \\ C(0,r)^2 &= \frac{1}{4}\epsilon^{\frac{4}{3}}K\frac{\cosh^2\left(\frac{r}{2}\right)}{\cosh^2\left(\frac{r}{3}\right)}, \\ D(0,r)^2 &= \frac{\epsilon^{\frac{4}{3}}}{6K^2\cosh^2\left(\frac{r}{3}\right)}. \end{aligned} \tag{4.27}$$

As these are derived from the static deformed conifold these initial conditions will yield a static metric, as was indeed found in our simulations by way of a check for the code.

4.6.3.1 Initial momentum

We added momentum of the following form

$$\frac{\dot{C}(0,r)}{C(0,r)} = \frac{\dot{D}(0,r)}{D(0,r)} = -P\left(\frac{r}{r_0}\right)^4 e^{-\left(\frac{r}{r_0}\right)^2}, \tag{4.28}$$

to initiate the dynamics, with the momenta for the A and B functions being determined by the constraint equations (E.9). By choosing the C and D momenta so related we are making the choice of maintaining the form of the three-sphere, at least initially. As in the resolved conifold initial conditions we note that the momentum decays away sufficiently fast that the energy input is finite, allowing for the possibility of forming a finite mass black hole.

4.6.4 Results

We used the same methods as described in section 2.2.2 to search for the appearance of an apparent horizon, thus indicating the presence of a horizon. The results are qualitatively similar to the collapse of the resolved conifold, with an apparent horizon appearing in all the cases we examined, these apparent horizons had a time development which involved the area growing initially but then asymptoting to a constant value and

so we are able to establish a final value for their area in most cases, which we take to be a good approximation to the area of the black hole horizon.

4.6.4.1 Results for a range of initial conditions

The final area of the black hole depends upon the initial momentum we have added, which we characterised by a magnitude P and a spatial extent r_0 in (4.28); varying these produced the range of final areas displayed in Fig. 4.7. For small values of P or r_0 the area of the apparent horizon did not converge sufficiently rapidly to acquire an accurate value for the horizon area, so we have left such regions blank in Fig. 4.7 however, for all cases an apparent horizon was observed to form.

In addition to plotting the final area we can also show the apparent horizon's appearance and growth in time, as seen in Fig. 4.8 and in Fig. 4.9. These figures also show that for initial momentum which are too small, the area of the apparent horizon is not sufficiently converged to read off a final area and so cannot be accurately plotted in Fig. 4.7, examples include $r_0 = 0.9$ $P = 2.6$ and $r_0 = 1.2$ $P = 2.2$. Despite the lack of a measured area, these initial conditions clearly result in an apparent horizon (and hence an event horizon) and so cannot be used for any conifold transition.

4.6.5 Conclusions

From these numerical simulations of the evolution of the deformed conifold, we again cannot form the conical singularity necessary for any topology transition to take place. We inevitably get an apparent horizon, an event horizon and hence a black hole spacetime. Again a range of possible initial momenta were tested and we still got a black hole solution (though other details such as the area and timescale were dependent upon this initial condition).

4.7 The Seven dimensional black hole solution

For both the case of a collapsing resolved conifold and a collapsing deformed conifold we have seen that an apparent horizon always forms, for our choice of initial momen-

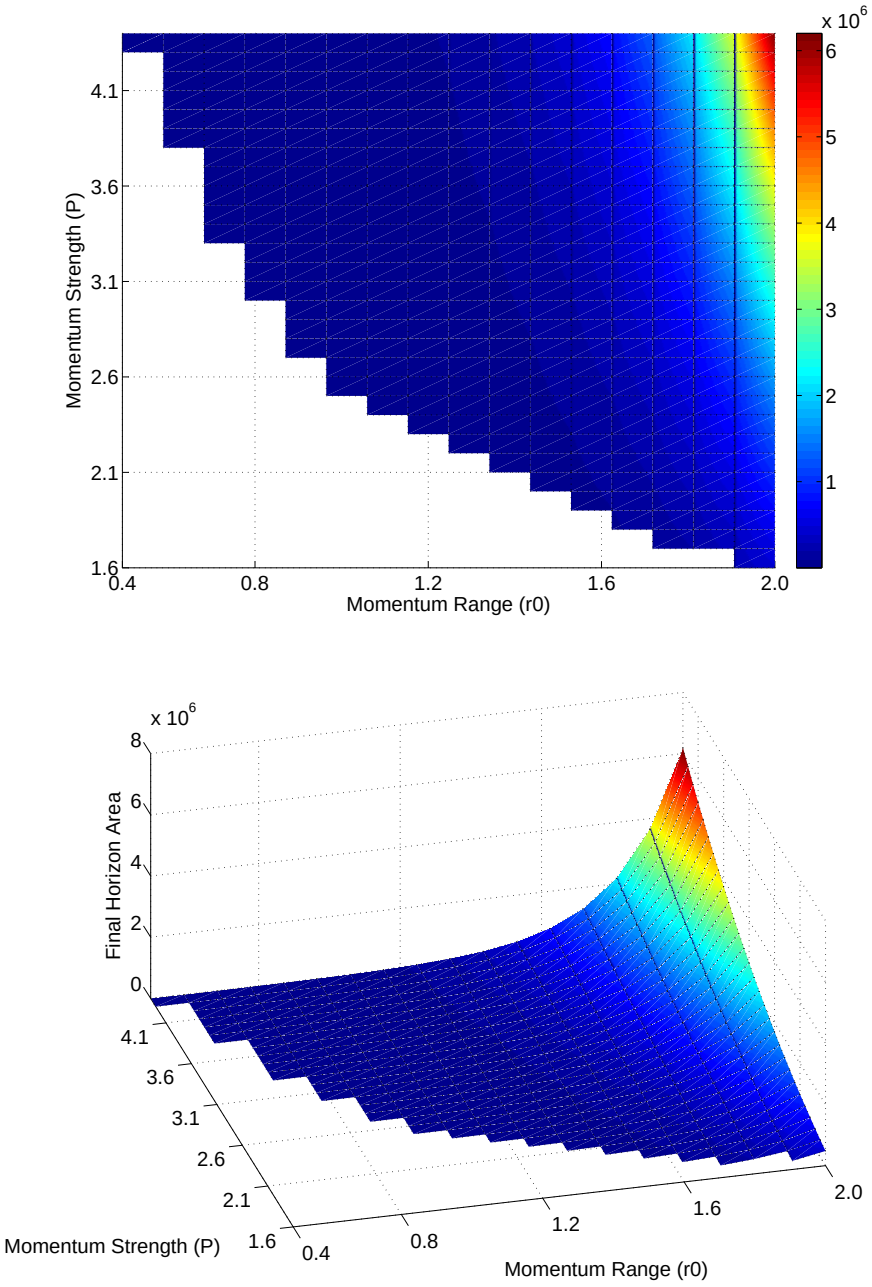

Figure 4.7: The effects on the creation of a black hole and its final area due to differing the initial P and r_0.

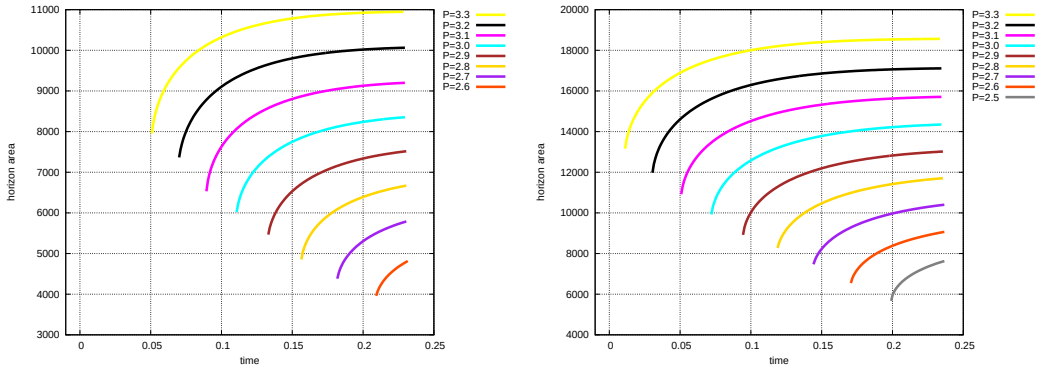

(a) $r_0 = 0.9$

(b) $r_0 = 1.0$

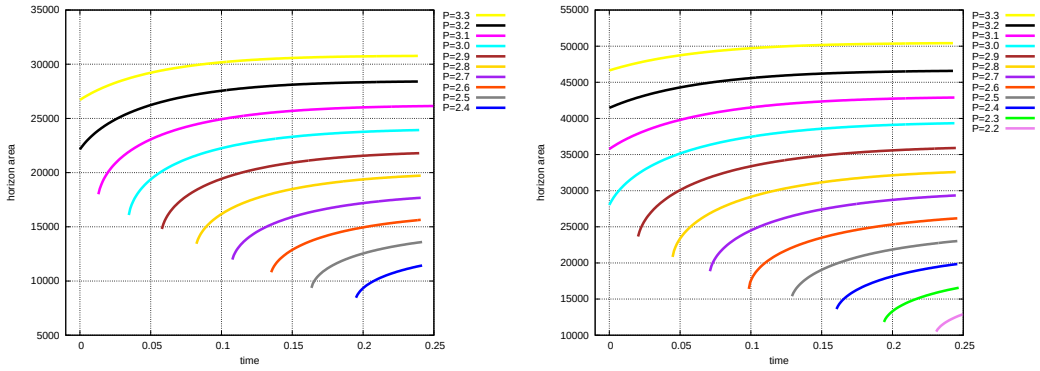

(c) $r_0 = 1.1$

(d) $r_0 = 1.2$

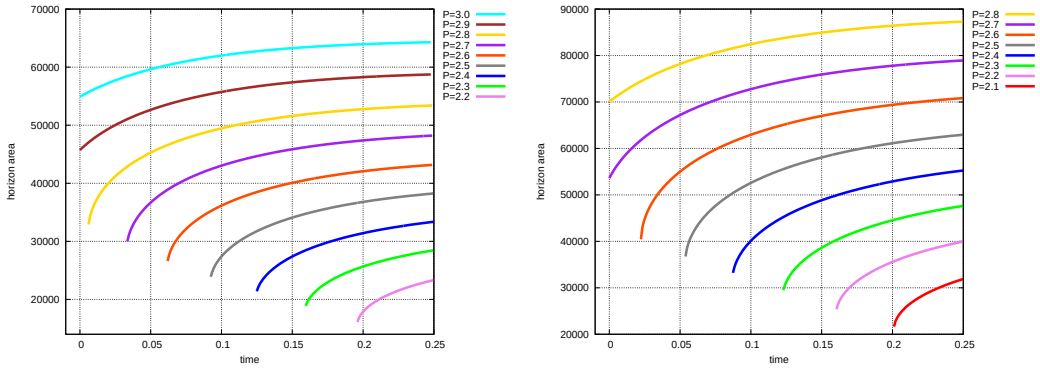

(e) $r_0 = 1.3$

(f) $r_0 = 1.4$

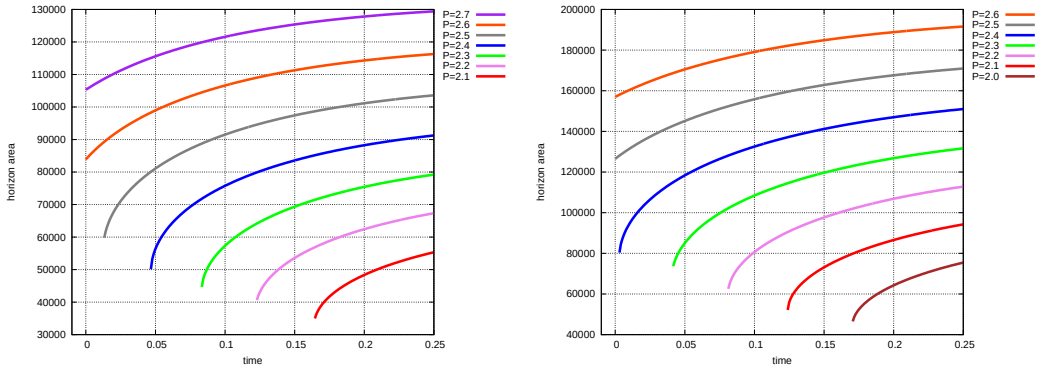

(g) $r_0 = 1.5$

(h) $r_0 = 1.6$

Figure 4.8: The effect of changing the strength of the momentum while keeping its range at a fixed value

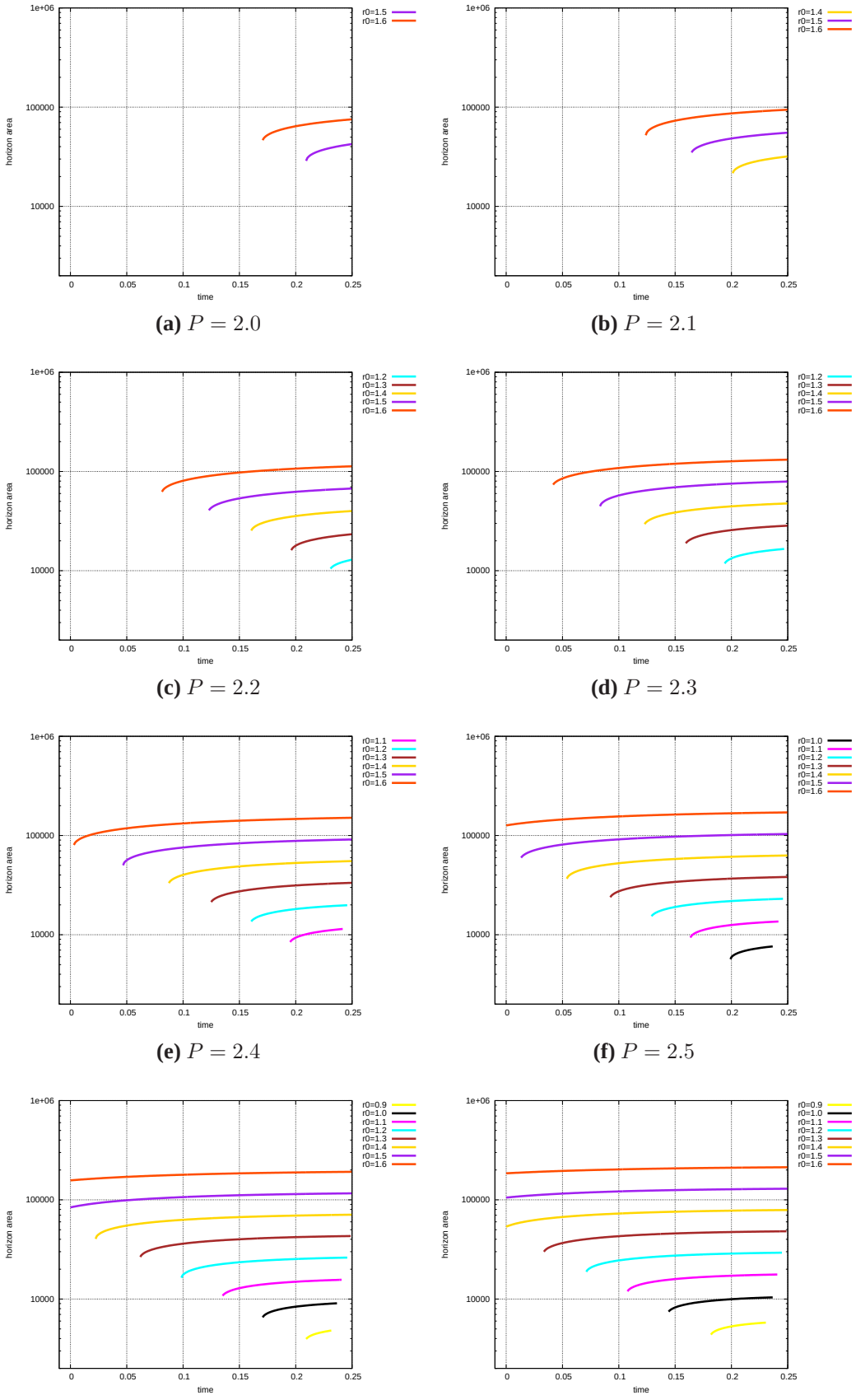

(a) $P = 2.0$ **(b)** $P = 2.1$

(c) $P = 2.2$ **(d)** $P = 2.3$

(e) $P = 2.4$ **(f)** $P = 2.5$

(g) $P = 2.6$ **(h)** $P = 2.7$

Figure 4.9: The effect of changing the range of the momentum while keeping its strength at a fixed value (log scale)

tum, and this therefore implies the presence of an event horizon. We have also seen that quantities such as the area of the apparent horizon, and the squashing modes of the angular part settle down to a constant value by the end of the simulation. This suggests that the final state of such collapses is a static black hole and so we hope to suggest a possible candidate for the resultant black hole.

We suggest a metric of the form

$$\begin{aligned} ds^2 = -f(r)dt^2 + \frac{1}{f(r)}dr^2 &+ b(r)^2(\sigma_1^2 + \sigma_2^2) \\ &+ c(r)^2(\Sigma_1^2 + \Sigma_2^2) \\ &+ d(r)^2(\sigma_3 + \Sigma_3)^2, \end{aligned} \tag{4.29}$$

as a candidate for the final state. So starting from this ansatz we found the equations for the profile functions by requiring Ricci flatness, these are given in the appendix E.3 Unfortunately we were unable to derive an analytic solution to these equations, but we have been able to solve them numerically, showing that sensible solutions exist, one such solution with an event horizon at $r = 1$ is presented in Fig. 4.10. At the location of the event horizon we have that f vanishes, with df/dr finite and non-zero, showing that it is simply a coordinate singularity. At the horizon we see that the profile functions b, c and d are all different, indicating that the horizon has a squashed angular geometry. We also see that the profile function, d, associated to the $U(1)$ direction $\sigma_3 + \Sigma_3$ tends to a constant, rather than increasing linearly as b and c do. This shows that the spatial section of the black hole is not asymptotically a conifold. This behaviour was also seen in the case of collapsing cycles in section 3.4.6 where the black hole formed in section 3.7 picks out a $U(1)$ direction to acquire a constant radius asymptotically.

These are candidates for the black holes formed by the collapse of the resolved conifold or, with appropriate coordinate transformations, the deformed conifold. We should of course be careful about the asymptotic structure of the solution which should not be altered by the collapse process near the origin. The discrepancy between the initial condition being asymptotically conifold and the black hole asymptotics is explained because the collapse takes an infinite amount of time to become the black hole, with a wave propagating outward from the collapse such that the interior is given by the black hole, and the exterior by the conifold.

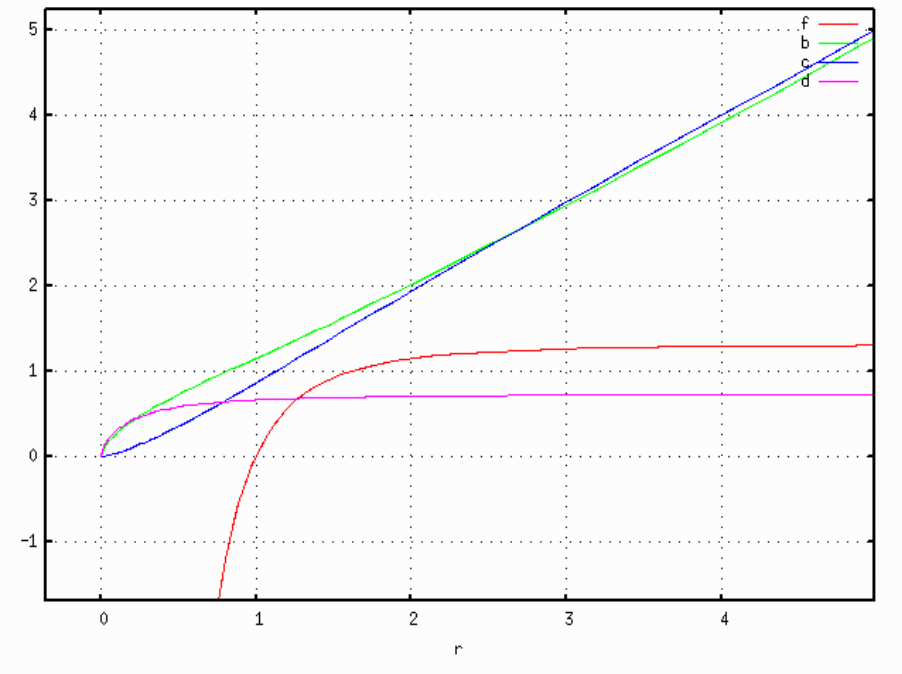

Figure 4.10: The defining functions of the static black hole, with horizon conditions $r = 1, f' = 4, f = 0, b = \frac{1}{2}\sqrt{3}$ and $d = \frac{2}{3}$.

4.8 Seven dimensional summary

In order to study the processes leading to the collapse of a two-sphere or a three-sphere, we have performed numerical simulations of two different, but related, cases of collapse. The resolved conifold, which involves a collapsing two-sphere, and the deformed conifold, which involves a collapsing three-sphere. These spaces are formed by two different methods of smoothing out a singular conifold, and it is using this singular conifold geometry that allows string theory to join the moduli spaces of these two regular, distinct geometries[54].

We have found that horizons are formed by the collapse of cycles in either of the two regular conifold solutions. These horizons take the form of two-sphere crossed with a squashed three-sphere. Such a horizon was formed in all the cases we studied, which is different to the situation found in five dimensional simulations where a study of the collapsing cycle in an Eguchi-Hanson geometry revealed cases where the cycle stopped collapsing, with no horizon being generated in section 3.4.6. However, there is a very large possible range of initial conditions, and the ubiquitous formation of a horizon may be an artifact of our choice.

Having established that horizons can form we have also found a possible candidate for the resulting black hole, by numerical means. This is a static black hole which also has a horizon comprising of a two-sphere crossed with a squashed three-sphere. An intriguing feature of this black hole, and one that it shares with the black hole of section 3.7, is that the asymptotic geometry contains a constant radius circle.

In cases where the horizon size is greater than the scale of the strings the field theory should be a valid approximation, but this may not be the case. This presents us with the natural extension of this work, as we have not yet introduced any stringy effects(that may resolve the singularity) such as those of section 2.6.3.1 despite the importance of these effects if horizons form at string scales, we shall go on to introduce the supergravity effects as we increase the dimensions to ten.

Chapter 5

Ten dimensional evolution

The procession from seven dimensions to ten brings many more applications to the results we produce. Ten dimensions are well used within string theories as superstring theories actually require there to be ten dimensions. Observing that we see three extended dimensions in our space and one timelike dimension, it is often thought that the remaining six are compactified into a closed manifold. While the previous simulations may have applications for this internal manifold, the coming results will better encompass the effects we may see within the supergravity approximation to string theory.

We shall introduce the fluxes which arise by supergravity and are predicted by string theory. While these can be consistently turned off and so result in a purely gravitational situation, we do not believe this to be the a good choice due to the strengths of flux compactification. Introducing these fluxes is necessary if we want results applicable to flux compactified internal manifolds.

The ten dimensional simulation also introduces the three extended spacelike dimensions. Even if we insist that the 4 extended dimensions have maximal symmetry (making them conformally Minkowski, de Sitter or anti-de Sitter) the conformal scale factor shall still be dependent upon r and t. Changes to the scale factor in time and in space will result in changes to the dynamics of the internal manifold due to the effects of Hubble damping whereby growth of the scale factor damps energy which would otherwise remain in the internal manifold. The reduction in the energy density can slow the changes to the internal manifold or prevent the energy density from forming black

holes.

All these effects are possible but a true simulation will show if they are realised in an actual case. This requires a starting initial manifold and a good choice of initial momentum.

There exists a solution which represents a supersymmetric deformed conifold that is held in place by the presence of fluxes [80], and has found many applications in the realm of flux compactification [84] and brane inflation [85]. Such calculations rely on this static Klebanov-Strassler geometry, without taking into account its own dynamics. If the dynamics of the Klebanov-Strassler geometry become significant then these calculations would need to be re-visited.

5.1 The Klebanov-Strassler static solution

A static warped throat solution exists which was found by Klebanov and Strassler [80]. This in turn made use of the deformed conifold which we described in section 4.3. This static six dimensional manifold can act as a good approximation to a region of the six compact dimensions used in a flux compactification. The remaining extended dimensions could be formed by a product of the deformed conifold with a 3+1 Minkowski metric $ds_{1,3}$.

$$ds_{10}^2 = ds_{1,3} + ds_{Def}^2. \tag{5.1}$$

However this approach is only the simplest case, the Klebanov-Strassler solution also includes D-branes along with the fluxes of type IIB supergravity and the resulting energy momentum tensor produces a warped metric and a warped throat.

5.1.1 D-brane sourced fluxes

If we introduce N D3-branes and further supplement this with M D5-branes wrapped around the two-sphere of a deformed conifold (these have previously been coined "fractional D3-branes") then it corresponds to taking a Calabi-Yau manifold with deformed conifold singularity and introducing a large flux through the three-sphere[86,

87]. The effect of combining ds_{Def} with (fractional) D-branes is to source fluxes which contribute to the Energy-Momentum tensor of the Einstein equation. The fluxes of the static case are described in terms of the metric coordinates and the one forms g^i as described in section B.3.

5.1.1.1 Dilaton

The dilaton in this static solution is a constant, which is given by the string coupling of the IIB string theory,

$$e^{\phi} = g_s = constant. \tag{5.2}$$

5.1.1.2 Neveu-Schwarz flux

The NS two-form field takes the form

$$B = B_\alpha(r)\, g^1 \wedge g^2 + B_\beta(r)\, g^3 \wedge g^4 \tag{5.3}$$

where

$$B_\alpha(r) = g_s M \frac{r\, \coth(r) - 1}{2\, \sinh(r)} (\cosh(r) - 1) \tag{5.4}$$

$$B_\beta(r) = g_s M \frac{r\, \coth(r) - 1}{2\, \sinh(r)} (\cosh(r) + 1) \tag{5.5}$$

This leads to the three-form field strength H by (2.23).

5.1.1.3 Ramond-Ramond fluxes

The Klebanov-Strassler solution has no C_0 term and so has no one-form Ramond-Ramond flux which means there is no axion

$$F_1 = 0. \tag{5.6}$$

There is a potential which sources the Ramond-Ramond three-form flux,

$$C_2 = M \frac{\sinh(r) - r}{2\, \sinh(r)}\, (g^1 \wedge g^3 + g^2 \wedge g^4) \tag{5.7}$$

this potential contributes to a three-form flux via (2.21). In addition there is also a contribution to this three-form flux coming from the charged sources which we have placed at the origin, this comes from the stack of M D3-branes and contributes an additional (closed) term to the flux in the direction of the blown up sphere $g^5 \wedge g^3 \wedge g^4$, giving

$$F_3 = M\, g^5 \wedge g^3 \wedge g^4 + dC_2. \tag{5.8}$$

The final Ramond-Ramond flux is the five-form, self dual F_5. Its self duality condition along with the equation of motion and our choices of F_3 and H lead to the solution that,

$$F_5 = B \wedge F_3 + *(B \wedge F_3). \tag{5.9}$$

5.1.2 Warp factor

The fluxes cause a warping of the metric, changing it from a Ricci flat metric to a metric with curvature, this is appropriate since the fluxes contribute to the energy momentum tensor. The new fluxes require a change to the metric (5.1), making the Minkowski scale factor depend upon the radius of the deformed conifold component and so we get conformal symmetry breaking (for non-zero M). This r dependence is introduced by means of a function, $h(r)$.

$$ds_{10}^2 = h^{-\frac{1}{2}}(r)\,(ds_{1,3}) + h^{\frac{1}{2}}(r)\left(ds_{Def}^2\right) \tag{5.10}$$

The introduction of this $h(r)$ changes the scales and removes the conformal invariance. The nature of $h(r)$ in the static case is given by a differential equation.

$$\frac{d\,h(r)}{dr} = -\alpha\,\frac{2^{\frac{2}{3}}}{4}\,\frac{r\,\coth(r) - 1}{\sinh^2(r)}\,\left(\sinh(2r) - 2r\right)^{\frac{1}{3}}. \tag{5.11}$$

To totally define $h(r)$ we also need a boundary condition (to complement the 1st order differential equation), Klebanov and Strassler impose the restriction that h must vanish at high r, this fully defines $h(r)$ which is plotted in Fig. 5.1.

$$\lim_{r\to\infty} h(r) = 0. \tag{5.12}$$

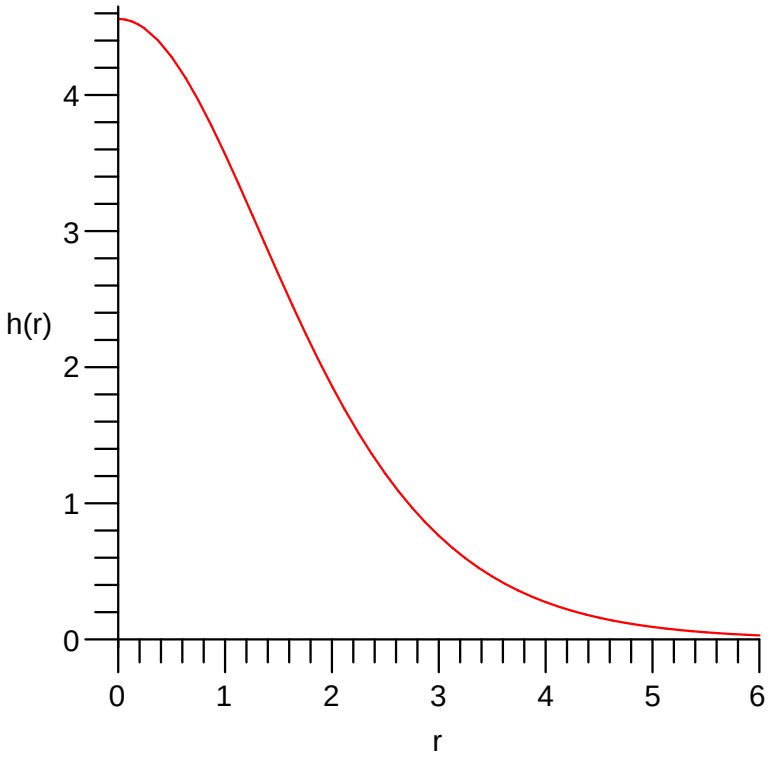

Figure 5.1: The warp factor vanishes at high r

The vanishing warp factor means that the radius of the three-sphere (which grew like r in ds_{Def}) now grows only very slowly, in fact the radius only grows like $r^{1/4}$ leading to the expression ”throat”, Fig. 5.2.

5.1.3 Superpotential and stabilised moduli

The introduction of the flux leads to a potential which can be found from the Hamiltonian constraint, as is described in [21] and used in [88]. This potential is then used to find a prediction to the evolution of the moduli field. Taking a slice through this moduli space along which only the volume of the three-sphere is permitted to change, we find the potential as a function of this volume[89]. This method results in a potential of the form plotted in Fig. 5.3. The potential diverges very quickly as the volume gets small, it permits a minima at a position determined by the other moduli and parameters (such as M), and tends to grow (albeit quite slowly) as the volume gets very large. The minima represents the static warped deformed throat solution of Klebanov

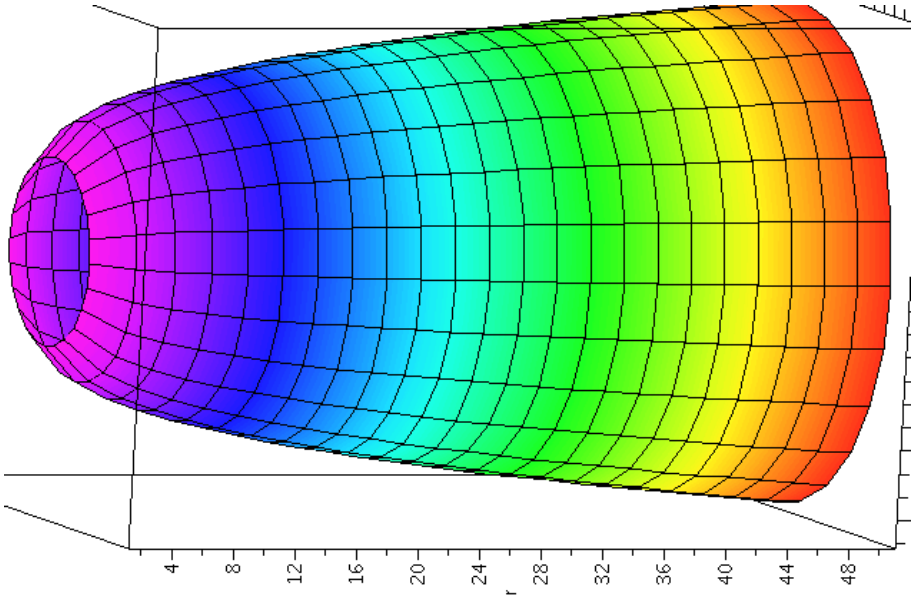

Figure 5.2: The radius of the three-sphere growing only very slowly at high r

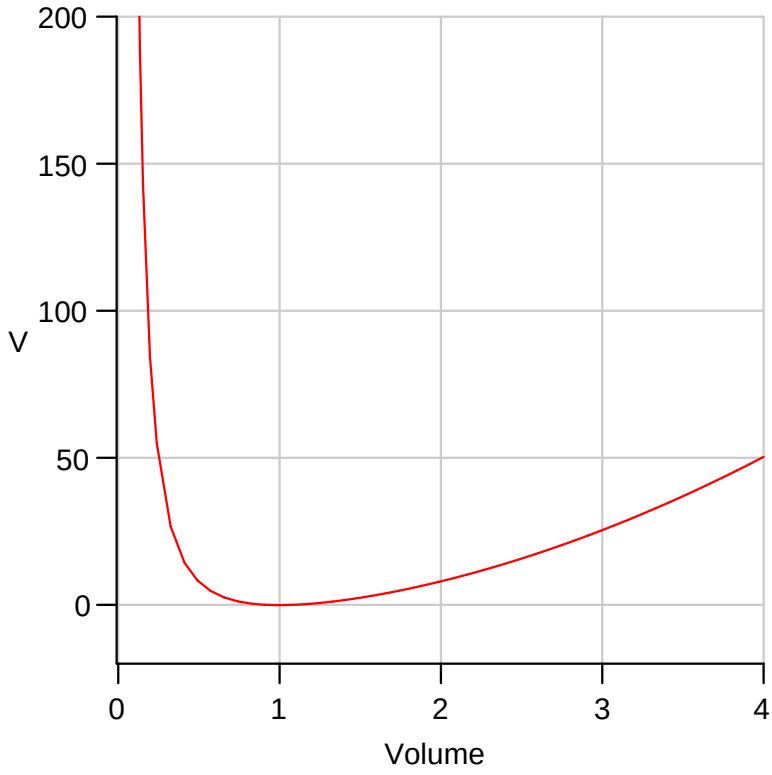

Figure 5.3: The potential as a function of the volume of the three-sphere in Planck units

and Strassler. The scale of the compactified dimensions is now set by the fluxes, the size of the three-sphere at the origin (ϵ of (4.6)) is stabilised according to the minima of the potential and is no longer a free modulus, in the static case it must conform to

$$\epsilon = \left(\frac{16 M^2 g_{string}}{\alpha} \right)^{3/8} . \tag{5.13}$$

This potential shows that other values of epsilon are not static and it gives a good estimation as to how unfavourable other values of the moduli are. We will later use our knowledge of the behaviour of the moduli to estimate how the volume of the three-sphere (a physical property of the throat which is initially related to the value of ϵ) will evolve.

5.2 Uses of the Klebanov-Strassler solution

The Klebanov-Strassler solution is not compact and so it is not a candidate for a global flux compactification, however it is thought that the warped throat possessed by the solution may be a good approximation to some other warped throat which makes up part of a compact manifold which could be used for compactification. Using the Klabanov-Strassler solution has allowed people to find the effects of having a warped throat as part of the internal compact manifold. Internal manifolds with throats can lead to useful consequences for the four extended dimensions.

Warped throats have been used in a wide range of inflation models such as warm inflation, DBI inflation, spinflation, hybrid inflation and brane inflation where further branes and anti-branes are included in the compactification to produce slow roll inflation scenarios[90, 91, 92, 93].

It has been suggested that the warped throat in the extra dimensions could be preventing us from seeing dark matter[94]. Matter which is trapped in the gravitational potential of the throat will be hidden from us if the standard model is located elsewhere. It is also suggested that this hidden dark matter could later be detected by its decay (probably via other intermediate particles) into standard model particles.

There have been attempts to recreate the standard model localised at the tip of the throat. Some[95] attempt this by finding a D-brane configuration creating the local

properties of the model (e.g. massless matter, gauge group, running of coupling) and then combining this with a compactification manifold to determine global features. Localising the model to the tip of the throat can naturally create a hierarchy due to the strong warping near the tip, this could go to explain the difference between the Planck scale and the electroweak scale[96] which would go to further explain the features and scales within the standard model. In the throat there is an IR scale below the UV compactification scale which helps justify the hierarchy[97].

5.3 Dynamical evolution of the Klebanov-Strassler solution

The Klebanov-Strassler solution is a static solution and so should not change in time (it has a timelike killing vector which we take to be the time). However it is possible that the Klebanov-Strassler solution matches a single timeslice of an evolving spacetime which will go on to change at later times. If this timeslice is taken as the initial condition we arise at a situation where a Klebanov-Strassler solution changes in time due to an initial momentum which causes it to evolve. The future evolution of the timeslice is a Cauchy problem and can be found using the Einstein field equations. This evolution also prompts the fluxes to change so these too must be allowed to change according to the equations of motion.

5.3.1 Moduli and perturbative approximations to the dynamics

Some approximations to the dynamical changes the Klebanov-Strassler solution will undergo can be made by looking only at the changes to one of the moduli at a time. These dynamics will likely only be true for short periods of time (as was the case in section 3.4.6.1) but they can give a good approximation to the dynamics of a single feature. The feature we choose to follow is the volume of the three-sphere at the tip of the solution. Our approximation relies heavily upon the potential we found in section 5.1.3, not only does this give the value of the moduli ϵ in the static case, it also shows that the moduli is stable. This implies the volume is also a stable property. Since we

do not have an analytic expression for the potential the predictions we make will also not be analytic (unlike section 3.4.1) however they still give us the behaviour.

The steep potential of ϵ smaller than the static case leads to the prediction that the volume will be especially stable against effects which would go to reduce the volume. The potential raises to a high value as we approach a vanishing ϵ so it should be very difficult to produce a very small volume. Also the moduli is unstable at these small values so it is unlikely that the volume will remain at rest there.

If the size of the three-cycle begins to rise then the same claims are true, the potential raises as ϵ goes up and so the growth of the volume is not predicted to continue for ever but should tend to slow down, we would also predict that it would tend to fall back to its stable value however the shallower potential gives rise to a weaker restoring force.

These predictions rely on a potential formed by the assumption that only one modulus changes. This shall not be the case however as any initial momentum applied shall not change only one modulus but will directly or indirectly cause other features of the spacetime solution to change. These other changes are not accounted for by this type of approximation and these predictions are incapable of testing for black hole formation so further investigation of the dynamics must be performed.

Earlier work[98, 99, 100] has attempted to discover the dynamics of warped throats by using perturbative methods. These permit only very small initial momentum to be added to the initial surface and are only applicable to scales below those of later numerical investigation. If the momentum were added in a general fashion then it would tend to violate what we call our momentum constraint so not being a solution to all the Einstein equations. This has sometimes been addressed by the inclusion of compensators which act to correct this difficulty. They can be viewed as Lagrange multipliers used to enforce the otherwise violated constraints.

These perturbative methods have gone to show that the throat is stable against sufficiently tiny introductions of momentum[98, 99, 100]. However the results can only be applicable to low order and to low energy scales so a full numerical investigation of the dynamics must still be performed.

5.3.2 Numerical evolution of the Klebanov-Strassler solution

If we start with the static solution then no change will happen as we move to later times, however with only a small initial perturbation the metric and the fluxes are observed to evolve. It is our intention to introduce an initial perturbation that changes the size of the three-sphere at the origin of the deformed conifold, possible outcomes include the formation of a black hole solution; the collapse of the three-sphere to a naked singularity; or the sphere may change size without collapsing all the way to zero. To observe the effects of an initial deformation we use a more general metric and flux ansatz, a system with the capacity to be time dependent, and then observe the effects we can incite with a small initial perturbation[89].

5.3.3 Time dependent spacetime ansatz

5.3.3.1 Spacetime coordinates

We choose a metric that is capable of changing in time and is also able to evolve numerically at the origin.

$$\begin{aligned} ds_{10}^2 = \quad & T^2(t,r)\, h^{-\frac{1}{2}}(r)\, (ds_{1,3}) \\ & + a^2(t,r)\, h^{\frac{1}{2}}(r)\, \frac{1}{2}\epsilon^{\frac{4}{3}}\, K(r)\, \left(\frac{1}{3K^3(r)}\right) dr^2 \\ & + b^2(t,r)\, h^{\frac{1}{2}}(r)\, \frac{1}{2}\epsilon^{\frac{4}{3}}\, K(r)\, \left(\sinh^2(r/2)\right) ((g^1)^{\,2} + (g^2)^{\,2}) \\ & + c^2(t,r)\, h^{\frac{1}{2}}(r)\, \frac{1}{2}\epsilon^{\frac{4}{3}}\, K(r)\, \left(\cosh^2(r/2)\right) ((g^3)^{\,2} + (g^4)^{\,2}) \\ & + d^2(t,r)\, h^{\frac{1}{2}}(r)\, \frac{1}{2}\epsilon^{\frac{4}{3}}\, K(r)\, \left(\frac{1}{3K^3(r)}\right) ((g^5)^{\,2}), \end{aligned} \tag{5.14}$$

where $K(r)$ is defined in (4.7). The profiles $T(t,r)$,$a(t,r)$,$b(t,r)$,$c(t,r)$ and $d(t,r)$ define the metric at all times.

We also had to impose boundary conditions at the origin of the simulation. These conditions were to ensure that local flatness remained at later times[66].

$$c^2(t,r)|_{r=0} = d^2(t,r)|_{r=0}, \tag{5.15}$$

$$b^2(t,r)|_{r=0} = a^2(t,r)|_{r=0}. \tag{5.16}$$

We also required that all these profile functions were always even at the origin.

$$\begin{aligned} T(t,r) &\sim T^0(t) + \mathcal{O}(r^2), \\ a(t,r) &\sim a^0(t) + \mathcal{O}(r^2), \\ b(t,r) &\sim b^0(t) + \mathcal{O}(r^2), \\ c(t,r) &\sim c^0(t) + \mathcal{O}(r^2), \\ d(t,r) &\sim d^0(t) + \mathcal{O}(r^2), \end{aligned} \tag{5.17}$$

$$a^0(t) = b^0(t), \quad c^0(t) = d^0(t) \tag{5.18}$$

At later times the size of the three-sphere at the origin can be found from $c^0(t)$ and $d^0(t)$.

5.3.3.2 Flux ansatz

Of course we must also allow the fluxes to change with time (as they almost certainly will when the metric is numerically evolved).

Initially the axion is constant and the equations of motion show this can continue to be the case even at later times,

$$F_1 = 0. \tag{5.19}$$

Also the dilaton is initially constant at all points however this is now required to change at later times,

$$\phi = \phi(t,r). \tag{5.20}$$

The M fractional branes that we have placed at the origin will not change but will always give R-R flux through the three-sphere, however the potential C_2 can now change in time, but is dependent upon only a single function we call $C_\alpha(t,r)$,

$$C_2 = C_\alpha(t,r)\ \left(g^1 \wedge g^3 + g^2 \wedge g^4\right). \tag{5.21}$$

F_3 is still the combination of the flux from the M fractional branes and the potential C_2 as in (5.8).

The NS-NS three-form flux, H, is initially described by two separate functions of r labeled $B_\alpha(r)$ and $B_\beta(r)$, these are used as a description of B in (5.3).

We now promote these radial profiles to time dependent functions,

$$B = B_\alpha(t,r)g^1 \wedge g^2 + B_\beta(t,r)g^3 \wedge g^4. \tag{5.22}$$

giving just these two functions time dependence allows H to change at later times according to (2.23).

Even at later times the R-R five-form flux is still determined by the other fluxes according to (5.9).

This means that all the fluxes are defined by the metric and four profile functions, $\phi(t,r)$, $C_\alpha(t,r)$, $B_\alpha(t,r)$ and $B_\beta(t,r)$. It is these functions that we will evolve using the equations of motion.

In addition to the equations of motion, we also imposed boundary conditions on these functions, we required that $B_\alpha(t,r)$ and $B_\beta(t,r)$ be odd, $\phi(t,r)$ be even and $C_\alpha(t,r)$ be even and must vanish at the origin, as can be seen from the equations of motion in appendix F.3.

$$\begin{aligned} \phi(t,r) &\sim \phi^0(t) + \mathcal{O}(r^2), \\ B_\alpha(t,r) &\sim \mathcal{O}(r), \\ B_\beta(t,r) &\sim \mathcal{O}(r), \\ C_\alpha(t,r) &\sim 0 + \mathcal{O}(r^2). \end{aligned} \tag{5.23}$$

This choice of fluxes is capable of acting as the initial conditions and also evolving consistently to later times.

5.3.4 Initial conditions

By comparing the static warped deformed conifold metric (5.10), and our time dependent ansatz (5.14), we can read off the initial metric conditions a term at a time.

$$T^2(0,r) = a^2(0,r) = b^2(0,r) = c^2(0,r) = d^2(0,r) = 1 \tag{5.24}$$

Flux is added when we give M a non-zero value (we introduce fractional branes), its strength depends upon our string coupling g_{string} and the number of branes M. The initial values of the fluxes can be found by comparing the ansatz in section 5.3.3.2 to the solution in section 5.1.1.

$$e^{\phi(0,r)} = g_{string}, \tag{5.25}$$

$$B_\alpha(0,r) = g_{string} M \frac{r\,\coth(r)-1}{2\sinh(r)}(\cosh(r)-1), \tag{5.26}$$

$$B_\beta(0,r) = g_{string} M \frac{r\,\coth(r)-1}{2\sinh(r)}(\cosh(r)+1), \tag{5.27}$$

$$C_\alpha(0,r) = M\frac{\sinh(r)-r}{2\sinh(r)}. \tag{5.28}$$

This also requires that $h(r)$ is still defined as it was in (5.11) and also tends to zero asymptotically. We found $h(r)$ numerically as we input the initial conditions.

These initial conditions give the static solution, so if all the momenta (e.g. $\dot{T}$) are zero to begin with then no evolution should occur. If instead we start with non zero momenta we perturb the metric away from the static case and can go on to see the future evolution.

5.3.4.1 Initial momentum

In order to best represent a physical system we make our perturbation localised by choosing a momentum which will vanish as we go to large r. So we add momentum going like:

$$\frac{\dot{c}}{c} = \frac{\dot{d}}{d} = -Pe^{-r^2}. \tag{5.29}$$

So a positive value of P will cause the size of the three-sphere at the origin to initially fall but this may only be temporary, whereas a negative P will cause the three-sphere to grow (the symmetry between c and d maintains the local flatness (5.15)).

Our initial momentum must also conform to the constraints upon the Hamiltonian and the momentum imposed by the Einstein equations (in appendix F.2). This requirement was used to numerically find the initial values of $\dot{a}$ and $\dot{b}$, we started by imposing the constraint

$$\dot{a}|_{r=0} > 0 \qquad \dot{b}|_{r=0} > 0. \tag{5.30}$$

The choice of $\dot{T}$ was made to aid the numerical integration:

$$\frac{\dot{T}}{T} = Pe^{-r^2}. \tag{5.31}$$

We kept the values of the string coupling and the number of fractional branes consistent throughout all plotted simulations, $Mg_{string} = 120$ and $M = 30$, we also specified the warping α so that the static solution was at $\epsilon = 1$.

5.3.5 Results

In order to best summarise the results of our perturbed evolution we were constantly watching the size of the three-cycle at the origin of the solution. If this shrinks it shows that the origin is becoming closer to that of a conifold, approaching the formation of a conical singularity, with the three-sphere vanishing being the most extreme case. Alternatively we can find other outcomes, such as the formation of black holes.

We will attempt to discover if and when black holes have formed by looking for apparent horizons on the timeslice. If the area of the apparent horizon converges upon a constant value then we can take this value to be a good estimate to the area of the resultant event horizon.

5.3.5.1 Bounce of the cycle

In order to prompt the size of the three-sphere to drop we introduce a momentum of the form described in section 5.3.4.1 with $P > 0$, this forces a drop in the size of the sphere but our results show that this is a temporary effect. As is seen in Fig. 5.4, after quickly reaching some minimum value (which depends on the strength of the momentum) the size of the three-sphere then proceeds to grow, tending back to a value close to its starting value. This is an expected behaviour since the size of the three-sphere is no longer a free modulus, in the static case it is determined by the fluxes passing through the cycle. Since the string coupling and the number of branes are unchanged by the momentum the static value or ground state is unchanged and so the three-sphere will tend to return to this value. The size of the three-sphere tends to flow to the flux-preferred value. This can be seen to be true and quickly realised even for

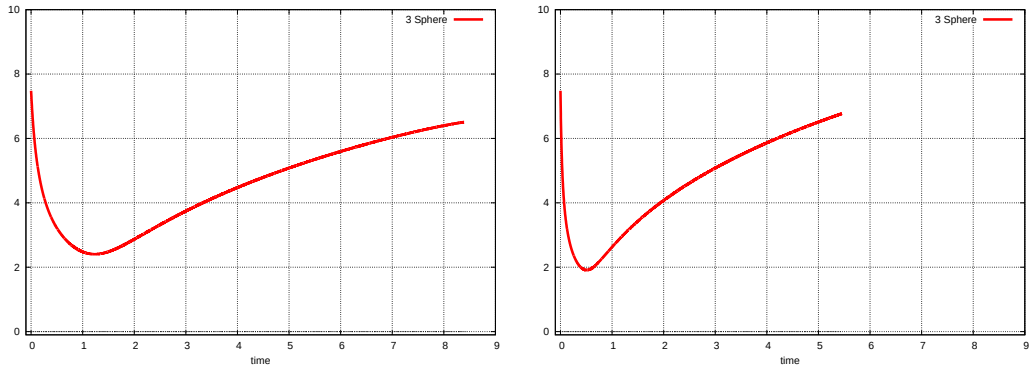

(a) $P = 50$ **(b)** $P = 200$

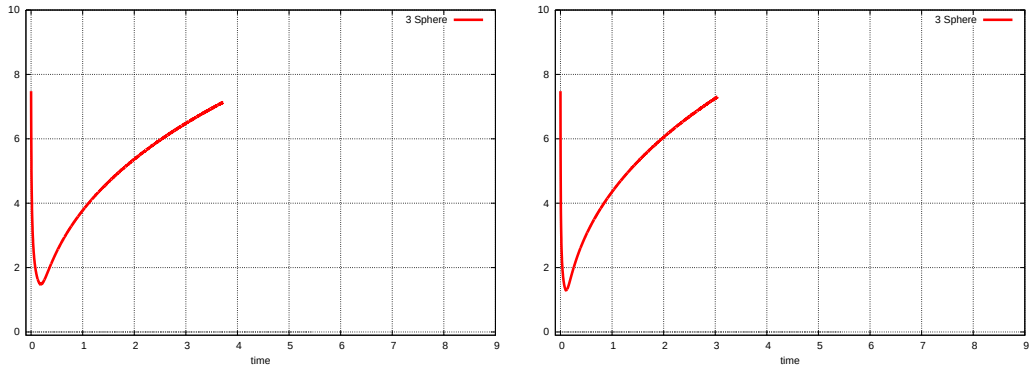

(c) $P = 900$ **(d)** $P = 2000$

Figure 5.4: The size of the three-sphere begins to fall but reaches a minima then returns to its starting value

initial momenta hundreds of times the warped deformed scale, showing the restoring force to be very strong indeed. This is expected behaviour due to the swift divergence of the potential at low radius, as shown Fig. 5.3.

In these cases we were constantly checking for the formation of a black hole however no apparent horizon is formed and so we believe the solution is free of black hole formation.

5.3.5.2 How low can it go?

Though the size of the three-sphere can be seen to return to its initial value, it first drops to a minimum value dependent upon the initial momentum. If we continue to increase the scale of initial momentum we can ask how low we can force the three-sphere to drop, could it be that there is some (very high) momentum which causes the sphere to drop to zero before it stops falling? We can find the lowest value which the three-sphere falls to for a range of initial momentum. As shown in Fig. 5.5 the size

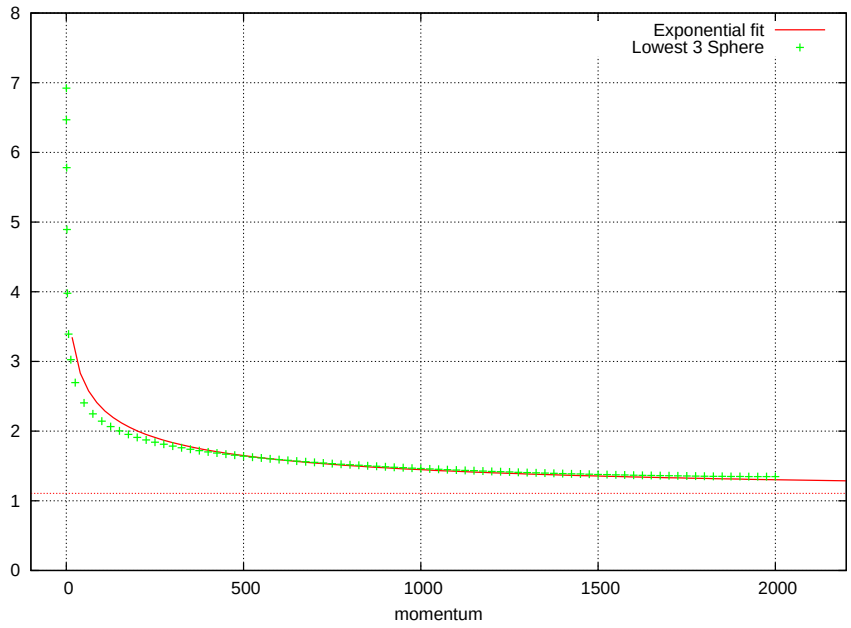

Figure 5.5: The smallest size the three-sphere reaches for a range of momenta

does drop with the initial momentum but it drops at a decreasing rate and it would take a huge momenta to even approach zero (it actually looks as though the asymptotic behaviour may not be to zero but to a constant, lowest possible, sphere size). We can fit this profile well to an exponential function of the form,

$$\alpha_0 + \beta_0 e^{-\gamma_0 P^{1/4}}. \tag{5.32}$$

(also plotted in Fig. 5.5) we can see that causing the sphere to vanish (if it is possible) would require incredible initial momentum way beyond the capabilities of our simulation.

5.3.5.3 Growth of the cycle

We also consider cases with similar initial momentum but obeying $P < 0$. These will tend to cause the size of the sphere at the origin to grow. Again we would expect (from our potential) this growth to be only temporary and that the size would fall back towards the starting value, as the static case is still determined by the fluxes and it is this value we would expect the size of the tip to flow to. We do see this slowing of the growth as is shown in Fig. 5.6, but slowing down takes so long that the restoration of the size is not seen within the timescale of the simulation, this can be attributed to a shallow restoring potential. We believe that the three-sphere would eventually return

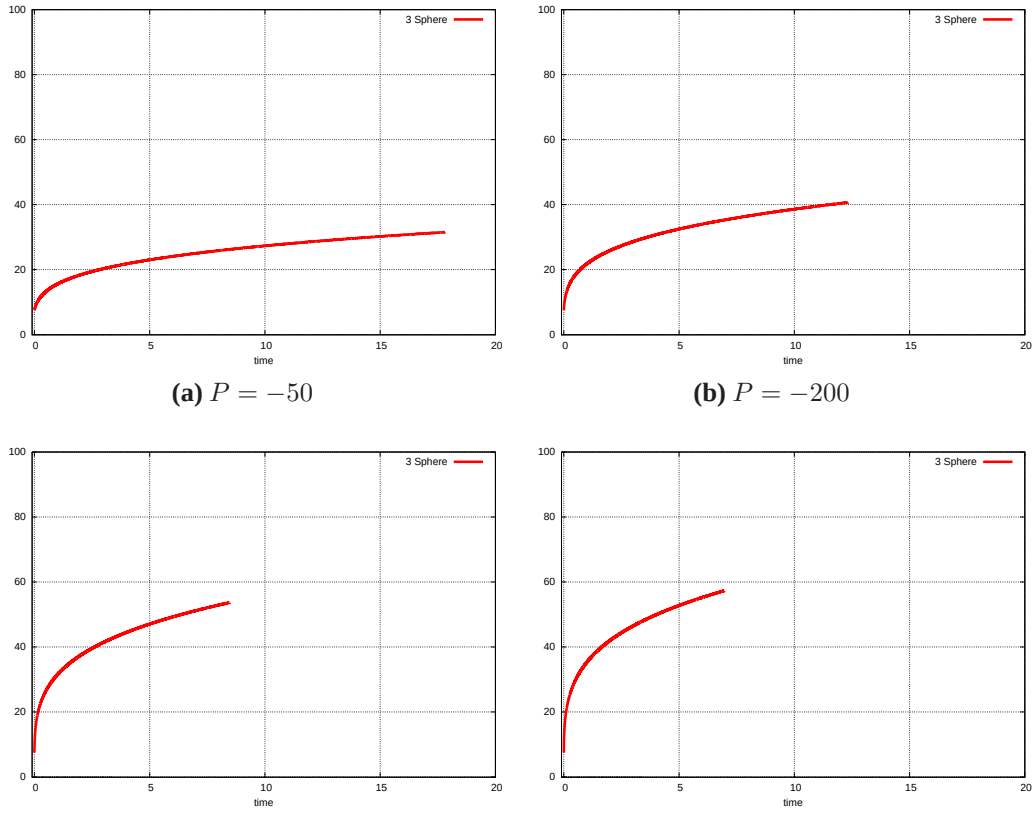

(a) $P = -50$ **(b)** $P = -200$

(c) $P = -900$ **(d)** $P = -2000$

Figure 5.6: The size of the three-sphere begins to grow but at a decelerating rate

to the starting value (the static case) but this takes a very long time. This situation was also free of apparent horizons.

5.3.5.4 Black hole formation

Relaxing the condition (5.30) was also attempted. This made the situation far more susceptible to the formation of black hole horizons, detectable by shells obeying the apparent horizon condition of section 2.2.2. The presence of an apparent horizon can often occur already in the initial conditions due to a high initial momentum giving an extrinsic curvature, but the late time creation and growth of an apparent horizon is also a strong possibility, as shown in the example of Fig. 5.7. These horizons would be intolerable if we wished to achieve results such as inflation, topology change or moduli stabilisation for the purposes of string phenomenology, any interesting effects would be enclosed behind the horizon. Even very weak initial conditions ($|P| = 1$) already contain apparent horizons before the simulations starts, and weaker conditions

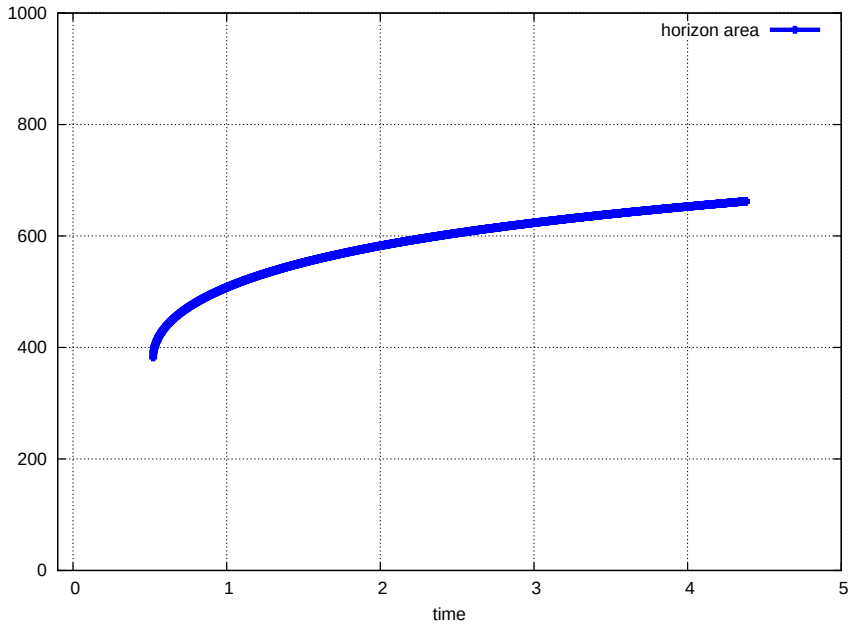

Figure 5.7: $P = 0.7$: The size of the horizon area begins to grow but at a decelerating rate

still form them within a small time.

This shows that adding even a small initial momentum to appropriate metric functions (g_{rr} and g_{11}, g_{22} in this case) introduces a risk of creating black holes. A momentum which would solely change the size of the three-sphere is disallowed by the Hamiltonian and momentum constraints, other changes to the initial conditions must be applied and the nature of these will determine the creation of a black hole.

5.4 Ten dimensional summary

So in summary, we have attempted to change a warped throat solution to a singular manifold by adding some initial momentum to a known static solution with a warped throat, the Klebanov-Strassler solution. The production of such a singular manifold would be essential for the initiation of a transition which could go on to change the topology of the internal manifold.

In cases where we insert momentum which tends to increase the size of the three-sphere then the growth slows down on a much longer timescale as one would expect on physical grounds by diluting flux-lines rather than squeezing them. This leads to a shallow potential in this direction, and a geometry that is more susceptible to growth

than collapse of the three-sphere. We believe the growth would eventually stop and the size of the three-sphere would tend back to its starting value, however this is not seen in simulation due to the much larger timescales involved.

More applicable were cases which reduced the size of the three-sphere and like the other simulations in lower dimensions we found no combination of initial momentum which could bring about the reduction of the three-cycle to a point while at the same time preventing the creation of a black hole spacetime. In some cases of momenta which would tend to reduce the volume of the tip we found the the size was stable against the change and went on to return to its starting value. This is attributed to a steep restoring potential which accompanies the branes and the fluxes of the Klebanov-Strassler solution. This restoration of the cycle prevented it from collapse and impeded the possibility of the transition. In other cases the momenta would form an apparent horizon in the spacetime and so obscure the cycle from an outside observer, again preventing a transition.

While these findings suggest that the transition cannot be achieved, they do not rule it out. Due to the limitless possibilities for initial momentum of both the spacetime and the fluxes, we cannot test all the possible combinations and so we cannot show that transitions are totally prevented, however these results do suggest that transitions will fail.

The results do numerically verify that the tip of the throat is stable against perturbations and so a warped throat can be used as a background for many of the processes described in section 5.2, without fear of it collapsing to zero size or even changing size much at all. The results also show that the creation of black hole solutions by changing the throat is a risk and any of the models which use this throat should check that the added effects are of a type and scale which will not result in a black hole.

Chapter 6

Discussion

One of the earlier problems we discussed in string theory was the requirement that it must be in a ten dimensional spacetime (and M theory would need eleven dimensions). These extra dimensions have never been seen and need to be accounted for. One possible resolution of this problem is compactification which means that the additional dimensions have previously gone unnoticed due to their small size. The small size dimensions would only be made visible by very high energy experiments beyond the capabilities of foreseeable accelerators.

Compactification possibilities are confined to an unwarped 3+1 Minkowski metric and some internal manifold which is Calabi-Yau. These compactifications retain N=2 supersymmetry and they are plagued by the possibilities of degenerate moduli which would be visible as scalars in the low energy theory and would violate the equivalence principle. Flux compactification offers more freedom of manifold and additional strengths. It brings the possibility of moduli stabilisation whereby the potentially difficult scalar fields which arise due to the degeneracy of the compactification under continuous deformations are given a potential with a local minima. This is a stable point from which they will be resistant to change and it would be seen as a mass in the scalar field, preventing the force being of infinite range and would restore the equivalence principle.

While compactification and flux compactification allow us to bypass the difficulty of the unseen extra dimensions, much of the uniqueness of string theory is lost due to the

large number of possible compactification methods, each manifold we can compactify upon leads to an alternative effective theory and would cause string theory to make different predictions about particle masses, interactions and couplings. Without predictive possibilities string theory will lose all the physical applications it may have had and cannot be verified as a true description of the universe.

6.1 Hopes of transition

Just as fluxes assign potential to the moduli space, potential which hopefully have local minima in which the moduli sit, so too will each topology have a different range of potentials, with some global minimum isolating one topology and one point within its moduli space. If it is possible for the universe to arrive at this topology and to fall to this minimal point in the potential we can predict the properties of the universe by finding the effective theory at this topology and at these moduli. With such predictions we can test string theory by experiment.

These predictions require that it is possible to change from an arbitrary topology to the preferred topology. While the moduli can vary continuously to arrive at the minimum, the topologies are discrete and separate, so continuous passage between them would seem to be impossible. The use of manifolds exhibiting conical singularities was thought to offer a method by which this marvel could be achieved, by changing moduli continuously to arrive at a conical singularity (which does not have a single defined topology) then continuously expanding the conical singularity to a manifold with different topology we could continuously arrive at the global minima, this would connect the different points by continuous (and finite) paths in moduli space. This would recover some of the predictive power of string theory.

This method brings with it risks however, most obviously are the events at the conical singularity and the change of topology while singular. This risk has been well studied and it has been found that the conical point can be made sense of within string theory and the risk can be bypassed. We however intently studied the gravitational effects of the process, notably the collapse of the cycle to a size small enough to initiate the transition. The reduction of the cycle to such a small size would require a great

concentration of energy in a small region. This presents the risk of creating black holes which would prevent the process being seen by an outside observer. The observer would merely see the concentrated energy forming a black hole solution as is predicted by existing theory, we could not verify string theory or gain any insight about the effects enclosed within the event horizon of the black hole.

6.2 Dynamical studies

In chapter 3 we investigated transitions within five dimensions, these would not be as drastic as some other transitions we suggested but the results still applied and they worked to indicate the possible outcomes. The first cycle we attempted to collapse belonged to an Eguchi-Hanson instanton, its collapse would have been the start of a flop transition, a change of topology under which many of the topological invariants are left unchanged. This could not be initiated however (despite the predictions of the moduli space approximation) as the cycle could not be collapsed. In low energy cases the cycle began to shrink in response to our initial conditions but this soon changed and the cycle re-expanded and grew beyond its starting size. In higher energy situations, the creation of a black hole was inevitable. Such a black-hole has an interesting asymptotic structure, namely there is a compact circle at infinity, and this leads us to an unexpected mechanism for compactificaction. If, instead of picturing the Eguchi-Hanson space as a portion of a compact internal space, we start with the full Eguchi-Hanson space, with its four large dimensions, we see that the final state has a compact dimension and corresponds to the Kaluza-Klein black-hole of [70].

The other five dimensional instanton we studied was the Taub-bolt instanton, it too possessed a cycle which could not be reduced to a singular point. In this case however the creation of a black hole was always the cause of the difficulty and the cycle could never return to the starting value once it had been perturbed. This indicated that the outcome resulted in the initial instanton and the initial momentum, while one instanton with a two-cycle invariably created a black hole, a different instanton's outcome depended upon the nature of the initial momentum even though it too possessed a two-cycle at its tip.

In chapter 4 we went on to simulate the possible dynamical creation of conical singularities in even higher dimensional situations. The possibility of transitions in seven dimensions is even more intriguing than five, this is because of the conifold transitions of seven dimensions which offer a way to change the topology even more drastically than the five dimensional flop transition. While a flop transition would change just the intersection numbers, a conifold transition would change Hodge numbers also. This may have more profound effect upon any lower dimensional observer (someone looking at only the particles of the low energy effective theory), the process could change the spectrum of particles even introducing the possibility of new types of particle coming into existence. This would be a more substantial change to the effective theory than would be seen during a flop transition.

The results we presented in this chapter however have suggested that this too cannot be dynamically achieved due to the inevitable creation of black hole spacetimes. In these simulations with seven dimensions and general relativity the creation of black holes seemed to be inevitable, just as it was for the Taub-bolt instanton of five dimensions. The tendency to return to the starting value (seen in the Eguchi-Hanson instanton) was never observed in these seven dimensional simulations.

In chapter 5 we performed our largest simulation, using a ten dimensional spacetime and introducing the fluxes of type IIB supergravity. This was also the simulation which we thought most applicable to our own situation and to other ongoing work since ten dimensions are predicted by string theory and the supergravity which arises from string theory is a major topic of study at the moment. This simulation was not only applicable for models involving transitions which could change the topology, but it will have applications to any theories which attempt to use the Klebanov-Strassler warped throat. This acted as a numerical test as to the stability of this solution, it is often taken to be the case that this solution is highly stable due to its the fluxes passing through the tip of its warped throat. The numerical simulations worked to test these assumptions under deformations larger than small perturbations and could test stability at even very larger perturbations still (though there is a minimum scale below which perturbative methods are superior).

These results produced a range of possible outcomes, not only dependent upon the

scale of initial momentum but also dependent upon the exact nature and which terms within the metric received the momentum. In section 5.3.5 we discussed situations which could only change the tip of the solution temporarily, though the size did increase due to our initial momentum it soon returned to the starting value. We also found that the restoration occurred even with very strong initial momentum which showed the tip to be very stable against this form of change. We could raise the initial momentum so high without reducing the tip to zero size that Fig. 5.5 suggested this could not be done using this form of initial momentum. Causing the three-cycle to expand was also possible but we believe this too is only a temporary change, though the time taken to return was much larger than the time it took for the cycle to recover from shrinking.

Alternatively there were some forms of initial momentum which created black hole solutions, these black holes would obscure the tip of the throat from the outside and would have to be accounted for in any theory using the throat. Forming these black holes would prevent the possibility of topology change also.

6.3 Evaporation of the black holes

While it seems classically that the topology change cannot be initiated but is prevented by the black holes which are often produced, when we include quantum mechanics we know that black holes do not in fact exist forever. Instead the black hole will radiate energy and will decrease in size until its area vanishes and it ”evaporates”. In section 2.3.3 we discussed that the interior of the black hole is completely disclosed from the rest of the spacetime and so has an unknown topology. This means that the relic left behind after evaporation may not have the same topology as the spacetime in which it was formed which presents an alternative method of topology change by a classical collapse of the spacetime to a black hole followed by a quantum evaporation to a new black hole free spacetime.

6.4 Closing statement

Our investigations have shown that the risks gravity poses to topology changing transitions being realised in classical GR are very significant as we have found no case where a singular manifold has been formed without a surrounding black hole to shroud the effects from any outside observers. This is a great impediment to the unification of the regions of the string landscape with different topology and so reduces the hope that the predictive power of string theory could be restored by changing the topology in response to the superpotential generated by flux compactifications.

However the inclusion of some quantum mechanics means that the black holes could later evaporate leaving a relic of unknown topology. This could act to change the topology by means of an intermediate black hole. This or any other method of changing the topology could be enougth to unite the string landscape and so return some predictive power to string theory.

String theory needs to make some predictions if we are to discover if we ourselves are comprised of some vibrating strings and whether our four dimensions are the left overs of a higher dimensional compactification.

Appendices

Appendix A

Conventions and computation

A.1 Conventions

In the following we will use a mostly plus metric signature and an antisymmetric tensor obeying

$$\epsilon_{0\,1\,2\,3\ldots} = +1. \tag{A.1}$$

This is used in the definition of the ten dimensional Hodge dual, given by

$$*e^{abc..} = \frac{1}{n!}\,\epsilon^{abc..}{}_{i_1 i_2..i_n} e^{i_1 i_2..i_n}. \tag{A.2}$$

We have used units such that $c = 1$ and $\bar{h} = 1$. We defined $8\pi G = 1$ which means that $G^{ab} = T^{ab}$.

A.2 Computational methods

All the numerical work was written from scratch in C++ and the simulations were carried out upon a desktop computer. The longest ten dimensional simulations took up to a week to run, lower dimensional problems took considerably less time. Any spatial derivatives which needed to be taken were performed using a fourth order five-point stencil. Apparent horizons were detected using an algorithm described in [19]. Plots were made using gnuplot.

Appendix B

Groups, forms and sets

B.1 Coset space geometry

We will work within groups formed by the quotient of a Lie group G and a subgroup of G which we call H (i.e. $H \subset G$). In order to find the line element of G/H and its associated curvatures we employ a coset method[82, 101]. If H is generated by $\{H_i$;i=1..dimH$\}$ and if G is generated by $\{H_i, E_a$;a=1..dimG-dimH$\}$, then the group G/H can be generated by E_a. The commutators of the generators can be written in terms of structure constants $C_{ij}{}^k$, defined by.

$$[H_i, H_j] = C_{ij}{}^k H_k, \tag{B.1}$$

$$[H_i, E_a] = C_{ia}{}^b E_b, \tag{B.2}$$

$$[E_a, E_b] = C_{ab}{}^d E_d + C_{ab}{}^i H_i. \tag{B.3}$$

If we let L be a general element of the group G then we can then define left invariant one-forms θ^a and h^i by the expressions

$$\Sigma = L^{-1} dL, \tag{B.4}$$

$$\Sigma = \theta^a E_a + h^i H_i. \tag{B.5}$$

When we construct the line element we use only the θ^a forms,

$$ds^2 = g_{ab} \theta^a \theta^b. \tag{B.6}$$

The ambiguity in the choice of L gives rise to various different one-forms. Using the expression (B.4) we can find that

$$\begin{aligned} d\Sigma &= dL^{-1} \wedge dL, \\ &= -L^{-1}dL \wedge L^{-1}dL, \\ &= -\Sigma \wedge \Sigma. \end{aligned} \tag{B.7}$$

Combining the equations (B.5) and (B.7) we can find that,

$$\begin{aligned} d\theta^a E_a + dh^i H_i &= -\theta^a \wedge \theta^b E_a E_b - \theta^a \wedge h^j E_a H_j - h^i \wedge \theta^b H_i E_b - h^i \wedge h^j H_i H_j, \\ &= -\frac{1}{2}\theta^a \wedge \theta^b [E_a, E_b] - \theta^a \wedge h^j [E_a, H_j] - \frac{1}{2} h^i \wedge h^j [H_i, H_j], \\ &= -\frac{1}{2}\theta^a \wedge \theta^b \left(C_{ab}{}^d E_d + C_{ab}{}^i H_i \right) - \theta^a \wedge h^j \left(C_{aj}{}^b E_b \right) \\ &\quad -\frac{1}{2} h^i \wedge h^j \left(C_{ij}{}^k H_k \right). \end{aligned} \tag{B.8}$$

The equation (B.8) can be split into two separate equations to give,

$$d\theta^a = -\frac{1}{2}\theta^b \wedge \theta^c C_{bc}{}^a - h^i \wedge \theta^b C_{ib}{}^a \tag{B.9}$$

$$dh^i = -\frac{1}{2}\theta^a \wedge \theta^b C_{ab}{}^i - \frac{1}{2} h^j \wedge h^k C_{jk}{}^i. \tag{B.10}$$

With these equations for the differentials of the one-forms we can go on to calculate the curvatures.

There is an additional constraint upon the coefficients of the line element (B.6), the constraint that,

$$0 = C_{ha}{}^c g_{cb} + C_{hb}{}^c g_{ac}. \tag{B.11}$$

This restriction ensures that Riemann curvature tensor only includes terms of the form θ^a and has no dependence upon h^i. The Levi-Civita connections are expressed in terms of one-forms $\omega^a{}_b$ defined by their metric compatability,

$$dg_{ab} - \omega^c{}_b g_{ac} - \omega^c{}_a g_{cb} = 0, \tag{B.12}$$

and also their lack of any torsion,

$$d\theta^a + \omega^a{}_b \theta^b = 0. \tag{B.13}$$

Using these connections we can go on to calculate the curvature tensors by the equation,

$$R^a{}_{bcd}\theta^c \wedge \theta^d = d\left(\omega^a{}_b\right) + \omega^a{}_c \wedge \omega^c{}_b. \tag{B.14}$$

This can then give the Ricci tensors and the Ricci scalar, which in turn give the Einstein tensor,

$$\begin{aligned} R_{ab} &= R^c{}_{acb} && \text{(B.15)} \\ R &= g^{ab}R_{ab} && \text{(B.16)} \\ G_{ab} &= R_{ab} - \frac{1}{2}g_{ab}R. && \text{(B.17)} \end{aligned}$$

It is these tensors, used in the Einstein equation, which give the equations of motion used to evolve the system.

B.2 The Special unitary group; $SU(2)$

One elegant way to write a metric in higher dimensional space is using the special unitary group. This group can conveniently be used to represent a three-sphere[62] since its parameter space can be identified with the manifold of the three-sphere. This $SU(2)$ also acts as a (double) covering of SO(3) and so could also be used as a representation of rotations. This section describes the conventions we have used when writing $SU(2)$ forms. We have used the conventional left-invariant one-forms, which are defined by the exterior derivitive

$$d\sigma_i = -\frac{1}{2}\epsilon_{ijk}\sigma_j \wedge \sigma_k. \tag{B.18}$$

This is equivalent to the requirement upon the Lie algebra of the $SU(2)$ generators

$$[\sigma_i, \sigma_j] = \epsilon_{ijk}\sigma_k. \tag{B.19}$$

In fact we will later use two distinct sets of the conventional left-invariant one-forms of $SU(2)$ both of which obey the equations of (B.18),

$$\begin{aligned} d\sigma^i &= -\frac{1}{2}\epsilon_{ijk}\sigma^j \wedge \sigma^k, \\ d\Sigma^i &= -\frac{1}{2}\epsilon_{ijk}\Sigma^j \wedge \Sigma^k. && \text{(B.20)} \end{aligned}$$

Though (B.18) is sufficient to define the one-forms, there are still multiple representations of $SU(2)$ which could be used. Since we intend to use the forms to represent a three-sphere it is most intuitive to investigate their properties using some angular coordinates. We used the representation

$$\begin{aligned} \sigma_1 &= sin\psi\, d\theta - sin\theta\, cos\psi\, d\phi, \\ \sigma_2 &= cos\psi\, d\theta + sin\theta\, sin\psi\, d\phi, \\ \sigma_3 &= d\psi + cos\theta\, d\phi. \end{aligned} \tag{B.21}$$

where

$$0 < \psi < 4\pi,\ 0 < \theta < \pi,\ 0 < \phi < 2\pi \tag{B.22}$$

Within this representation we can find the properties of the σ forms such as their volume and relation to the three-sphere and the two-sphere.

The Three-sphere S^3

The $SU(2)$ group can be used as a representation of S^3 when we use all three one-forms, the line element is then given by

$$ds^2 = \left(\frac{r}{2}\right)^2 \left(\sigma_1^2 + \sigma_2^2 + \sigma_3^2\right). \tag{B.23}$$

It then follows that the volume element is

$$dV = \left(\frac{r}{2}\right)^3 \sigma_1\sigma_2\sigma_3 \tag{B.24}$$

which can be calculated within our angular representation.

$$\begin{aligned} \int \sigma_1\sigma_2\sigma_3 &= \int (sin\psi\, d\theta - sin\theta\, cos\psi\, d\phi)\,(cos\psi\, d\theta + sin\theta\, sin\psi\, d\phi)\,(d\psi + cos\theta\, d\phi) \\ &= \int (d\theta\, sin\theta\, d\phi)\left(cos\psi^2 + sin\psi^2\right)(d\psi + cos\theta\, d\phi) \\ &= \int (sin\theta\, d\theta\, d\phi\, d\psi) \\ &= \int sin\theta\, d\theta \int d\phi \int d\psi \\ &= [-cos\theta]_0^\pi\, [\phi]_0^{2\pi}\, [\psi]_0^{4\pi} \\ &= 16\pi^2. \end{aligned} \tag{B.25}$$

This can give the volume of our S^3

$$\begin{aligned} \int dV &= \left(\frac{r}{2}\right)^3 \int \sigma_1\sigma_2\sigma_3 \\ V &= 2\pi^2 r^3 \end{aligned} \tag{B.26}$$

which is the correct volume for an S^3 with radius r.

The Two-sphere S^2

We can also use the forms of $SU(2)$ to represent a two-sphere, though it would require a different metric. Using just two of the forms gives the angular line element we recognise.

$$\begin{aligned} ds^2 &= r^2\left(\sigma_1^2 + \sigma_2^2\right) \\ &= r^2\left(cos\psi^2 + sin\psi^2\right)\left(d\theta^2 + sin^2\theta\, d\phi^2\right) \\ &= r^2\left(d\theta^2 + sin^2\theta\, d\phi^2\right). \end{aligned} \tag{B.27}$$

This line element, along with the correct range of angular values as given in (B.22) gives us the S^2. It has volume

$$\begin{aligned} \int \sigma_1\sigma_2 &= \int (sin\psi\, d\theta - sin\theta\, cos\psi\, d\phi)\,(cos\psi\, d\theta + sin\theta\, sin\psi\, d\phi) \\ &= \int (sin\theta\, d\theta\, d\phi) \\ &= \int sin\theta\, d\theta \int d\phi \\ &= [-cos\theta]_0^\pi\, [\phi]_0^{2\pi} \\ &= 4\pi. \end{aligned} \tag{B.28}$$

As before we can again form a volume from this S^2

$$\begin{aligned} \int dV &= r^2 \int \sigma_1\sigma_2 \\ V &= 4\pi r^2 \end{aligned} \tag{B.29}$$

which is the expected volume for an S^2 with radius r.

B.3 g^i one-forms

Within the coming analysis it is convenient to define a set of one-forms which are commonly used throughout. Labeled g^i, these are not a closed Lie group but a quotient. They are defined in terms of the two sets of $SU(2)$ forms, (B.20), to be

$$g^1 = (\sigma^1 - \Sigma^1)/\sqrt{2} \tag{B.30}$$

$$g^2 = (\sigma^2 + \Sigma^2)/\sqrt{2} \tag{B.31}$$

$$g^3 = (\sigma^1 + \Sigma^1)/\sqrt{2} \tag{B.32}$$

$$g^4 = (\sigma^2 - \Sigma^2)/\sqrt{2} \tag{B.33}$$

$$g^5 = (\sigma^3 + \Sigma^3). \tag{B.34}$$

Following section B.1 we see that the exterior derivatives of certain combinations are permitted, other combinations do not produce forms expressibile in terms of the g^i forms. The exterior derivatives expressible in g^i comprise of a limited number of combinations of two-forms,

$$d(g^1 \wedge g^2) = -\frac{1}{2}(g^1 \wedge g^3 \wedge g^5 + g^2 \wedge g^4 \wedge g^5), \tag{B.35}$$

$$d(g^3 \wedge g^4) = +\frac{1}{2}(g^1 \wedge g^3 \wedge g^5 + g^2 \wedge g^4 \wedge g^5), \tag{B.36}$$

$$d(g^1 \wedge g^3 + g^2 \wedge g^4) = (g^1 \wedge g^2 \wedge g^5 + g^3 \wedge g^4 \wedge g^5), \tag{B.37}$$

$$d(g^1 \wedge g^4 + g^2 \wedge g^3) = 0. \tag{B.38}$$

Along with a small number of three-forms ,

$$d(g^1 \wedge g^2 \wedge g^5) = 0, \tag{B.39}$$

$$d(g^3 \wedge g^4 \wedge g^5) = 0, \tag{B.40}$$

$$d(g^1 \wedge g^3 \wedge g^5 + g^2 \wedge g^4 \wedge g^5) = 0. \tag{B.41}$$

These restrictions can be used to limit the possibilities for fluxes and potentials.

Appendix C

Five dimensional Einstein equations for Taub-Bolt

The choice of metric (3.44) means that we can find the Ricci terms expressed in terms of A,B and C. These equations will allow our profile functions, A, B and C to be evolved dynamically in time and will also give two additional equations which must hold. These additional constraint equations must be imposed initially and can be used to test the numerics at later times.

We describe these more conveniently by defining some new functions:

$$\begin{aligned}
\alpha &= \left(1+\frac{R^2}{N^2}\right)e^{2A(t,R)}, \\
\beta &= N^2\left(1+\frac{R^4}{N^4}\right)e^{2B(t,R)}, \\
\gamma &= \frac{R^2}{\left(4+\frac{R^2}{N^2}\right)}e^{2C(t,R)}.
\end{aligned} \tag{C.1}$$

$$\begin{aligned}
K_A &= -\dot{A} \qquad & D_A &= A' + \frac{R}{N^2+R^2}, \\
K_B &= -\dot{B} \qquad & D_B &= B' + \frac{2R^3}{N^4+R^4}, \\
K_C &= -\dot{C} \qquad & D_C &= C' - \frac{R}{4N^2+R^2}.
\end{aligned} \tag{C.2}$$

Using these we can write the equations which come from the vanishing curvature.

C.1 Equations of motion

The Ricci terms must be used to evolve the metric into the future, they gave the evolution of the functions which describe the spacetime.

$$\begin{aligned}
\dot{K_A} &= K_A^2 - K_B^2 - 2\,K_B\,K_C + \frac{\gamma}{\beta^2} - \frac{4}{\beta} \\
&\quad + \frac{1}{\alpha}(D_B^2 + 2\,D_B\,(D_C + \frac{1}{R})) \\
\dot{K_B} &= 2\,K_B^2 + K_B\,K_C + K_B\,K_A - \frac{2\,\gamma}{\beta^2} + \frac{4}{\beta} \\
&\quad + \frac{1}{\alpha}(D_B\,D_A - 2\,D_B^2 - D'_B - D_B\,(D_C + \frac{1}{R})) \\
\dot{K_C} &= -K_B^2 + K_C^2 - 2\,K_B\,K_A + \frac{3\,\gamma}{\beta^2} - \frac{4}{\beta} \\
&\quad + \frac{1}{\alpha}(3\,D_B^2 - 2\,D_B\,D_A + 2\,D'_B).
\end{aligned} \tag{C.3}$$

C.2 Constraint equations

There were two remaining non-zero Ricci terms, these go to give the constraint equations:

$$\begin{aligned}
0 = &- K_A\,(2\,K_B + K_C) - K_B\,(K_B + 2\,K_C) + \frac{\gamma}{\beta^2} - \frac{4}{\beta} \\
&+ \frac{1}{\alpha}\left(-D_A\,(D_C + \frac{1}{R}) + 2\,D_B\,(D_C + \frac{1}{R}) + \frac{2\,D_C}{R}\right) \\
&+ \frac{1}{\alpha}\left(-2\,D_A\,D_B + 3\,D_B^2 + 2\,D'_B + D'_C + D_C^2\right),
\end{aligned} \tag{C.4}$$

and

$$K_A\,(D_C + 2\,D_B + \frac{1}{R}) = 2\,K'_B + K'_C + 2\,K_B\,D_B + K_C\,(D_C + \frac{1}{R}). \tag{C.5}$$

These are refered to as Hamiltonian and momentum constraints and must be imposed as we initiate the simulation.

Appendix D

Uniqueness of the squashed 5d black hole

In order to see if the black hole described in section 3.7 is the only option for a final state, we must find if it is unique. Firstly we write a metric capable of giving the most general form obeying the symmetries of (3.46).

$$ds^2 = -f(r)dt^2 + \frac{k(r)^2}{f(r)}dr^2 + \frac{r^2}{4}\left[\frac{b(r)^2}{d(r)^2}(\sigma_1^2 + \sigma_2^2) + d(r)^2\sigma_3^2\right]. \tag{D.1}$$

We make a gauge choice by defining r using the expression:

$$f = 1 - \frac{M^2}{r^2}. \tag{D.2}$$

Then we can solve the Einstein equation for R_{00} directly, with no loss of generality giving the expression

$$k(r) = \kappa\frac{b(r)^2}{d(r)}. \tag{D.3}$$

A coordinate rescaling and parameter redefinition permits the simplification (still with no loss of generality)

$$r \to \kappa r\,, \quad M \to \kappa M, \tag{D.4}$$

resulting in the expressions

$$f(r) = 1 - \frac{M^2}{r^2}, \tag{D.5}$$

$$k(r) = \frac{b(r)^2}{d(r)}, \tag{D.6}$$

while leaving $b(r)$ and $d(r)$ still unknown functions of r. Next we write these remaining unknown functions as a series

$$b(r) = \frac{r}{2}\left(b_0 + b_2 r^2 + b_4 r^4 + b_6 r^6 + b_8 r^8 + b_{10} r^{10} + b_{12} r^{12} ...\right), \tag{D.7}$$

$$d(r) = \frac{r}{2}\left(d_0 + d_2 r^2 + d_4 r^4 + d_6 r^6 + d_8 r^8 + d_{10} r^{10} + d_{12} r^{12} ...\right). \tag{D.8}$$

Expand the Einstein equations for R_{11} and R_{22} in r and make each term in the power series vanish. This will give us the values of the coefficients b_n and d_n

$$\begin{aligned} b_2 &= -\frac{b_0}{M^2}(b_0^2 - 1)\,, \quad d_2 = -\frac{1}{2M^2}(d_0^2 - 1)(d_0^2 + 1) \\ b_4 &= +\frac{b_0}{M^4}(b_0^2 - 1)^2\,, \quad d_4 = +\frac{3}{8M^4}(d_0^2 - 1)^2(d_0^2 + 1)^2 \\ &\vdots \end{aligned} \tag{D.9}$$

We then have to attempt to find the pattern to this series of coefficients. We found the coefficients to be given by

$$b_n = \frac{b_0}{M^n}(-1)^{n/2}(b_0^2 - 1)^{n/2}, \tag{D.10}$$

$$d_n = d_0 \prod_{i=1..n}\left(-\frac{1}{2}\frac{(2i-1)}{i}\frac{(d_0^4 - 1)}{M^2}\right). \tag{D.11}$$

This gives us the ability to write the infinite sum as an analytic expression

$$b(r) = \frac{M^2 b_0}{M^2 + b_0^2 r^2 - r^2}, \tag{D.12}$$

$$d(r) = \frac{M d_0}{\sqrt{M^2 + d_0^4 r^2 - r^2}}. \tag{D.13}$$

This is enough to define the most general 5d black hole which obeys the symmetries of (3.46). It seems to have one more degree of freedom than the uncharged version of (3.46) with the three parameters b_0,d_0 and M. However by the coordinate transformation

$$R = d(r)\, r, \tag{D.14}$$

$$T = d_0^2 t, \tag{D.15}$$

$$\bar{M} = \frac{M}{d_0}, \tag{D.16}$$

$$R_\infty = \frac{M\, d_0}{\sqrt{d_0^4 - b_0^2}}, \tag{D.17}$$

we arrive at the metric

$$ds^2 = -F(R)dT^2 + \frac{K(R)^2}{F(R)}dR^2 + \frac{R^2}{4}\left[K(R)(\sigma_1^2 + \sigma_2^2) + \sigma_3^2\right], \tag{D.18}$$

$$F(R) = 1 - \frac{\bar{M}^2}{R^2}, \tag{D.19}$$

$$K(R) = \frac{1 - \bar{M}^2/R_\infty^2}{(1 - R^2/R_\infty^2)^2}. \tag{D.20}$$

We see that this is identical to the uncharged case of (3.46). This is the only possible black hole solution which could result from our collapsing five dimensional instantons.

Appendix E

Seven dimensional Einstein equations

In both our seven dimensional simulations we used the vacuum Einstein-Hilbert action to evolve the initial surface to later times. The equations are given in full here.

E.1 Resolved conifold Einstein equations

The choice of metric (4.15) means that we can find the Ricci terms expressed in terms of A,B,C and D. These equations will allow our profile functions, A,B,C and D to be evolved dynamically in time and will also give two additional equations which must hold. These additional constraint equations must be imposed initially and can be used to test the numerics at later times.

We describe these more conveniently by defining the new functions

$$\begin{aligned} a(t,r) &= A^2(t,r), \\ b(t,r) &= r^2 B^2(t,r), \\ c(r,t) &= (6{\alpha_0}^2 + r^2) C^2(t,r), \\ d(t,r) &= r^2 D^2(t,r), \end{aligned} \tag{E.1}$$

each with associated momenta and derivative.

$$\begin{aligned} K_b &= \frac{\dot{b}}{b} \qquad & D_b &= \frac{b'}{ab}, \\ K_c &= \frac{\dot{c}}{c} \qquad & D_c &= \frac{c'}{ac}, \\ K_d &= \frac{\dot{d}}{d} \qquad & D_d &= \frac{d'}{ad}, \\ K_a &= \frac{\dot{a}}{a}. \end{aligned} \tag{E.2}$$

Using these we can find the equations from the vanishing curvature.

E.1.1 Equations of motion

The first four Ricci terms must be used to evolve the metric into the future, they gave the evolution of the four functions which describe the spacetime.

$$\begin{aligned} R_{11} = R_{22} = \quad & \dot{K_b} + K_b \left(K_a + 2K_b + 2K_c + K_d\right) \\ & -\frac{D_b'}{a} - D_b \left(2D_b + 2D_c + D_d\right) + \frac{1}{b^2} - \frac{d^2}{2b^4}, \\ R_{33} = R_{44} = \quad & \dot{K_c} + K_c \left(K_a + 2K_b + 2K_c + K_d\right) \\ & -\frac{D_c'}{a} - D_c \left(2D_b + 2D_c + D_d\right) + \frac{1}{c^2} - \frac{d^2}{2c^4}, \\ R_{55} = \quad & \dot{K_d} + K_d \left(K_a + 2K_b + 2K_c + K_d\right) \\ & -\frac{D_d'}{a} - D_d \left(2D_b + 2D_c + D_d\right) + \frac{d^2}{2b^4} + \frac{d^2}{2c^4}, \\ R_{rr} = \quad & \dot{K_a} + K_a \left(K_a + 2K_b + 2K_c + K_d\right) \\ & -2\frac{D_b'}{a} - 2\frac{D_c'}{a} - \frac{D_d'}{a} - \left(2D_b^2 + 2D_c^2 + D_d^2\right). \end{aligned} \tag{E.3}$$

E.1.2 Constraint equations

There were two remaining non-zero Ricci terms,

$$\begin{aligned} R_{tr} &= 2\left(\dot{D_b} + K_b D_b\right) + 2\left(\dot{D_c} + K_c D_c\right) + \left(\dot{D_d} + K_d D_d\right), \\ R_{tt} &= -\left(\dot{K_a} + K_a^2 + 2\dot{K_b} + 2K_b^2 + 2\dot{K_c} + 2K_c^2 \dot{K_d} + K_d^2\right). \end{aligned} \tag{E.4}$$

These are refered to as Hamiltonian and momentum constraints and must be imposed as we initiate the simulation.

E.2 Deformed conifold Einstein equations

Ansatz (4.24) produces the Ricci curvature dependent upon A,B,C and D (along with their derivatives) these are used as the equations of motion and constraint equations.

E.2.1 Equations of motion

Four of the Einstein equations were used to evolve the spacetime dynamically, the future state of the system is described by the four functions A,B,C and D. These are changed in time using the equations of motion which are found by ensuring the Ricci curvature vanishes.

Writing these Ricci terms is easier with the newly defined funcions

$$\begin{aligned} a(t,r) &= \left(A(t,r)\cosh\left(\frac{r}{3}\right)\right), \\ b(t,r) &= \left(B(t,r)\sinh\left(\frac{r}{3}\right)\right), \\ c(r,t) &= \left(C(t,r)\cosh\left(\frac{r}{3}\right)\right), \\ d(t,r) &= \left(D(t,r)\cosh\left(\frac{r}{3}\right)\right). \end{aligned} \tag{E.5}$$

We also associate each with functions describing momenta and the derivative:

$$\begin{aligned} K_b &= \frac{\dot{b}}{b} \qquad D_b = \frac{b'}{ab}, \\ K_c &= \frac{\dot{c}}{c} \qquad D_c = \frac{c'}{ac}, \\ K_d &= \frac{\dot{d}}{d} \qquad D_d = \frac{d'}{ad}, \\ K_a &= \frac{\dot{a}}{a}. \end{aligned} \tag{E.6}$$

The four Ricci terms below are used to form the equations of motion:

$$
\begin{aligned}
R_{rr} &= \dot{K_a} + K_a\left(K_a + 2K_b + 2K_c + K_d\right) \\
&\quad -2\frac{D_b'}{a} - 2\frac{D_c'}{a} - \frac{D_d'}{a} - \left(2D_b^2 + 2D_c^2 + D_d^2\right), \\
R_{11} = R_{22} &= \dot{K_b} + K_b\left(K_a + 2K_b + 2K_c + K_d\right) \\
&\quad -\frac{D_b'}{a} - D_b\left(2D_b + 2D_c + D_d\right) \\
&\quad +\frac{1}{2b^2} + \frac{b^2}{8c^2d^2} - \frac{c^2}{8b^2d^2} - \frac{d^2}{8c^2b^2}, \\
R_{33} = R_{44} &= \dot{K_c} + K_c\left(K_a + 2K_b + 2K_c + K_d\right) \\
&\quad -\frac{D_c'}{a} - D_c\left(2D_b + 2D_c + D_d\right) \\
&\quad +\frac{1}{2c^2} + \frac{c^2}{8b^2d^2} - \frac{b^2}{8c^2d^2} - \frac{d^2}{8c^2b^2}, \\
R_{55} &= \dot{K_d} + K_d\left(K_a + 2K_b + 2K_c + K_d\right) \\
&\quad -\frac{D_d'}{a} - D_d\left(2D_b + 2D_c + D_d\right) \\
&\quad +\frac{1}{2d^2} + \frac{d^2}{4b^2c^2} - \frac{b^2}{4c^2d^2} - \frac{c^2}{4d^2b^2}.
\end{aligned} \tag{E.7}
$$

E.2.2 Constraint equations

The two remaining non-zero Ricci terms acts as constraints, equations which are not used to evolve the system but should continue to hold provided they are true in the initial conditions

$$
\begin{aligned}
R_{tr} = \quad & -2\left(\frac{K_b'}{a} + D_b(K_b - K_a)\right) \\
& -2\left(\frac{K_c'}{a} + D_c(K_c - K_a)\right) \\
& -\left(\frac{K_d'}{a} + D_d(K_d - K_a)\right), \qquad \text{(E.8)} \\
R_{tt} &= -\left(\dot{K_a} + K_a^2 + 2\dot{K_b} + 2K_b^2 + 2\dot{K_c} + 2K_c^2\dot{K_d} + K_d^2\right). \qquad \text{(E.9)}
\end{aligned}
$$

These are called the Hamiltonian constraint and the momentum constraint, they were monitored during the course of the simulation to ensure the accuracy was sufficient.

E.3 Static black hole equations

As we wish to find a candidate for a black hole solution in seven dimensions in section 4.7, we use the Einstein equations to find vacuum solutions with event horizons. The need for Ricci flatness imposes restrictions upon the profile function of the metric (4.29). These are calculated to be,

$$\begin{aligned}
f'' &= -2f'\left(\frac{b'}{b}+\frac{c'}{c}+\frac{d'}{2d}\right)\\
b'' &= -\frac{f'b'}{f}+\frac{4}{bf}-\frac{d^2}{2fb^3}-\frac{b'b'}{b}-\frac{2b'c'}{c}-\frac{b'd'}{d}\\
c'' &= -\frac{f'c'}{f}+\frac{4}{cf}-\frac{d^2}{2fc^3}-\frac{c'c'}{c}-\frac{2b'c'}{b}-\frac{c'd'}{d}\\
d'' &= -\frac{f'd'}{f}+2\left(\frac{d^3}{4fb^4}-\frac{d'b'}{b}+\frac{d^3}{4fc^4}-\frac{d'c'}{c}\right)\\
0 &= f'\left(\frac{2b'}{b}+\frac{2c'}{c}+\frac{d'}{d}\right)+\frac{d^2}{2b^4}+\frac{d^2}{2c^4}-\frac{8}{b^2}-\frac{8}{c^2}\\
&\quad +f\left(2\left(\frac{b'}{b}\right)^2+2\left(\frac{c'}{c}\right)^2+8\frac{b'c'}{bc}+4\frac{b'd'}{bd}+4\frac{d'c'}{dc}\right).
\end{aligned} \tag{E.10}$$

Appendix F

Ten dimensional equations

Using the supergravity equations of section 2.6.3.1 along with the spacetime ansatz of section 5.3.3 leads to very elaborate eqution of motion. In order to write these in a more concise form we define new functions:

$$\begin{aligned}
\tilde{T}^2(t,r) = &\quad T^2(t,r)\, h^{-\frac{1}{2}}(r) \\
\tilde{a}^2(t,r) = &\quad a^2(t,r)\, h^{\frac{1}{2}}(r)\, \frac{1}{2}\epsilon^{\frac{4}{3}}\, K(r)\, \left(\frac{1}{3K^3(r)}\right) \\
\tilde{b}^2(t,r) = &\quad b^2(t,r)\, h^{\frac{1}{2}}(r)\, \frac{1}{2}\epsilon^{\frac{4}{3}}\, K(r)\, \left(sinh^2(r/2)\right) \\
\tilde{c}^2(t,r) = &\quad c^2(t,r)\, h^{\frac{1}{2}}(r)\, \frac{1}{2}\epsilon^{\frac{4}{3}}\, K(r)\, \left(cosh^2(r/2)\right) \\
\tilde{d}^2(t,r) = &\quad d^2(t,r)\, h^{\frac{1}{2}}(r)\, \frac{1}{2}\epsilon^{\frac{4}{3}}\, K(r)\, \left(\frac{1}{3K^3(r)}\right).
\end{aligned} \tag{F.1}$$

We also associate each metric function with functions describing momenta and the derivative:

$$\begin{aligned}
K_{\tilde{b}} &= \frac{\dot{\tilde{b}}}{\tilde{T}\tilde{b}} \qquad & D_{\tilde{b}} &= \frac{\tilde{b}'}{\tilde{a}\tilde{b}} \\
K_{\tilde{c}} &= \frac{\dot{\tilde{c}}}{\tilde{T}\tilde{c}} \qquad & D_{\tilde{c}} &= \frac{\tilde{c}'}{\tilde{a}\tilde{c}} \\
K_{\tilde{d}} &= \frac{\dot{\tilde{d}}}{\tilde{T}\tilde{d}} \qquad & D_{\tilde{d}} &= \frac{\tilde{d}'}{\tilde{a}\tilde{d}} \\
K_{\tilde{a}} &= \frac{\dot{\tilde{a}}}{\tilde{T}\tilde{a}} & & \\
K_{\tilde{T}} &= \frac{\dot{\tilde{T}}}{\tilde{T}^2} \qquad & D_{\tilde{T}} &= \frac{\tilde{T}'}{\tilde{a}\tilde{T}}.
\end{aligned} \tag{F.2}$$

We also give the fluxes a momenta and derivative function:

$$\begin{aligned} K_{B_\alpha} &= \dot{B}_\alpha \frac{\tilde{a}\tilde{T}^2\tilde{c}^2\tilde{d}}{\tilde{b}^2} & D_{B_\alpha} &= B'_\alpha \frac{\tilde{T}^4\tilde{c}^2\tilde{d}}{\tilde{a}\tilde{b}^2} \\ K_{B_\beta} &= \dot{B}_\beta \frac{\tilde{a}\tilde{T}^2\tilde{b}^2\tilde{d}}{\tilde{c}^2} & D_{B_\beta} &= B'_\beta \frac{\tilde{T}^4\tilde{b}^2\tilde{d}}{\tilde{a}\tilde{c}^2} \\ K_{C_\alpha} &= \dot{C}_\alpha \tilde{d}\tilde{a}\tilde{T}^2 & D_{C_\alpha} &= C'_\alpha \frac{\tilde{d}\tilde{T}^4}{\tilde{a}} \\ K_\phi &= \dot{\phi}\tilde{a}\tilde{T}^2\tilde{b}^2\tilde{c}^2\tilde{d} & D_{\tilde{T}} &= \phi' \frac{\tilde{T}^4\tilde{b}^2\tilde{c}^2\tilde{d}}{\tilde{a}}. \end{aligned} \tag{F.3}$$

We also use the fact that the fluxes have traces given by

$$F_{(3)}{}^2 = -12\left(\frac{\dot{C}_\alpha}{\tilde{T}\tilde{b}\tilde{c}}\right)^2 + 12\left(\frac{C'_\alpha}{\tilde{a}\tilde{b}\tilde{c}}\right)^2 + 6\frac{M - C_\alpha}{\tilde{c}^2\tilde{d}} + 6\frac{C_\alpha}{\tilde{b}^2\tilde{d}} \tag{F.4}$$

$$\begin{aligned} H^2 = {} & -6\left(\frac{\dot{B}_\alpha}{\tilde{T}\tilde{c}^2}\right)^2 - 6\left(\frac{\dot{B}_\beta}{\tilde{T}\tilde{b}^2}\right)^2 + 6\left(\frac{B'_\alpha}{\tilde{a}\tilde{c}^2}\right)^2 + 6\left(\frac{B'_\beta}{\tilde{a}\tilde{b}^2}\right)^2 \\ & + 12\left(\frac{B_\beta - B_\alpha}{2\tilde{b}\tilde{c}\tilde{d}}\right)^2. \end{aligned} \tag{F.5}$$

F.1 Equations of motion

The Ricci terms result from the metric ansatz and equation (B.15):

$$\begin{aligned}
R_{rr} = \; & \tfrac{\dot{K}_{\tilde{a}}}{\tilde{T}} + K_{\tilde{a}}\left(K_{\tilde{a}} + 3K_{\tilde{T}} + 2K_{\tilde{b}} + 2K_{\tilde{c}} + K_{\tilde{d}}\right) \\
& -4\tfrac{D'_{\tilde{T}}}{\tilde{a}} - 2\tfrac{D'_{\tilde{b}}}{\tilde{a}} - 2\tfrac{D'_{\tilde{c}}}{\tilde{a}} - \tfrac{D'_{\tilde{d}}}{\tilde{a}} \\
& -4D_{\tilde{T}}^2 - 2D_{\tilde{b}}^2 - 2D_{\tilde{c}}^2 - D_{\tilde{d}}^2
\end{aligned}$$

$$\begin{aligned}
R_{xx} = \; & \tfrac{\dot{K}_{\tilde{T}}}{\tilde{T}} + K_{\tilde{T}}\left(K_{\tilde{a}} + 3K_{\tilde{T}} + 2K_{\tilde{b}} + 2K_{\tilde{c}} + K_{\tilde{d}}\right) \\
& -\tfrac{D'_{\tilde{T}}}{\tilde{a}} - D_{\tilde{T}}(4D_{\tilde{T}} + 2D_{\tilde{b}} + 2D_{\tilde{c}} + D_{\tilde{d}})
\end{aligned}$$

$$\begin{aligned}
R_{11} = \; & \tfrac{\dot{K}_{\tilde{b}}}{\tilde{T}} + K_{\tilde{b}}\left(K_{\tilde{a}} + 3K_{\tilde{T}} + 2K_{\tilde{b}} + 2K_{\tilde{c}} + K_{\tilde{d}}\right) \\
& -\tfrac{D'_{\tilde{b}}}{\tilde{a}} - D_{\tilde{b}}(4D_{\tilde{T}} + 2D_{\tilde{b}} + 2D_{\tilde{c}} + D_{\tilde{d}}) \\
& +\tfrac{1}{16\tilde{b}^2\tilde{c}^2\tilde{d}^2}(2\tilde{b}^4 - 2\tilde{c}^4 - 8\tilde{d}^4 + 16\tilde{c}^2\tilde{d}^2)
\end{aligned}$$

$$\begin{aligned}
R_{33} = \; & \tfrac{\dot{K}_{\tilde{c}}}{\tilde{T}} + K_{\tilde{c}}\left(K_{\tilde{a}} + 3K_{\tilde{T}} + 2K_{\tilde{b}} + 2K_{\tilde{c}} + K_{\tilde{d}}\right) \\
& -\tfrac{D'_{\tilde{c}}}{\tilde{a}} - D_{\tilde{c}}(4D_{\tilde{T}} + 2D_{\tilde{b}} + 2D_{\tilde{c}} + D_{\tilde{d}}) \\
& +\tfrac{1}{16\tilde{b}^2\tilde{c}^2\tilde{d}^2}(2\tilde{c}^4 - 2\tilde{b}^4 - 8\tilde{d}^4 + 16\tilde{b}^2\tilde{d}^2)
\end{aligned}$$

$$\begin{aligned}
R_{55} = \; & \tfrac{\dot{K}_{\tilde{d}}}{\tilde{T}} + K_{\tilde{d}}\left(K_{\tilde{a}} + 3K_{\tilde{T}} + 2K_{\tilde{b}} + 2K_{\tilde{c}} + K_{\tilde{d}}\right) \\
& -\tfrac{D'_{\tilde{d}}}{\tilde{a}} - D_{\tilde{d}}(4D_{\tilde{T}} + 2D_{\tilde{b}} + 2D_{\tilde{c}} + D_{\tilde{d}}) \\
& +\tfrac{1}{16\tilde{b}^2\tilde{c}^2\tilde{d}^2}(16\tilde{d}^4 - 4\tilde{b}^4 - 4\tilde{c}^4 + 8\tilde{b}^2\tilde{c}^2).
\end{aligned} \tag{F.6}$$

The flux ansatz and equation (2.32) give another set of equations for the same Ricci terms:

$$
\begin{aligned}
R_{rr} &= \frac{1}{2\tilde{a}^2}\phi'^2 - \frac{1}{4}\left(\frac{(M-C_\alpha)B_\alpha + C_\alpha B_\beta}{\tilde{b}^2\tilde{c}^2\tilde{d}}\right)^2 \\
&\quad + \frac{1}{4}e^{\phi}\left(4\left(\frac{C'_\alpha}{\tilde{a}\tilde{b}\tilde{c}}\right)^2 - \frac{1}{12}\left(F_{(3)}{}^2\right)\right) \\
&\quad + \frac{1}{4}e^{-\phi}\left(2\left(\frac{B'_\alpha}{\tilde{a}\tilde{b}^2}\right)^2 + 2\left(\frac{B'_\beta}{\tilde{a}\tilde{c}^2}\right)^2 - \frac{1}{12}\left(H^2\right)\right) \\
R_{xx} &= -\frac{1}{4}\left(\frac{(M-C_\alpha)B_\alpha + C_\alpha B_\beta}{\tilde{b}^2\tilde{c}^2\tilde{d}}\right)^2 \\
&\quad + \frac{1}{4}e^{\phi}\left(-\frac{1}{12}\left(F_{(3)}{}^2\right)\right) \\
&\quad + \frac{1}{4}e^{-\phi}\left(-\frac{1}{12}\left(H^2\right)\right) \\
R_{11} &= \frac{1}{4}\left(\frac{(M-C_\alpha)B_\alpha + C_\alpha B_\beta}{\tilde{b}^2\tilde{c}^2\tilde{d}}\right)^2 \\
&\quad + \frac{1}{4}e^{\phi}\left(2\left(\frac{C_\alpha}{\tilde{b}^2\tilde{d}}\right)^2 - 2\left(\frac{\dot{C}_\alpha}{\tilde{T}\tilde{b}\tilde{c}}\right)^2 + 2\left(\frac{C'_\alpha}{\tilde{a}\tilde{b}\tilde{c}}\right)^2 - \frac{1}{12}\left(F_{(3)}{}^2\right)\right) \\
&\quad + \frac{1}{4}e^{-\phi}\left(2\left(\frac{B_\beta - B_\alpha}{2\tilde{b}\tilde{c}\tilde{d}}\right)^2 - 2\left(\frac{\dot{B}_\alpha}{\tilde{T}\tilde{c}^2}\right)^2 + 2\left(\frac{B'_\alpha}{\tilde{a}\tilde{c}^2}\right)^2 - \frac{1}{12}\left(H^2\right)\right) \\
R_{33} &= \frac{1}{4}\left(\frac{(M-C_\alpha)B_\alpha + C_\alpha B_\beta}{\tilde{b}^2\tilde{c}^2\tilde{d}}\right)^2 \\
&\quad + \frac{1}{4}e^{\phi}\left(2\left(\frac{M-C_\alpha}{\tilde{c}^2\tilde{d}}\right)^2 - 2\left(\frac{\dot{C}_\alpha}{\tilde{T}\tilde{b}\tilde{c}}\right)^2 + 2\left(\frac{C'_\alpha}{\tilde{a}\tilde{b}\tilde{c}}\right)^2 - \frac{1}{12}\left(F_{(3)}{}^2\right)\right) \\
&\quad + \frac{1}{4}e^{-\phi}\left(2\left(\frac{B_\beta - B_\alpha}{2\tilde{b}\tilde{c}\tilde{d}}\right)^2 - 2\left(\frac{\dot{B}_\beta}{\tilde{T}\tilde{b}^2}\right)^2 + 2\left(\frac{B'_\beta}{\tilde{a}\tilde{b}^2}\right)^2 - \frac{1}{12}\left(H^2\right)\right) \\
R_{55} &= \frac{1}{4}\left(\frac{(M-C_\alpha)B_\alpha + C_\alpha B_\beta}{\tilde{b}^2\tilde{c}^2\tilde{d}}\right)^2 \\
&\quad + \frac{1}{4}e^{\phi}\left(2\left(\frac{C_\alpha}{\tilde{b}^2\tilde{d}}\right)^2 + 2\left(\frac{M-C_\alpha}{\tilde{c}^2\tilde{d}}\right)^2 - \frac{1}{12}\left(F_{(3)}{}^2\right)\right) \\
&\quad + \frac{1}{4}e^{-\phi}\left(4\left(\frac{B_\beta - B_\alpha}{2\tilde{b}\tilde{c}\tilde{d}}\right)^2 - \frac{1}{12}\left(H^2\right)\right)
\end{aligned}
\tag{F.7}
$$

By combining (F.7) and (F.6) we arrive at our equations of motion for the terms in the metric.

F.2 Constraint equations

The two Ricci terms which will be used as constraints also come from the metric ansatz and equation (B.15):

$$\begin{aligned} R_{tt} = \quad & -(\tfrac{\dot{K}_{\tilde{a}}}{\tilde{T}} + K_{\tilde{a}}^2 - \tfrac{D'_{\tilde{T}}}{\tilde{a}} - D_{\tilde{T}}^2) \\ & -3(\tfrac{\dot{K}_{\tilde{T}}}{\tilde{T}} + K_{\tilde{T}}^2 - D_{\tilde{T}}^2) \\ & -2(\tfrac{\dot{K}_{\tilde{b}}}{\tilde{T}} + K_{\tilde{b}}^2 - D_{\tilde{T}} D_{\tilde{b}}) \\ & -2(\tfrac{\dot{K}_{\tilde{c}}}{\tilde{T}} + K_{\tilde{c}}^2 - D_{\tilde{T}} D_{\tilde{c}}) \\ & -(\tfrac{\dot{K}_{\tilde{d}}}{\tilde{T}} + K_{\tilde{d}}^2 - D_{\tilde{T}} D_{\tilde{d}}), \end{aligned}$$

$$\begin{aligned} R_{tr} = \quad & -3(\tfrac{K'_{\tilde{T}}}{\tilde{a}} + K_{\tilde{T}} D_{\tilde{T}} - K_{\tilde{a}} D_{\tilde{T}}) \\ & -2(\tfrac{K'_{\tilde{b}}}{\tilde{a}} + (K_{\tilde{b}} - K_{\tilde{a}}) D_{\tilde{b}}) \\ & -2(\tfrac{K'_{\tilde{c}}}{\tilde{a}} + (K_{\tilde{c}} - K_{\tilde{a}}) D_{\tilde{c}}) \\ & -(\tfrac{K'_{\tilde{d}}}{\tilde{a}} + (K_{\tilde{d}} - K_{\tilde{a}}) D_{\tilde{d}}). \end{aligned} \tag{F.8}$$

Another set of expressions for the Ricci terms comes from the flux ansatz and equation (2.32):

$$\begin{aligned} R_{tt} \quad = \quad & \frac{1}{2\tilde{T}^2}\dot{\phi}^2 + \frac{1}{4}\left(\frac{(M - C_\alpha)B_\alpha + C_\alpha B_\beta}{\tilde{b}^2\tilde{c}^2\tilde{d}}\right)^2 \\ & + \frac{1}{4}e^{\phi}\left(4\left(\frac{\dot{C}_\alpha}{\tilde{T}\tilde{b}\tilde{c}}\right)^2 + \frac{1}{12}\left(F_{(3)}{}^2\right)\right) \\ & + \frac{1}{4}e^{-\phi}\left(2\left(\frac{\dot{B}_\alpha}{\tilde{T}\tilde{b}^2}\right)^2 + 2\left(\frac{\dot{B}_\beta}{\tilde{T}\tilde{c}^2}\right)^2 + \frac{1}{12}\left(H^2\right)\right) \\ R_{tr} \quad = \quad & \frac{1}{2\tilde{T}\tilde{a}}\dot{\phi}\phi' \\ & + \frac{1}{4}e^{\phi}\left(-4\left(\frac{\dot{C}_\alpha}{\tilde{T}\tilde{b}\tilde{c}}\right)\left(\frac{C'_\alpha}{\tilde{a}\tilde{b}\tilde{c}}\right)\right) \\ & + \frac{1}{4}e^{-\phi}\left(-2\left(\frac{\dot{B}_\alpha}{\tilde{T}\tilde{b}^2}\right)\left(\frac{B'_\alpha}{\tilde{a}\tilde{b}^2}\right) - 2\left(\frac{\dot{B}_\beta}{\tilde{T}\tilde{c}^2}\right)\left(\frac{B'_\beta}{\tilde{a}\tilde{c}^2}\right)\right). \end{aligned} \tag{F.9}$$

Combining these relations gives us the constraint equations which must be obeyed upon the initial surface and should continue to be true throughout the simulation.

F.3 Flux equations

These equations come from (2.25) and allow us to evolve the fluxes to later times.

$$\begin{aligned} & e^{-\phi}\left(\dot{\phi}K_{B_\alpha} - \phi' D_{B_\alpha} - \dot{K_{B_\alpha}} + D'_{B_\alpha} + \frac{\tilde{a}\tilde{T}^4}{2\tilde{d}}\left(B_\beta - B_\alpha\right)\right) \\ & = \frac{\tilde{a}\tilde{T}^4\left(M - C_\alpha\right)}{\tilde{b}^2\tilde{c}^2\tilde{d}}\left(\left(M - C_\alpha\right)B_\alpha + C_\alpha B_\beta\right) \end{aligned} \tag{F.10}$$

$$\begin{aligned} & e^{-\phi}\left(\dot{\phi}K_{B_\beta} - \phi' D_{B_\beta} - \dot{K_{B_\beta}} + D'_{B_\beta} - \frac{\tilde{a}\tilde{T}^4}{2\tilde{d}}\left(B_\beta - B_\alpha\right)\right) \\ & = \frac{\tilde{a}\tilde{T}^4 C_\alpha}{\tilde{b}^2\tilde{c}^2\tilde{d}}\left(\left(M - C_\alpha\right)B_\alpha + C_\alpha B_\beta\right) \end{aligned} \tag{F.11}$$

$$\begin{aligned} & e^{\phi}\left(\dot{\phi}K_{C_\alpha} - \phi' D_{C_\alpha} + \dot{K_{C_\alpha}} - D'_{C_\alpha} + \frac{\tilde{a}\tilde{T}^4}{2\tilde{d}}\left(-\frac{\tilde{b}^2}{\tilde{c}^2}(M - C_\alpha) + \frac{\tilde{c}^2}{\tilde{b}^2}C_\alpha\right)\right) \\ & = \frac{-\tilde{a}\tilde{T}^4}{2\tilde{b}^2\tilde{c}^2\tilde{d}}\left(\left(M - C_\alpha\right)B_\alpha + C_\alpha B_\beta\right)\left(B_\beta - B_\alpha\right) \end{aligned} \tag{F.12}$$

$$\begin{aligned} -\dot{K}_\phi + D'_\phi \;=\; & -\frac{1}{2}e^{\phi}\left(\frac{2}{\tilde{d}\tilde{a}\tilde{T}^2}K^2_{C_\alpha} - \frac{2\tilde{a}}{\tilde{d}\tilde{T}^4}D^2_{C_\alpha} - \frac{\tilde{a}\tilde{T}^4}{\tilde{d}}\left(\frac{\tilde{b}^2}{\tilde{c}^2}(M - C_\alpha)^2 + \frac{\tilde{c}^2}{\tilde{b}^2}C^2_\alpha\right)\right) \\ & + \frac{1}{2}e^{-\phi}\left(\frac{1}{\tilde{d}\tilde{a}\tilde{T}^2}\left(\frac{\tilde{b}^2}{\tilde{c}^2}K^2_{B_\alpha} + \frac{\tilde{c}^2}{\tilde{b}^2}K^2_{B_\beta}\right) - \frac{\tilde{a}}{\tilde{d}\tilde{T}^4}\left(\frac{\tilde{b}^2}{\tilde{c}^2}D^2_{B_\alpha} + \frac{\tilde{c}^2}{\tilde{b}^2}D^2_{B_\beta}\right)\right) \\ & + \frac{1}{2}e^{-\phi}\left(-\frac{\tilde{a}\tilde{T}^4}{2\tilde{d}}(B_\beta - B_\alpha)^2\right) \end{aligned} \tag{F.13}$$

Bibliography

[1] T. Kaluza, *On the Problem of Unity in Physics*, *Sitzungsber. Preuss. Akad. Wiss. Berlin (Math. Phys.)* (1921) 966–972.

[2] O. Klein, *Quantum theory and five-dimensional theory of relativity*, *Z. Phys.* **37** (1926) 895–906.

[3] R. d'Inverno, *Introducing Einstein's relativity*, . Oxford, UK: Clarendon (1992) 383 p.

[4] R. M. Wald, *General Relativity*. University Of Chicago Press, June, 1984.

[5] J. Polchinski, *String theory. Vol. 2: Superstring theory and beyond*, . Cambridge, UK: Univ. Pr. (1998) 531 p.

[6] J. Polchinski, *Lectures on D-branes*, `hep-th/9611050`.

[7] J. Polchinski, *Dirichlet-Branes and Ramond-Ramond Charges*, *Phys. Rev. Lett.* **75** (1995) 4724–4727, [`hep-th/9510017`].

[8] V. A. Rubakov and M. E. Shaposhnikov, *Do We Live Inside a Domain Wall?*, *Phys. Lett.* **B125** (1983) 136–138.

[9] M. Nakahara, *Geometry, topology and physics*, . Boca Raton, USA: Taylor and Francis (2003) 573 p.

[10] R. S. Ward and R. O. Wells, *Twistor geometry and field theory*, . Cambridge, UK: Univ. Pr. (1990) 520 p.

[11] M. Grana, *Flux compactifications in string theory: A comprehensive review*, *Phys. Rept.* **423** (2006) 91–158, [`hep-th/0509003`].

[12] S.-T. Yau, *Calabi's Conjecture and some new results in algebraic geometry*, *Proc. Nat. Acad. Sci.* **74** (1977) 1798–1799.

[13] B. R. Greene, *String theory on Calabi-Yau manifolds*, `hep-th/9702155`.

[14] S. Hawking and G. Ellis, *The Large Scale Structure of Space-Time*. Cambridge Monographs on Mathematical Physics. Cambridge University Press, Cambridge, U.K., 1973.

[15] J. D. Bekenstein, *Black holes and entropy*, *Phys. Rev.* **D7** (1973) 2333–2346.

[16] J. M. Bardeen, B. Carter, and S. W. Hawking, *The Four laws of black hole mechanics*, *Commun. Math. Phys.* **31** (1973) 161–170.

[17] S. W. Hawking, *Black hole explosions*, *Nature* **248** (1974) 30–31.

[18] S. W. Hawking, *Particle Creation by Black Holes*, *Commun. Math. Phys.* **43** (1975) 199–220.

[19] J. Thornburg, *Finding apparent horizons in numerical relativity*, *Phys. Rev.* **D54** (1996) 4899–4918, [gr-qc/9508014].

[20] J. Michell, *On the Means of Discovering the Distance, Magnitude, and c. of the Fixed Stars, in Consequence of the Diminution of the Velocity of Their Light*, *Philosophical Transactions of the Royal Society of London* **74** (1784) 35–57.

[21] C. W. Misner, K. S. Thorne, and J. A. Wheeler, *Gravitation*, . San Francisco 1973, 1279p.

[22] R. L. Arnowitt, S. Deser, and C. W. Misner, *Coordinate invariance and energy expressions in general relativity*, *Phys. Rev.* **122** (1961) 997.

[23] R. L. Arnowitt, S. Deser, and C. W. Misner, *The dynamics of general relativity*, gr-qc/0405109.

[24] L. F. Abbott and S. Deser, *Stability of Gravity with a Cosmological Constant*, *Nucl. Phys.* **B195** (1982) 76.

[25] S. W. Hawking and G. T. Horowitz, *The Gravitational Hamiltonian, action, entropy and surface terms*, *Class. Quant. Grav.* **13** (1996) 1487–1498, [gr-qc/9501014].

[26] R. L. Arnowitt, S. Deser, and C. W. Misner, *Dynamical Structure and Definition of Energy in General Relativity*, *Phys. Rev.* **116** (1959) 1322–1330.

[27] L. Lehner, *Numerical relativity: A review*, *Class. Quant. Grav.* **18** (2001) R25–R86, [gr-qc/0106072].

[28] N. S. Manton, *A Remark on the Scattering of BPS Monopoles*, *Phys. Lett.* **B110** (1982) 54–56.

[29] W. Press, B. Flannery, S. Teukolsky, and W. Vetterling, *Numerical Recipes in C: The Art of Scientific Computing*. Cambridge University Press, 1992.

[30] D. C. J. R. J. Hosking and J. C. Turner, *First steps in numerical analysis*. Hodder and Stoughton, London, 1978.

[31] S. R. Coleman and J. Mandula, *All Possible Symmetries Of The S Matrix*, *Phys. Rev.* **159** (1967) 1251–1256.

[32] Y. A. Golfand and E. P. Likhtman, *Extension of the Algebra of Poincare Group Generators and Violation of p Invariance*, *JETP Lett.* **13** (1971) 323–326.

[33] M. Dine, *Supersymmetry and string theory: Beyond the standard model*, . Cambridge, UK: Cambridge Univ. Pr. (2007) 515 p.

[34] P. C. West, *Introduction to supersymmetry and supergravity*, . Singapore: World Scientific (1990) 425 p.

[35] F. Gliozzi, J. Scherk, and D. I. Olive, *Supersymmetry, Supergravity Theories and the Dual Spinor Model*, *Nucl. Phys.* **B122** (1977) 253–290.

[36] E. Cremmer, B. Julia, and J. Scherk, *Supergravity theory in 11 dimensions*, *Phys. Lett.* **B76** (1978) 409–412.

[37] P. G. O. Freund and M. A. Rubin, *Dynamics of Dimensional Reduction*, *Phys. Lett.* **B97** (1980) 233–235.

[38] P. K. Townsend, *Four lectures on M-theory*, `hep-th/9612121`.

[39] M. Cvetic, H. Lu, and C. N. Pope, *Brane-world Kaluza-Klein reductions and branes on the brane*, *J. Math. Phys.* **42** (2001) 3048–3070, [`hep-th/0009183`].

[40] M. Cvetic, H. Lu, and C. N. Pope, *Brane resolution through transgression*, *Nucl. Phys.* **B600** (2001) 103–132, [`hep-th/0011023`].

[41] E. A. Bergshoeff, M. de Roo, S. F. Kerstan, and F. Riccioni, *IIB Supergravity Revisited*, *JHEP* **08** (2005) 098, [`hep-th/0506013`].

[42] M. B. Green and J. H. Schwarz, *Anomaly Cancellation in Supersymmetric D=10 Gauge Theory and Superstring Theory*, *Phys. Lett.* **B149** (1984) 117–122.

[43] D. J. Gross, J. A. Harvey, E. J. Martinec, and R. Rohm, *The Heterotic String*, *Phys. Rev. Lett.* **54** (1985) 502–505.

[44] D. J. Gross, J. A. Harvey, E. J. Martinec, and R. Rohm, *Heterotic String Theory. 1. The Free Heterotic String*, *Nucl. Phys.* **B256** (1985) 253.

[45] D. J. Gross, J. A. Harvey, E. J. Martinec, and R. Rohm, *Heterotic String Theory. 2. The Interacting Heterotic String*, *Nucl. Phys.* **B267** (1986) 75.

[46] P. Candelas, G. T. Horowitz, A. Strominger, and E. Witten, *Vacuum Configurations for Superstrings*, *Nucl. Phys.* **B258** (1985) 46–74.

[47] S. Gurrieri, *N = 2 and N = 4 supergravities as compactifications from string theories in 10 dimensions*, `hep-th/0408044`.

[48] B. de Carlos, J. A. Casas, F. Quevedo, and E. Roulet, *Model independent properties and cosmological implications of the dilaton and moduli sectors of 4-d strings*, *Phys. Lett.* **B318** (1993) 447–456, [`hep-ph/9308325`].

[49] M. Dine and N. Seiberg, *Is the Superstring Weakly Coupled?*, *Phys. Lett.* **B162** (1985) 299.

[50] L. Susskind, *The anthropic landscape of string theory*, `hep-th/0302219`.

[51] P. Candelas, P. S. Green, and T. Hubsch, *Finite distances between distinct calabi-yau vacua: (other worlds are just around the corner)*, *Phys. Rev. Lett.* **62** (1989) 1956.

[52] P. Candelas, P. S. Green, and T. Hubsch, *Rolling Among Calabi-Yau Vacua*, *Nucl. Phys.* **B330** (1990) 49.

[53] A. Lukas, E. Palti, and P. M. Saffin, *Type IIB conifold transitions in cosmology*, *Phys. Rev.* **D71** (2005) 066001, [hep-th/0411033].

[54] A. Strominger, *Massless black holes and conifolds in string theory*, *Nucl. Phys.* **B451** (1995) 96–108, [hep-th/9504090].

[55] M. Brandle and A. Lukas, *Flop transitions in M-theory cosmology*, *Phys. Rev.* **D68** (2003) 024030, [hep-th/0212263].

[56] L. Jarv, T. Mohaupt, and F. Saueressig, *Effective supergravity actions for flop transitions*, *JHEP* **12** (2003) 047, [hep-th/0310173].

[57] L. Jarv, T. Mohaupt, and F. Saueressig, *M-theory cosmologies from singular Calabi-Yau compactifications*, *JCAP* **0402** (2004) 012, [hep-th/0310174].

[58] E. Palti, P. Saffin, and J. Urrestilla, *The effects of inhomogeneities on the cosmology of type IIB conifold transitions*, *JHEP* **03** (2006) 029, [hep-th/0510269].

[59] B. R. Greene, D. R. Morrison, and C. Vafa, *A geometric realization of confinement*, *Nucl. Phys.* **B481** (1996) 513–538, [hep-th/9608039].

[60] P. Bizon, T. Chmaj, and G. Gibbons, *Nonlinear perturbations of the Kaluza-Klein monopole*, *Phys. Rev. Lett.* **96** (2006) 231103, [gr-qc/0604043].

[61] G. W. Gibbons and S. W. Hawking, *Classification of Gravitational Instanton Symmetries*, *Commun. Math. Phys.* **66** (1979) 291–310.

[62] T. Eguchi, P. B. Gilkey, and A. J. Hanson, *Gravitation, Gauge Theories and Differential Geometry*, *Phys. Rept.* **66** (1980) 213.

[63] T. Eguchi and A. J. Hanson, *Asymptotically Flat Selfdual Solutions to Euclidean Gravity*, *Phys. Lett.* **B74** (1978) 249.

[64] N. A. Butcher and P. M. Saffin, *Singular manifolds, topology change and the dynamics of compactification*, *JHEP* **11** (2007) 062, [arXiv:0709.2430].

[65] N. A. Butcher and P. M. Saffin, *The dynamics of topology change*, *AIP Conf. Proc.* **1122** (2009) 115–120.

[66] M. Alcubierre and J. A. Gonzalez, *Regularization of spherically symmetric evolution codes in numerical relativity*, *Comput. Phys. Commun.* **167** (2005) 76–84, [gr-qc/0401113].

[67] M. Ruiz, M. Alcubierre, and D. Nunez, *Regularization of spherical and axisymmetric evolution codes in numerical relativity*, *Gen. Rel. Grav.* **40** (2008) 159–182, [arXiv:0706.0923].

[68] B. J. Kelly *et. al.*, *A cure for unstable numerical evolutions of single black holes: adjusting the standard ADM equations*, *Phys. Rev.* **D64** (2001) 084013, [gr-qc/0103099].

[69] D. N. Page, *Taub - Nut Instanton with an horizon*, *Phys. Lett.* **B78** (1978) 249.

[70] G. W. Gibbons and D. L. Wiltshire, *Black Holes in Kaluza-Klein Theory*, *Ann. Phys.* **167** (1986) 201.

[71] P. Dobiasch and D. Maison, *Stationary, spherically symmetric solutions of Jordan's unified theory of gravity and electromagnetism*, *Gen. Rel. Grav.* **14** (1982) 231–242.

[72] H. Ishihara and K. Matsuno, *Kaluza-Klein black holes with squashed horizons*, *Prog. Theor. Phys.* **116** (2006) 417–422, [hep-th/0510094].

[73] P. Bizon, T. Chmaj, G. W. Gibbons, and C. N. Pope, *Gravitational solitons and the squashed seven-sphere*, *Class. Quant. Grav.* **24** (2007) 4751–4776, [hep-th/0701190].

[74] P. Candelas and X. C. de la Ossa, *Comments on Conifolds*, *Nucl. Phys.* **B342** (1990) 246–268.

[75] P. Candelas and X. de la Ossa, *Moduli space of calabi-yau manifolds*, *Nucl. Phys.* **B355** (1991) 455–481.

[76] P. Candelas, X. C. De La Ossa, P. S. Green, and L. Parkes, *A pair of Calabi-Yau manifolds as an exactly soluble superconformal theory*, *Nucl. Phys.* **B359** (1991) 21–74.

[77] P. S. Aspinwall, B. R. Greene, and D. R. Morrison, *Calabi-Yau moduli space, mirror manifolds and spacetime topology change in string theory*, *Nucl. Phys.* **B416** (1994) 414–480, [hep-th/9309097].

[78] R. Gwyn and A. Knauf, *The Geometric Transition Revisited*, hep-th/0703289.

[79] L. A. Pando Zayas and A. A. Tseytlin, *3-branes on resolved conifold*, *JHEP* **11** (2000) 028, [hep-th/0010088].

[80] I. R. Klebanov and M. J. Strassler, *Supergravity and a confining gauge theory: Duality cascades and chiSB-resolution of naked singularities*, *JHEP* **08** (2000) 052, [hep-th/0007191].

[81] K. Ohta and T. Yokono, *Deformation of conifold and intersecting branes*, *JHEP* **02** (2000) 023, [hep-th/9912266].

[82] R. Minasian and D. Tsimpis, *On the geometry of non-trivially embedded branes*, *Nucl. Phys.* **B572** (2000) 499–513, [hep-th/9911042].

[83] N. A. Butcher and P. M. Saffin, *The evolution of conifolds*, *JHEP* **12** (2008) 012, [arXiv:0809.1354].

[84] M. R. Douglas and S. Kachru, *Flux compactification*, *Rev. Mod. Phys.* **79** (2007) 733–796, [hep-th/0610102].

[85] S. Kachru and L. McAllister, *Bouncing brane cosmologies from warped string compactifications*, *JHEP* **03** (2003) 018, [hep-th/0205209].

[86] I. R. Klebanov and E. Witten, *AdS/CFT correspondence and symmetry breaking*, *Nucl. Phys.* **B556** (1999) 89–114, [hep-th/9905104].

[87] I. R. Klebanov and A. A. Tseytlin, *Gravity Duals of Supersymmetric SU(N) x SU(N+M) Gauge Theories*, *Nucl. Phys.* **B578** (2000) 123–138, [hep-th/0002159].

[88] R. Graham, *Supersymmetric Bianchi type IX cosmology*, *Phys. Rev. Lett.* **67** (1991) 1381–1383.

[89] N. A. Butcher and P. M. Saffin, *The gravitational dynamics of warped throats*, arXiv:0909.1675.

[90] X. Chen and S. H. H. Tye, *Heating in brane inflation and hidden dark matter*, *JCAP* **0606** (2006) 011, [hep-th/0602136].

[91] X. Chen, *Inflation from warped space*, *JHEP* **08** (2005) 045, [hep-th/0501184].

[92] S. Kecskemeti, J. Maiden, G. Shiu, and B. Underwood, *DBI inflation in the tip region of a warped throat*, *JHEP* **09** (2006) 076, [hep-th/0605189].

[93] A. Buchel and R. Roiban, *Inflation in warped geometries*, *Phys. Lett.* **B590** (2004) 284–294, [hep-th/0311154].

[94] X. Chen, *Decaying Hidden Dark Matter in Warped Compactification*, *JCAP* **0909** (2009) 029, [arXiv:0902.0008].

[95] J. F. G. Cascales, M. P. Garcia del Moral, F. Quevedo, and A. M. Uranga, *Realistic D-brane models on warped throats: Fluxes, hierarchies and moduli stabilization*, *JHEP* **02** (2004) 031, [hep-th/0312051].

[96] L. Randall and R. Sundrum, *A large mass hierarchy from a small extra dimension*, *Phys. Rev. Lett.* **83** (1999) 3370–3373, [hep-ph/9905221].

[97] S. B. Giddings, S. Kachru, and J. Polchinski, *Hierarchies from fluxes in string compactifications*, *Phys. Rev.* **D66** (2002) 106006, [hep-th/0105097].

[98] M. R. Douglas and G. Torroba, *Kinetic terms in warped compactifications*, arXiv:0805.3700.

[99] A. R. Frey, G. Torroba, B. Underwood, and M. R. Douglas, *The Universal Kaehler Modulus in Warped Compactifications*, *JHEP* **01** (2009) 036, [arXiv:0810.5768].

[100] G. Shiu, G. Torroba, B. Underwood, and M. R. Douglas, *Dynamics of Warped Flux Compactifications*, *JHEP* **06** (2008) 024, [arXiv:0803.3068].

[101] F. Mueller-Hoissen and R. Stuckl, *Coset spaces and ten-dimensional unified theories*, *Class. Quant. Grav.* **5** (1988) 27.